EXPERIMENTAL INVESTIGATION OF FILM COOLING EFFECTIVENESS ON GAS TURBINE BLADES

A Dissertation

by

ZHIHONG GAO

Submitted to the Office of Graduate Studies of
Texas A&M University
in partial fulfillment of the requirements for the degree of

DOCTOR OF PHILOSOPHY

August 2007

Major Subject: Mechanical Engineering

EXPERIMENTAL INVESTIGATION OF FILM COOLING EFFECTIVENESS ON GAS TURBINE BLADES

A Dissertation

by

ZHIHONG GAO

Submitted to the Office of Graduate Studies of
Texas A&M University
in partial fulfillment of the requirements for the degree of

DOCTOR OF PHILOSOPHY

Approved by:

Chair of Committee,	Je-Chin Han
Committee Members,	N.K. Anand
	Hamn-Ching Chen
	Sai Lau
Head of Department,	Dennis O'Neal

August 2007

Major Subject: Mechanical Engineering

ABSTRACT

Experimental Investigation of Film Cooling Effectiveness on Gas Turbine Blades.

(August 2007)

Zhihong Gao, B.E., Harbin Institute of Technology;

M.E., Harbin Institute of Technology;

M.S., National University of Singapore

Chair of Advisory Committee: Dr. Je-Chin Han

The hot gas temperature in gas turbine engines is far above the permissible metal temperatures. Advanced cooling technologies must be applied to cool the blades, so they can withstand the extreme conditions. Film cooling is widely used in modern high temperature and high pressure blades as an active cooling scheme. In this study, the film cooling effectiveness in different regions of gas turbine blades was investigated with various film hole/slot configurations and mainstream flow conditions. The study consisted of four parts: 1) effect of upstream wake on blade surface film cooling, 2) effect of upstream vortex on platform purge flow cooling, 3) influence of hole shape and angle on leading edge film cooling and 4) slot film cooling on trailing edge. Pressure sensitive paint (PSP) technique was used to get the conduction-free film cooling effectiveness distribution.

For the blade surface film cooling, the effectiveness from axial shaped holes and compound angle shaped holes were examined. Results showed that the compound angle

shaped holes offer better film effectiveness than the axial shaped holes. The upstream stationary wakes have detrimental effect on film effectiveness in certain wake rod phase positions.

For platform purge flow cooling, the stator-rotor gap was simulated by a typical labyrinth-like seal. Delta wings were used to generate vortex and modeled the passage vortex generated by the upstream vanes. Results showed that the upstream vortex reduces the film cooling effectiveness on the platform.

For the leading edge film cooling, two film cooling designs, each with four film cooling hole configurations, were investigated. Results showed that the shaped holes provide higher film cooling effectiveness than the cylindrical holes at higher average blowing ratios. In the same range of average blowing ratio, the radial angle holes produce better effectiveness than the compound angle holes. The seven-row design results in much higher effectiveness than the three-row design.

For the trailing edge slot cooling, the effect of slot lip thickness on film effectiveness under the two mainstream conditions was investigated. Results showed thinner lips offer higher effectiveness. The film effectiveness on the slots reduces when the incoming mainstream boundary layer thickness decreases.

DEDICATION

To Lixian Chen, Chengming Gao, Guiqin Wang and Chengjie Gao.

ACKNOWLEDGMENTS

I would like to express my deepest appreciation to Dr. Je-Chin Han for his continuous technical and financial support during my Ph.D. program. I also would like to thank Dr. N. K. Anand, Dr. H. C. Chen, and Dr. S. Lau for giving their precious time on the advisory committee. Their advice and suggestions are greatly appreciated.

Acknowledgments are also due to my colleagues from the Turbine Heat Transfer Laboratory.

Finally, I thank to my family for their support, understanding and patience.

NOMENCLATURE

C_D	Discharge coefficient
Co	Oxygen concentration
C_x	Axial chord length of the blade
d	Diameter of film-cooling holes
D	Diameter of leading edge model
I	Pixel intensity for an image
M	Average blowing ratio ($=\rho_c V_c / \rho_m V_m$)
LE	Leading edge of the blade
p	Spanwise distance between film cooling holes
P	Local static pressure
P_t	Total pressure at the cascade inlet
P_{O2}	Partial pressure of oxygen
PS	Blade pressure-side
s	Streamwise distance from the stagnation line row or slot height
t	Lip thickness
SS	Blade suction-side
TE	Trailing edge of the blade
Tu	Turbulence intensity level at the cascade inlet
x	Axial distance
y	Spanwise distance
z	Lateral distance
V_c	Averaged velocity of coolant air from all film cooling holes

δ	Boundary layer thickness
η	Local film-cooling effectiveness
$\bar{\eta}$	Spanwise averaged film cooling effectiveness
θ	Angle from the stagnation line along the surface
ρ_c	Density of coolant air
ρ_m	Density of mainstream air

Subscript

air	Mainstream air with air as coolant
c	Coolant
m	Mainstream
mix	Mainstream air with nitrogen as coolant
ref	Reference image with no mainstream and coolant flow
blk	Image without illumination (black)

TABLE OF CONTENTS

Page

Page

LIST OF FIGURES

Page

Page

Page

Page

Page

LIST OF TABLES

Page

1. INTRODUCTION

Gas turbines are widely used in aircraft propulsion and land-based power generation or industrial applications. Thermal efficiency and power output of gas turbine increase with increasing turbine rotor inlet temperatures. The operating temperatures are far above the permissible metal temperatures. Advanced cooling technologies must be applied to the airfoils, so they can withstand these extreme conditions. Han et al. [1] describes many cooling techniques that are commonly used in various combinations to increase the lifetime of the turbine blades. Impingement cooling, rib turbulated cooling, and pin-fin cooling are typically used to remove heat from the inner walls of the blades. In order to overcome the hazard from the severe environment and prevent failure of turbine components, film cooling has been widely accepted as an active cooling method. In a film cooled component, relatively cooler air is penetrated through discrete holes or slots to provide a protective film between the hot mainstream gas and the turbine component to maintain the surface at a lower temperature thus protect the turbine component surface. However, excessive use of coolant reduces the gain of the higher inlet temperature because the consumption of compressed air and the mixing between the hot mainstream flow and coolant reduce the thermal efficiency of entire system. Thus, much research has been conducted to understand the physical phenomena regarding the film cooling process and to find better configurations that can provide more protection with less coolant.

This dissertation follows the style of ASME Journal of Turbomachinery.

1.1 Literature Review on Turbine Blade Surface Film Cooling

Among the vast literatures related to the film cooling, majority of the recent work focuses on comparative assessment of two or more film cooling hole configurations. Among the variety of film cooling hole designs, four kinds of hole geometries are generally considered: cylindrical holes, laterally-diffused (fanshape) holes, forward-diffused (laidback) holes, and laterally- and forward-diffused (laidback fanshape) holes. Figure 1.1 shows the four kinds of hole geometries with the cross section view cutting along the hole centerline. Depending on the angle (β) of the projected hole centerline on the surface with respect to the mainstream direction, a film cooling hole can be identified as an axial hole (if $\beta = 0°$) or a compound angle hole (if $\beta > 0°$). Figure 1.1 also conceptually shows the film cooling effectiveness distribution associated with the various hole configurations. In general, the compound angle hole gives better effectiveness as the coolant is deflected by the mainstream and covers a larger surface area. The shaped holes performs better than the cylindrical holes because the expanded hole breakout area reduces the jet momentum and diminish the jet lift-off.

Film cooling on a flat plate is often chosen as a baseline study. Goldstein et al. [2] showed the benefits of film-cooling with shaped holes. They compared film-cooling effectiveness for straight round holes and axial shaped holes with lateral diffusion of 10°. The axis of both the hole geometries were inclined at 35° from the test surface. They reported a significant increase in the film-cooling effectiveness immediately downstream of the shaped holes as well as increased lateral coolant displacement. They attributed this effect primarily to the reduced mean velocity of the coolant at the hole exit causing the jet to stay closer to the surface. Thole et al. [3] carried out flow field measurements using LDV at the exit of three different hole

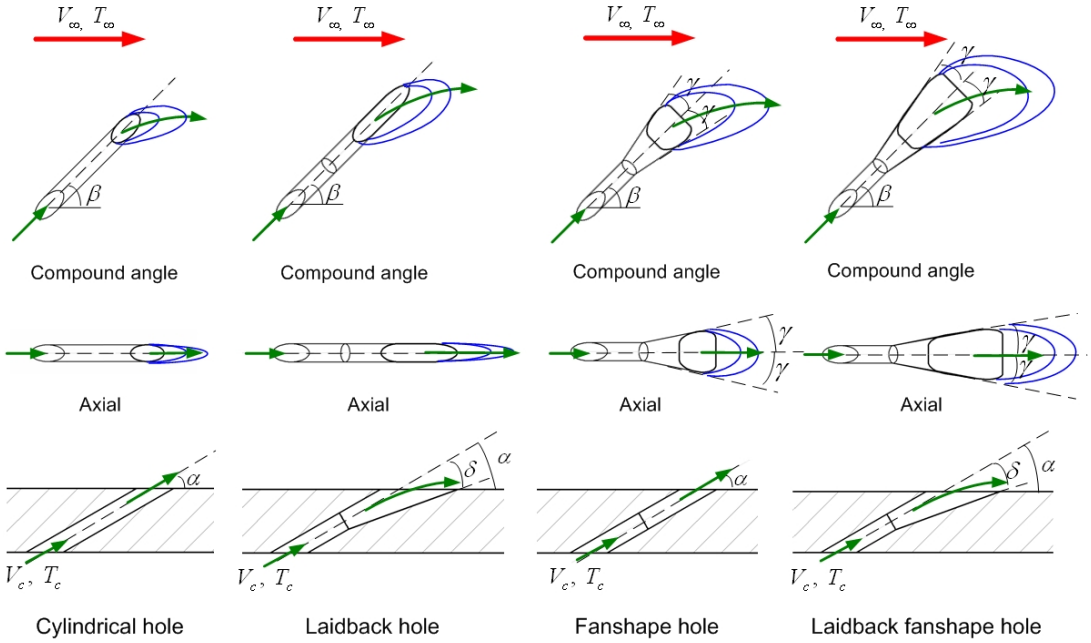

Fig. 1.1 Film cooling hole configurations

geometries. The hole geometries included a round hole, a hole with a laterally expanded exit, and a hole with a forward-laterally expanded exit. All holes were oriented at an angle of at 30° from the surface. Their findings showed that both the shaped holes had less shear mixing of the injection jet with the mainstream and greater lateral spreading of the coolant compared to that of a round hole. Additionally, the forward-laterally shaped hole had relatively lower film effectiveness than the laterally expanded shaped hole due to excessive diffusion of the coolant and subsequent mainstream interaction. Gritsch et al. [4] studied the same cooling hole configurations and orientations as [3] with a density ratio of 1.85. Their film-cooling effectiveness measurements were confined to x/D = 10 in order to focus in the nearfield of the cooling hole. As compared to the cylindrical hole, both expanded holes showed significantly improved thermal protection of the surface downstream of the ejection location, particularly at high blowing ratios. Along similar lines, Yu et al. [5] studied film-effectiveness and heat transfer distributions on a flat plate with straight circular hole, 10° forward diffusion shaped hole, and another type of hole with an additional 10° lateral diffusion. In each case, the axis of the hole was oriented 30° relative to the mainstream direction. The last mentioned hole provided the highest film cooling performance as well as overall heat transfer reduction.

All of the above studies were performed on a flat plate with axially oriented holes. Schmidt et al. [6] examined film-cooling performance of 60° compound angled holes on a flat plate surface, with and without forward expanded shaped exit, and compared that with cylindrical holes aligned with the mainstream. The round and shaped exit holes with compound angle had significantly greater effectiveness at larger momentum flux ratios. The compound angle holes with expanded exits had a much

improved lateral distribution of coolant near the hole for all momentum flux ratios. Dittmar et al. [7], in a slight deviation, conducted measurements on a model of a suction side of an actual turbine guide vane inside a wind tunnel. Four different cooling hole configurations - a double row of cylindrical holes, a double row of discrete slots, a single row of straight fan-shaped holes, and a single row of compound angle fan-shaped holes, were chosen to study adiabatic film-cooling effectiveness and heat transfer coefficient. Both the shaped holes featured expansion only in the lateral direction. The streamwise injection angle was 45° for all cases with an additional lateral angle of 35° from the mainstream direction for compound shaped holes. According to their study, fan-shaped holes provided good effectiveness values at moderate and high blowing ratios unlike the cylindrical holes which suffered from jet separation. In another study involving pressure and suction side models inside a wind tunnel, Chen et al. [8] investigated both axial and compound shaped holes with forward diffusion. The compound angle in their study was 45°. On the concave surface, improvement in laterally averaged effectiveness due to the addition of compound angle was found at high blowing ratio of 2. On the convex surface, significant improvement in effectiveness is seen at both low and high blowing ratios.

Hole shape study in linear cascades are fewer in comparison to those in flat plate and model airfoils. Teng and Han [9] studied one row of film holes near the gill-hole portion of the suction side. The hole geometries considered in their study were same as those of [3] and [4] but with a slightly higher inclined angle of 45^{o}. They reported that spanwise-averaged film effectiveness of shaped holes could be about two times higher than that of cylindrical holes. In addition, fan-shaped holes performed better than laidback fan-shaped holes. More recently, Mhetras et al. [10] observed the excellent

coolant coverage offered by compound shaped holes near the tip region of the pressure side. Their study showed that the shaped holes on the pressure side of the blade could be utilized in cooling the cut-back region of the tip cavity floor.

Effect of a rotating, unsteady wake on film cooling effectiveness and coolant jet temperature profiles on the suction side of a turbine blade were investigated by Teng et al. [11] in a low speed cascade. A spoked-wheel mechanism was used to generate the upstream wakes. They found that unsteady wake reduced the effectiveness magnitudes. Local heat transfer immediately downstream of the holes was found to increase by as much as 60% due to film injection. Ou et al. [12] simulated unsteady wake conditions using the same mechanism as [11] over a linear turbine blade cascade with film cooling. They tested no-wake case and wake Strouhal numbers of 0.1 and 0.3. Air and CO2 were used to study effect of density ratio. It was found that increasing wake passing frequency increases local Nusselt numbers for all blowing ratios, but this effect is reduced at higher blowing ratios. It was concluded that the additional increases in Nusselt numbers due to unsteady wake, blowing ratio, and density ratio were only secondary when compared to the dramatic increases in Nusselt numbers only due to film injection over the no film holes case. They concluded that heat transfer coefficients increase and film cooling effectiveness values decreased with an increase in unsteady wake strength. Further, Mehendale et al. [13], in the same test facility and for the same experimental conditions, found that an increase in wake Strouhal number leaded to a decrease in film effectiveness over most of the blade surface for both density ratio injections and at all blowing ratios. Du et al. [14] performed a similar experiment with the addition of trailing edge coolant ejection from the wake-producing bars. The addition of wake coolant had a relatively small effect on downstream blade heat transfer

coefficient, but reduced leading edge film effectiveness below the wake case with no coolant ejection. Detailed heat transfer measurements on transonic film-cooled blade with and without NGV shock waves and wakes were made by Rigby et al. [15]. It was found that there was a significant change of film-cooling behavior on the suction surface when simulated NGV unsteady effects were introduced. Heidmann et al. [16] studied the effect of wake passing on showerhead film cooling performance in an annular cascade with an upstream rotating row of cylindrical rods. A high wake Strouhal number was found to decrease effectiveness but it was also found to divert the coolant towards the pressure side resulting in slightly better cooling on the pressure side.

Most of experimental study of the film cooling was focused on the mid-span region only, the endwall effect was not captured. By using the Pressure Sensitive Paint (PSP) techniques, Mhetras et al.[17] and Narzary et. al. [18] were able to obtain detailed film cooling effectiveness distribution on a fully film cooled blade surface. Both tests were done in the same cascade. The flow conditions, film cooling hole locations and internal coolant supply cavities were similar for the two studies. Both test blades had three showerhead rows of cylindrical holes with 30° angle in radial direction in the leading region. However, the hole configurations on the blade surfaces were different. They were compound angle cylindrical holes in Mhetras et al. study [17], while the compound angle fan-shape laid-back holes in Narzary et. al. study[18]. During the film cooling test, the holes on both the pressure side and suction side were all open as well as the showerhead holes. They showed the coolant on the suction side was swept substantially to the mid-span region because of the tip leakage vortices and endwall vortices. It has been shown that the highest effectiveness was obtained at M=0.9 for

cylindrical holes, while shaped holes didn't present the optimal blowing ratio from M=0.3 to M=1.2. The effectiveness keeps increasing with increase of blowing in the range of blowing ratio studied for the shaped holes. Comparison of the two film cooling hole designs shows suction side gains higher effectiveness with the shaped holes. The effectiveness on the pressure side was comparable for the two hole configurations. The upstream wake effect was also simulated by the stationary rods periodically placed upstream of the blade. Depending on the wake rods positions, the film cooling effectiveness was degraded in different degree. In another paper by Mhetras and Han [19], they studied the upstream film cooling accumulation effect on the downstream film cooling using superposition method. Four rows and two rows of compound angle cylindrical holes were arranged on the pressure surface and suction surface, respectively. Results showed the film cooling effectiveness on the suction was much higher than on the pressure side, although pressure side had more film cooling holes. Superposition from individual film cooling holes showed good agreement with experimental data.

1.2 Literature Review on Fluid Flow, Heat Transfer and Film Cooling on Platform

Several reviews have been published by Han et al. [1], Langston [20], Chyu [21], Simon and Piggush [22], which give an overview of the flow near the endwall and platform regions, as well as heat transfer and film cooling on these regions. The secondary flows near the platform increase the heat transfer between the mainstream gases and the uncooled platform. The secondary flows also make film cooling on the platform more difficult. Studies by Langston et al. [23, 24] revealed some features of these flows. When a boundary layer flow approaches a blade or vane, as shown in

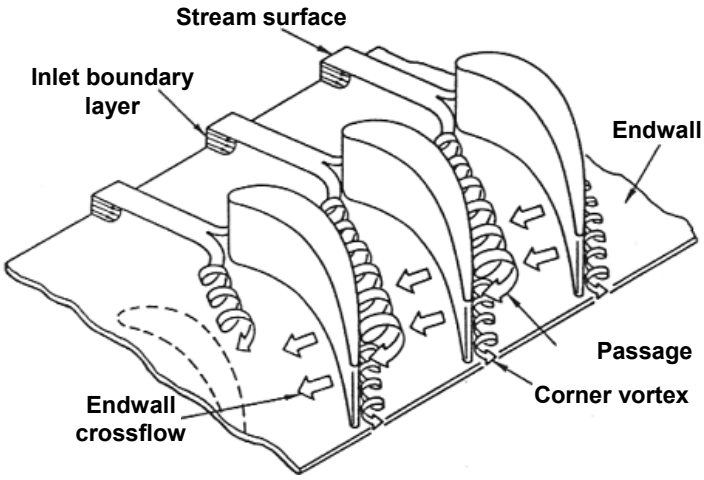

Fig. 1.2. Passage vortex in vane [24]

Fig. 1.2, vortex forms at the leading edge and continues along each side of the blade or vane forming a horseshoe vortex. The pressure distribution in each passage causes the suction side leg of the horseshoe vortex to follow the suction side of the blade near the endwall. The pressure side leg of the horseshoe vortex is carried across the passage and gains strength. This large vortex is often called the passage vortex and crosses the passage to meet the suction side leg of the horseshoe vortex on the adjacent blade. Goldstein and Spores [25] and Wang et al. [26] found several "corner" vortices that formed near the intersection of the blade surface and the endwall.

Film cooling is commonly used to protect the platform. Coolant may enter through discrete holes (similar to the midspan of the airfoil). Takeishi et al. [27] studied film cooling through discrete holes in three locations on a vane endwall. They found that the coolant was swept from the pressure side of the passage toward the suction side. Also, the film cooling effectiveness near the leading edge of the blade was very low due to the formation of the horseshoe vortex. Harasgama and Burton [28] placed film cooling holes evenly along an iso-Mach line near the leading edge of a passage. The pressure side of the passage received very little coolant. Similarly, Jabbari et al. [29] found that coolant from discrete holes in the downstream half of the passage did not produce uniform coverage, as the coolant moved away from the pressure side of the passage. Studies by Friedrichs et al. [30, 31] also showed that evenly spaced rows of coolant holes did not provide even coverage for the endwall. Using an ammonia and diazo technique, they measured the amount of coolant coverage at every point on the endwall. The horseshoe vortex prevented the coolant from covering the leading edge of the blade, while the passage vortex lifted the coolant in its path off of the surface. The coolant in the passage was swept from the pressure side toward the suction side by the

passage flow. Based on these results, Friedrichs et al. [32] repositioned the film cooling holes to attempt to cover the entire endwall with the same amount of coolant. Coverage in the majority of the passage was significantly improved, but the coverage near the leading edge and close to the suction surface was still poor, due to the horseshoe vortex and the suction side corner vortex. In a recent study, Barigozzi et al. [33] compared film cooling designs with cylindrical holes or fanshaped holes. With increasing blowing ratios, the passage vortex was weakened and cross flow in the passage was reduced.

Upstream of the inlet guide vane, a gap commonly exists between the combustion chamber and the vane endwall. A similar gap exists between the vane endwall and the rotor platform, ensuring the rotor can move freely. Coolant air is often injected through these gaps, or slots, in order to prevent hot mainstream gases from entering the engine cavity. This coolant air has a secondary effect of protecting the platform region, and if this air is used effectively, the need for discrete hole film cooling can be reduced. An early study by Blair [34] showed that the film cooling effectiveness for upstream slot injection varied greatly through the passage due to the secondary flows. Granser and Schulenberg [35] showed that coolant from an upstream slot could reduce the secondary flows in the passage by increasing the momentum of the boundary layer. Similarly, coolant slots used by Roy et al. [36] reduced the heat transfer near the leading edge. Burd et al. [37] and Oke et al. [38, 39] also studied film cooling through slots upstream of vanes. They found coolant from the slot could provide coverage for most of the passage. In order to provide adequate coverage for the entire endwall or platform, an upstream slot could be combined with discrete holes. Nicklas [40] measured the heat transfer coefficients and film cooling effectiveness with an upstream slot and three rows of discrete holes. Liu et al. [41] found that an increased blowing

ratio gave more uniform protection to the platform, for the densely spaced cooling holes they used to simulate upstream slot cooling. Zhang and Jaiswal [42] and Zhang and Moon [43] used pressure sensitive paint to measure the film cooling effectiveness for two rows of discrete holes upstream of the passage or for a single slot. They confirmed that effectiveness was significantly improved with increasing blowing ratio. Knost and Thole [44] found that areas that are typically difficult to cool, including the area near the leading edge, could be cooled effectively with upstream slot injection. Cardwell et al. [45] showed that effectiveness was reduced significantly if two adjacent vanes were not properly aligned. Wright et al. [46 – 48] considered a variety of stator-rotor seal configurations, discrete film hole combinations, and flow parameters. They concluded the film cooling effectiveness on the blade platform (within a linear cascade) was significantly affected by the upstream seal configuration. In addition, it is possible to minimize the purge flow, if the purge flow was thoughtfully combined with additional discrete film cooling.

Most of the studies have been performed on linear cascades or turbine vanes; few studies were done in rotating environment to examine the effect of upstream vane on rotor platform cooling. Suryanarayanan et al. [49, 50] studied the film cooling effectiveness by stator-rotor purge flow on the 1st stage rotor platform in a three-stage turbine facility. They also studied the discrete hole film cooling on the downstream of the platform and combined it with the stator-rotor purge flow cooling. They found that the film cooling effectiveness increased with increasing of purge coolant rate. Increasing the rotational speed, the film effectiveness from the stator-rotor purge flow also increased. However, for the downstream discrete film cooling, the best film protection

on the rotor platform took place at reference speed of 2550 rpm. For all rotational speed, local blowing ratio unity offered the best film coverage and effectiveness level.

Due to the inherent complexities in designing and instrumenting rotating systems, it would be useful if some of the upstream vane effect can be modeled in a cascade environment. Wright et al. [51] modeled the effect of the upstream passing vane on rotor platform film cooling in a low speed wind tunnel. Stationary cylindrical rods were used to simulate the upstream wake created by the trailing edge of the vanes. Delta wings were used to simulate the passage vortex created by the upstream vane. Fig 1.3 schematically shows vortex is created when the freestream passes over a delta wing. The platform was cooled by the purge flow from a simulated labyrinth-like seal. They found that wake rod didn't affect the platform film cooling effectiveness significantly, while the vortex created by the delta wings had a profound impact on the film cooling effectiveness.

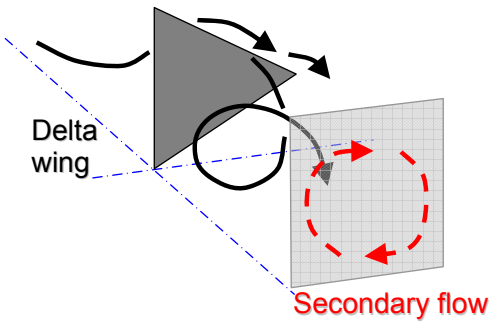

Fig. 1.3 Vortex created by delta wing [51]

1.3 Literature Review on Turbine Blade Leading Edge Heat Transfer and Film Cooling

The leading edge of the turbine blades is subject to the greatest heat load due to flow stagnation. Many researchers used cylinder or semicylinder to model the blade leading edge. The leading edge film cooling was investigated under different freestream conditions. Luckey et al. [52] simulated the airfoil leading edge using a cylinder with several rows of film cooling holes. They correlated their result for the optimum blowing ratio and injection angle. Karni and Goldstein [53] studied the effect of blowing ratio and injection location on the mass transfer coefficient. Mick and Mayle [54] studied the effect of coolant blowing ratio and film cooling hole location on the stagnation region. Mehendale and Han [55, 56] investigated the effect of Reynolds number and turbulence on heat transfer and film cooling effectiveness. Ou et al. [57] presented the effect of film hole location and inclined film slots on the leading edge film cooling heat transfer. Ekkad et al. [58] presented the effect of coolant density and free-stream turbulence. Using the same test facility, Gao et al. [59] assessed pressure sensitive paint (PSP) and transient infrared thermogrpahy technique. Funazaki et al. [60] studied the effect of unsteady wake on the leading edge film cooling effectiveness. Ou and Rivir [61] examined the effect of turbulence intensity, blowing ratio, and Reynolds number.

Some researches have been conducted in cascade environment. Nirmalan and Hylton [62] studied the effects of various parameters on film cooling in a turbine vane cascade under the conditions similar to the ranges of actual engines. Abuaf et al. [63] presented heat transfer coefficients and film effectiveness for a film cooled vane. Cruse et al. [64] studied the effect of leading-edge shapes. Ekkad et al. [65] studied the combined effect of unsteady wake and free stream turbulence on the film cooling

effectiveness and the heat transfer coefficient with air and CO_2 film injection. Cutbirth and Bogard [66] studied the effects of coolant density ratio on film cooling effectiveness on a simulated turbine vane. Mhetras et al. [67] studied the effect of upstream wake on the leading edge film cooling effectiveness in a 5-blade linear cascade. Some researchers studied leading edge film cooling under rotating environment. Dring et al. [68] investigated film cooling performance in a low speed rotating facility. Takeishi et al. [69] also reported the film cooling effectiveness distributions on a low speed stator-rotor stage using a rotating rig with a one-stage turbine model. Abhari and Epstein [70] investigated time-resolved measurements of heat transfer on a fully cooled transonic turbine stage. Using a short-duration blowdown turbine test facility, they simulated full engine parameters. Ahn et al. [71, 72] studied film cooling effectiveness on the leading edge with two-row and three-row hole injection under rotating condition in a three-stage turbine using PSP technique.

The film cooling holes in above studies were cylindrical holes and angle in the radial direction; recently, the shaped holes come into consideration for the leading edge film cooling. Mouzon et al. [73] compared the film performance between the laidback holes and cylindrical holes on a three row leading edge model. The holes were located at 0° and ±20°. They were inclined 45° to the surface and angle in radial (spanwise) direction. They found that the laidback holes resulted in much higher net heat flux reduction than the cylindrical holes. Falcoz et al [74] investigated cylindrical holes, conical holes and laidback (forward diffused) holes on a leading model. Four rows of film holes located at ±22.5° and ±7.5°. The holes were angle in the radial direction and inclined 45° to the surface. The hole to hole spacing was p/d=4. Their results indicated that the laidback holes showed a better lateral coverage. The best spanwise averaged

film cooling effectiveness was achieved by conical holes. Kim and Kim [75] studied cylindrical holes and laidback holes and tear-drop shaped (both laterally and forward expanded) holes. Three rows of radial angle hole were located at 0° and ±23° with a hole to hole spacing of p/d=7.5. The holes were inclined 30° to the surface. They showed that holes with a laidback type widened exits gave higher film cooling effectiveness than tear-drop shaped holes. Both laidback holes and tear-drop shaped holes were better than cylindrical holes. Reiss and Bölcs [76] studied effect of shaped hole with compound angle orientation. They compared cylindrical holes, laidback (forward diffused) holes and fanshaped (laterally diffused) holes. Five rows of leading edge film holes were located at 0°, ±20° and ±40°. The stagnation holes were angle in the radial direction while the rest holes were angle 60° to the mainstream direction. The holes were inclined 45° to the surface. They found that laidback holes gave the best overall film cooling performance. The fanshape holes performed better than cylindrical holes, but not as well as laidback holes. Lu et al. [77] also studied the effect of hole orientation and hole shape on leading edge film cooling. They examined compound angle cylindrical holes and compound angle laidback fanshaped holes. Three rows of film cooling holes were located at 0° and ±15° with a hole to hole spacing of p/d=4. These holes were inclined 30° to the surface. The compound angle holes were angled at 30° or 45° with respect to the local mainstream direction. They found that the shaped holes give much higher effectiveness than cylindrical holes. For the compound angle holes, the effectiveness was improved at lower blowing ratios, but reduced at higher blowing ratios due to jet liftoff.

1.4 Literature Review on Trailing Edge Slot Film Cooling

Trailing edge region is one of the regions on airfoils which are hard to cool because trailing edge must be thin to reduce aerodynamic losses. It is of great challenge to implement cooling design in a relatively small area of the airfoil. In addition to the internal cooling enhancement techniques, such as pin fins or blockage inserts, one of the cooling techniques frequently used by turbine blade designers is ejecting cooling air through spanwise slots located on the airfoil pressure side near the trailing edge. Several studies have been performed for aerodynamics and film cooling effectiveness by slot injection on the trailing edge. Uzol et al. [78] studied discharge coefficients from a cutback trailing edge with several cutback lengths, spanwise rib spacing, free stream Reynolds number and chordwise rib length. Aerodynamic loss characteristics using PIV flow measurement technique was studied by Uzol et al. [79] for different ejection rates and cutback lengths. An experimental and numerical investigation for trailing edge slot injection was performed by Holloway et al. [80, 81] under realistic engine flow conditions. Periodic vortex shedding from the pressure side lip was found to cause a relatively fast decay in film cooling effectiveness on the cutback portion of the trailing edge for larger lip thicknesses.

A comprehensive survey of film cooling investigations prior to 1971 was done by Goldstein [82] and included data for slots as well as discrete holes. Most of the slots cooling studies presented in [82] were two dimensional. Taslim et al. [83] reported a comprehensive parametric study of the effects of slot exit geometries on film cooling effectiveness. They found that lip-to-slot height ratio has strong impact on film cooling effectiveness. Martini et al. [84, 85] measured the film cooling effectiveness and heat transfer on the trailing edge cutback of gas turbine airfoils with different internal

cooling structures using IR camera. They showed the strong impact of internal design on the film cooling performance downstream of the ejection slot. They found fast decay in film cooling effectiveness was attributed to vortex shedding from the pressure side lip. Cunha et al. [86] studied the impact of trailing edge ejection on heat transfer using a closed form, analytical solution for temperature profiles for four different configurations. Impact of several geometrical design features on the trailing edge design and durability were investigated. Chen et al. [87] measured heat transfer and film cooling effectiveness on the slot floor with liquid crystal technique. They found the heat transfer coefficient on the slots increased due to mixing from internal cooling, however, the overall heat flux reduction was high with the slot cooling. Recently, Cakan and Talim [88] measured the mass/heat transfer coefficients on the trailing edge slot floor, slot sidewalls and lands using naphthalene sublimation method. They found that averaged mass transfer on the land sidewalls are higher than that on the slot floor surface.

1.5 Objective of the Present Study

As reviewed, the film cooling effectiveness is influenced by many factors, such as the blowing ratio, density ratios, incoming freestream flow properties (upstream wake, passage vortex, turbulence, etc), film hole or slot configurations (angle and shapes), film cooled surface conditions (curvature, roughness), and so on. Depending on the regions on the blade, these factors may not play an equally important role on local film cooling effectiveness distribution. The purpose of this study is to investigate gas turbine blade leading edge, trailing edge, and blade surface and platform regions film cooling under the impact of some of above factors. Three temperatures (coolant

temperature, free stream temperature and adiabatic surface temperature) involves in film cooling, so it is hard to get conduction-free effectiveness data in the conventional heat transfer experiments. Particularly with heavily distributed film cooling holes, correction of conduction is of great pain. In this study, pressure sensitive paint (PSP) is used to measurement the film cooling effectiveness distribution. PSP technique is based on heat/mass analogy. The conduction error associated with heat transfer experiment is eliminated.

For film cooling on the blade pressure side and suction side, most of experimental study of the film cooling was focused on the mid-span region only, the endwall effect and tip leakage effect were not captured. The objective of this study is to capture the film cooling effectiveness distribution on blade pressure side or suction side of fully film cooled blades. The effects of film hole configuration and upstream wake on the film cooling effectiveness are examined. Two kinds of hole configurations are considered: axial fan shaped laidback hole and compound angle fan shaped laidback holes. The upstream wake effect are simulated by periodically placed stationary metal rods. Test is done in a five-blade cascade at a relatively high Mach number and high pressure condition.

For the platform film cooling study, the objective is to examine the upstream vane passage vortex effect on the downstream blade platform film-cooling effectiveness. The coolant is purged through a new labyrinth-like slot, which is a typical stator-rotor seal used in the gas turbine engines. The effect of the upstream vane passage vortex is modeled by delta wings. Since the vane passage vortex varies depending on the vane configurations, it is hard to know the exact size and strength of passage vortex generated by upstream vanes. By varying the size of the delta wings and the flow attack

angles, a range of vortices' size and strength are simulated. Two sets of delta wings are selected in the test The delta wings are placed upstream of labyrinth-like seal at an attack angle of 30° and 45°, respectively. Test is done in a in the same high flow as blade surface film cooling study.

There is a lot of constraint for leading edge film cooling. The limited space, small wall thickness and high curvature are the obstacles of leading edge film cooling study. The research on shaped holes and varying hole angle is limited, especially for heavily film cooled designs. It is a challenge to achieving accurate effectiveness data in heat transfer experiment. In this study, by using Pressure Sensitive Paint (PSP) technique, accurate film cooling effectiveness are obtained for heavily film cooled leading edge models. Two leading edge film cooling designs are investigated: a heavily film cooled design with seven rows of film holes and moderately film cooled design with three rows. Four different film hole configurations are applied to the two designs: radial angle cylindrical holes, compound angle cylindrical holes, radial angle shaped holes and compound angle shaped holes.

The slot film cooling on the trailing edge is a complicated three dimensional problems. Effectiveness data were only available for the slot floor surface in the open literature. The lands play an important role to maintain the blade structure. However, similar to the squealer tip, the land is very narrow. Reliable adiabatic effectiveness data for the land is hard to obtain with heat transfer measurement due to conduction. In this study, Pressure sensitive paint (PSP) measurement technique is used to measure the film cooling effectiveness on the slots, lands and slot sidewalls. In the past studies, the trailing edge with pressure side cutback was simulated as an inclined plate. The mainstream flow was basically two dimensional. In the current study, the test is done on

a modeled airfoil placed in the middle of wind tunnel. The mainstream flow is closer to that in a cascade environment. The effect of slot lip thickness and incoming mainstream boundary layer thickness on the slot film cooling is investigated. Tests are done with several different blowing ratios.

2. PRESSURE SENSITIVE PAINT MEASUREMENT THEORY AND DATA ANALYSIS

Data for film cooling effectiveness were obtained using the Pressure Sensitive Paint (PSP) technique. Figure 2.1 schematically shows the PSP setup for film cooling effectiveness measurement. PSP is a photo-luminescent material that emits light when excited, with the emitted light intensity inversely proportional to the partial pressure of oxygen. This light intensity is recorded using a CCD camera. The image intensity obtained from PSP by the camera during data acquisition is normalized with a reference image intensity (I_{ref}) taken under no-flow condition. Background noise in the optical setup is removed by subtracting the image intensities with the image intensity obtained under no-flow conditions and without light excitation (I_{blk}). The resulting intensity ratio can be converted to pressure ratio using a pre-determined calibration curve and can be expressed as:

$$\frac{I_{ref} - I_{blk}}{I - I_{blk}} = f\left(\frac{\left(P_{O_2}\right)_{air}}{\left(P_{O_2}\right)_{ref}}\right) = f\left(P_{ratio}\right) \tag{2.1}$$

where I denotes the intensity obtained for each pixel and $f(P_{ratio})$ is the relationship between intensity ratio and pressure ratio obtained after calibration.

Calibration of PSP system was performed using a vacuum chamber at several known pressures varying from 0 to 1.8atm. The same optical setup that was used during experiments was chosen for calibration. The calibration curve is shown in Fig. 2.2. PSP is also sensitive to temperature with higher temperatures resulting in lower light emission. Hence, the paint was also calibrated at different temperatures. It was observed that if the emitted light intensity at a certain temperature was normalized with the

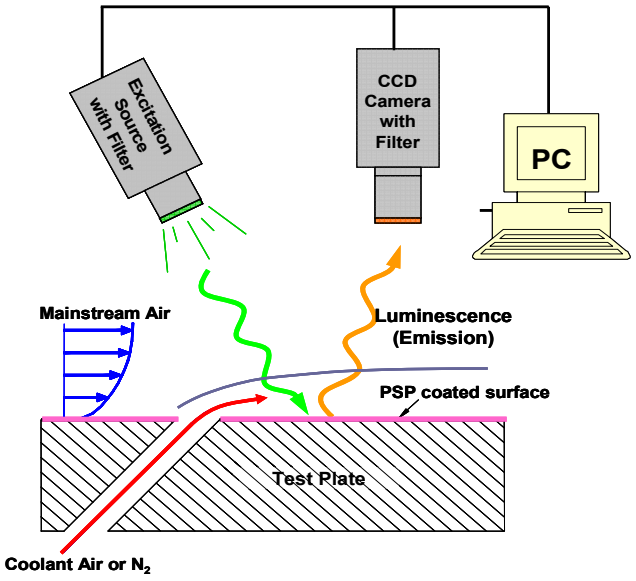

Fig. 2.1 PSP setup for film cooling effectiveness measurement

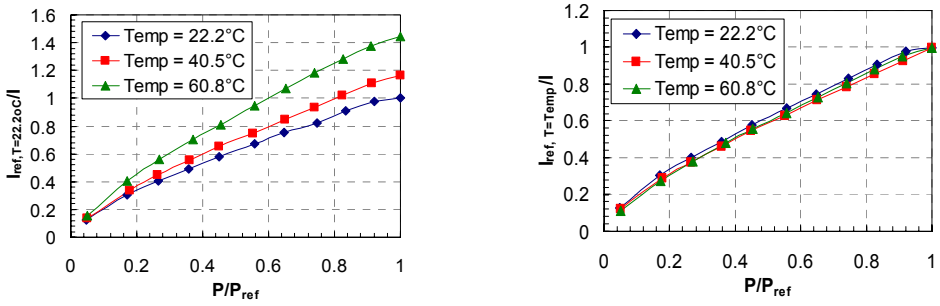

(a) **(b)**

Fig. 2.2 (a) PSP calibration at single reference temperature
(b) PSP calibration at corresponding reference temperature

reference image intensity taken at the same temperature, the temperature sensitivity can be minimized as shown in Fig. 2.2(b). Hence, during experiments, the reference (I_{ref}) and black (I_{blk}) images were acquired immediately after stopping the mainstream flow so that the test surface temperature does not change appreciably.

To obtain film cooling effectiveness, air and nitrogen were used alternately as coolant. Nitrogen which has nearly the same molecular weight as that of air displaces the oxygen molecules on the surface causing a change in the emitted light intensity from PSP. By noting the difference in partial pressure between the air and nitrogen injection cases, the film cooling effectiveness can be determined using the following equation.

$$\eta = \frac{C_{mix} - C_{air}}{C_{N_2} - C_{air}} = \frac{C_{air} - C_{mix}}{C_{air}} = \frac{\left(P_{O_2}\right)_{air} - \left(P_{O_2}\right)_{mix}}{\left(P_{O_2}\right)_{air}} \tag{2.2}$$

where C_{air}, C_{mix} and C_{N2} are the oxygen concentrations of mainstream air, air/nitrogen mixture and nitrogen on the test surface respectively. The definition of film effectiveness in Eq. (2.2) based on mass transfer analogy assumes similar form as that of adiabatic film cooling effectiveness given in Eq. (2.3).

$$\eta = \frac{T_{mix} - T_m}{T_c - T_m} \tag{2.3}$$

The accuracy of the PSP technique for measuring film-cooling effectiveness has been compared by Wright et al [89] on a flat plate with compound angled film holes using steady-state Infra-Red (IR) technique and steady-state Temperature Sensitive Paint (TSP) technique. Results were obtained for a range of blowing ratios and showed reasonable agreement with each other. All three measurement techniques agreed within 15% of each other. Larger uncertainties for heat transfer techniques such as IR and TSP

methods were due to lateral heat conduction in the flat plate as corrections for heat conduction were not included in the presented results.

The film cooled platform was coated with PSP using an air brush. It was excited by a strobe light fitted with a narrow band-pass interference filter (optical wavelength = 520nm). Upon excitation, the PSP coated surface emitted light with a wavelength higher than 600nm. A 12-bit scientific grade CCD camera (Cooke Sensicam QE with CCD temperature maintained at -15^{o}C using 2-stage peltier cooler), fitted with a 35mm lens and a 600nm long-pass filter, recorded images. The filter mounted on the camera was chosen such that it did not allow any reflected light from the illumination source to pass through. The camera and the strobe light were triggered simultaneously using a TTL signal from a function generator. A total of 200 TIF images were captured and ensemble-averaged to get the individual intensities. A computer program was used to convert these pixel intensities into pressure using the calibration curve and then into film cooling effectiveness.

Uncertainty calculations were performed based on a confidence level of 95% and are based on the uncertainty analysis method of Coleman and Steele [90]. Lower effectiveness magnitudes have higher uncertainties. For an effectiveness magnitude of 0.3, uncertainty was around ±1% while for effectiveness magnitude of 0.05, uncertainty was as high as ±8%. This uncertainty is the result of uncertainties in calibration (4%), image capture (1%), and blowing ratio (4%).

3. EFFECT OF UPSTREAM WAKE ON FILM-COOLING EFFECTIVENESS DISTRIBUTION ON GAS TURBINE BLADES WITH SHAPED HOLES

3.1 Experimental Facilities

The measurements were conducted in a 5-blade linear cascade facility as shown in Fig. 3.1. Some of important dimensions of the cascade are listed in Table 3.1. The inlet cross section of the test section was 19.6cm (width) x 12.7cm (height) while the exit cross section was 12.9cm (width) x 12.7cm (height). The top plate which acted as the shroud for the blades and the outer side walls of the test section were machined out of 1.27cm thick acrylic sheets for optical access. The three middle blades in the cascade had a span of 12.64cm and an axial chord length of 8.13cm. The tip gap clearance was about 0.5% of the blade span. A honeycomb mesh, 7.62cm long with a cell size of 1.27cm, was put 1.78m upstream to the blade leading edge to obtain uniform velocity distribution. Flow conditions in adjacent passages of the center blade were ensured to be identical by adjusting the trailing edge tailboards for the cascade. The mainstream air was supplied by a centrifugal compressor that could deliver a volume flow rate up to 6.2m^3/s. The cascade inlet and exit velocities were set to be 96m/s and 156m/s corresponding to inlet and exit Mach numbers of 0.27 and 0.44, respectively. The Reynolds number based on the axial chord length and exit velocity was 750,000 and the overall pressure ratio (P_t/P) was 1.14 (where P_t is inlet total pressure and P is exit static pressure). Turbulence intensity and boundary layer thickness was recorded 6.3cm upstream of the middle blade using. The boundary layer thickness was about 1.5cm. Along the span, the turbulence intensity (Tu) varied from 6% at the centre to about 11% close to the walls. The mainstream flow conditions are listed in Table 3.2.

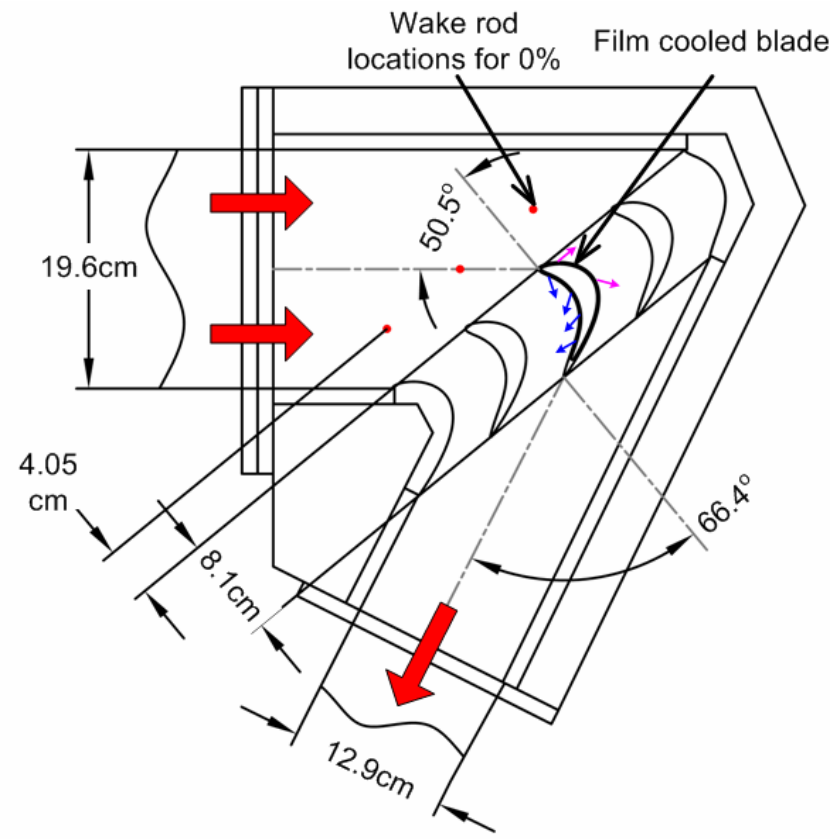

Fig. 3.1 Schematic of the cascade with film cooled blade

Table 3.1 Cascade and Blade Parameters

Blade span (cm)	12.64	Inlet area (cm^2)	249
Tip clearance (cm)	0.064	Exit area (cm^2)	164
Axial chord length (cm)	8.13	Inlet angle (°)	50.5
Pitch (cm)	7.69	Exit angle (°)	66.4

Table 3.2 Mainstream Flow Conditions

Inlet Mach No.	0.27	Pressure ratio (Pt/P)	1.14
Exit Mach No.	0.44	Turbulence intensity	6%
Reynolds No.	750,000	Boundary layer thickness (cm)	1.5

As indicated in Fig. 1.1, four different discrete holes configuration are generally used in blade film cooling. In this study, the blades were cooled with laidback fanshaped holes. Two film cooling designs were presented and the effect of hole angle with respect to mainstream direction was investigated in current study. The holes were oriented in axial direction in one design (Blade 1); and angled 45° to the axial direction in the other design (Blade 2). Two film cooled test blades were made using Stereolithography (SLA). They had a squealer tip with a recess of 2.4% (2.84mm) of blade span while the two adjacent blades had a flat tip. The tip gap clearance for the test blade and the two adjacent guide blades was 1% of the blade span. The leading edge of the blade could be approximated as an arc with a radius of 2.4mm. Figure 3.2 and Fig. 3.3 show the film cooling hole configurations on the test blades with the internal coolant passage geometry. Some of important parameters of the film cooling hole configurations are listed in Table 3.3. The film cooling holes locations on the blade surface were the same for the two blades. All these laidback fanshaped holes were inclined 45° to the blade surface. The laidback fanshape holes were featured with a lateral diffusion angle (γ) of 10° from the hole centerline and a forward expansion angle (δ) of 10° to the blade surface. Four rows of shaped holes were arranged on the pressure side at axial locations of 1.24cm (PS1, 23 holesl), 3.62cm (PS2, 22 holes), 5.01cm (PS3, 23 holes) and 6.1cm (PS4, 22 holes). Two rows were provided on the suction side at axial locations of 0.38cm (SS1, 23 holes) and 3.56cm (SS2, 22 holes). The rows of holes were staggered; therefore, PS2, PS4 and SS2 had one hole less than PS1, PS3 and SS1. The spanwise spacing was kept constant, i.e., s/d ratio was maintained at 8.2. All these holes had a diameter 0.65mm of the metering part (before expansion). For the axial shaped holes (Blade 1), the total length of the hole was 6.8 times of hole diameter of metering part.

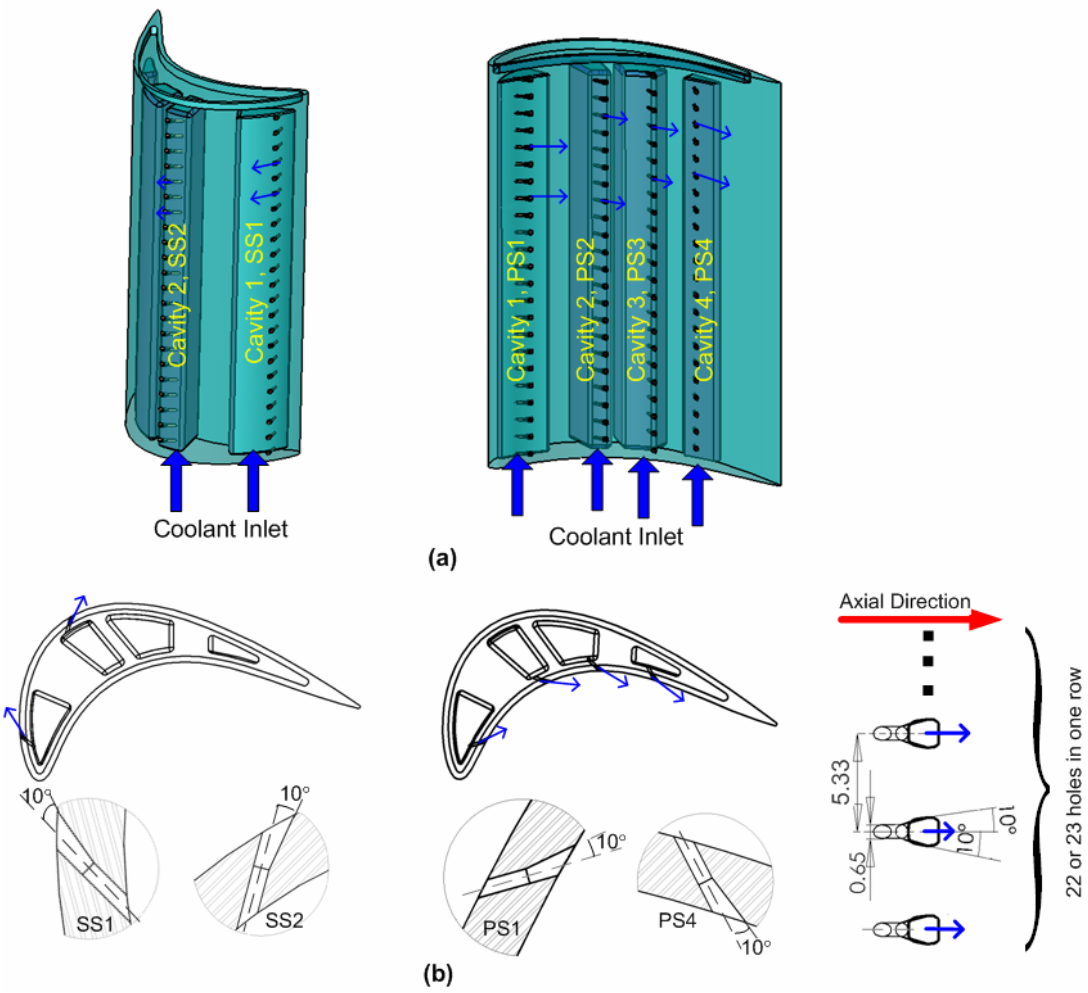

Fig. 3.2 Film cooled blade with axial shaped holes (Blade 1)
(a) film cooling holes and cavities (b) film cooling hole configuration

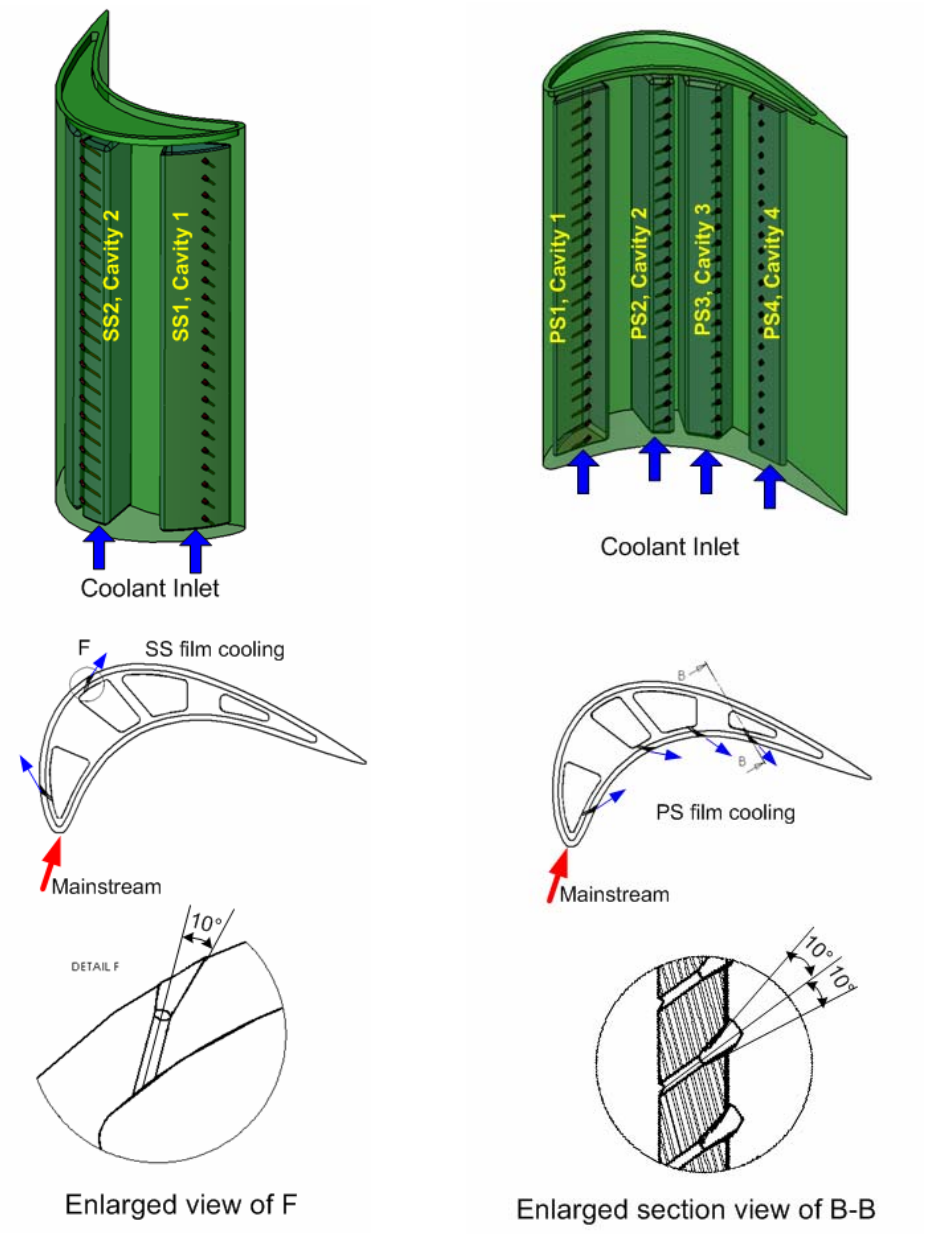

Fig. 3.3 Film cooled blade with compound angle shaped holes (Blade 2)

Table 3.3 Film Cooling Hole Configurations

	Axial shaped hole (Blade 1)	**Compound angle shaped hole (blade 2)**
Angle to blade surface (°)	45	45
Axial angle (°)	0	45
Radial angle (°)	90	45
No. of hole rows	PS: 4; SS: 2	PS: 4; SS: 2
No. of holes in each row	22 or 23	22 or 23
Hole diameter (d, mm)	0.65	0.65
Lateral diffusion angle (°)	10	10
Forward diffusion angle(°)	10	10
Hole to hole spacing (s/d)	8.2	8.2
Hole length (L)	6.8d	9d
Hole Expansion length	2.9d	4.25d
Exit to inlet area ratio	3.7	4.5

The expansion starting at 3.9 times of hole diameter, resulted in a area ratio of 3.7 between exit cross section to inlet cross section. For the compound angle shaped holes (Blade 2), the total length of the hole was 9 times of hole diameter of metering part. The expansion started at 4.75 times of hole diameter, which resulted in a area ratio of 4.5 between exit cross section to the inlet cross section of a hole.

Coolant was supplied to the film holes via 4 cavities numbered from 1 to 4. The cavity cross sections were modeled similar to the internal cooling passages in turbine blades with coolant injection through the bottom of the blade. The coolant was heated to same temperature as mainstream before fed into the coolant cavity. The coolant flow rate in each cavity was monitored by a dedicated rotameter. The PS1 holes and SS1 holes shared the first cavity; likewise, the PS2 holes and SS2 holes shared the secondary cavity. The remaining two cavities supplied coolant to the rows PS3 and PS4, respectively. During the test, coolant was only allowed to eject to either pressure side or suction side, so film cooling holes on the other side were sealed.

The effects of wake generated by upstream vane were simulated by stationary rods. The rods were inserted periodically upstream of the cascade inlet to simulate stationary upstream wakes. A rod diameter of 4.8mm was selected to simulate typical airfoil trailing edge. They were placed upstream of the blades at a distance equal to 50% of axial chord. The rods were placed at four equally spaced positions corresponding to the blade pitch. The four positions divided the passage into quarters. The rod locations are shown in Fig. 3.4. The rod directly upstream of the leading edge was indicated as the 0% phase location and was 6.3cm upstream of the leading edge in the flow direction. Rod locations for 25%, 50% and 75% were progressively located along the blade pitch. The periodically placed upstream rods may be thought as a progressing wake in a

rotating turbine. Four sets of experiments were conducted to cover all phase locations. Two rods were placed with one in the pressure side passage of the test blade and the other at the corresponding periodic location in the suction side passage for 25%, 50% and 75% phase locations while a single rod was placed in front of the stagnation line of the test blade for phase location 0%.

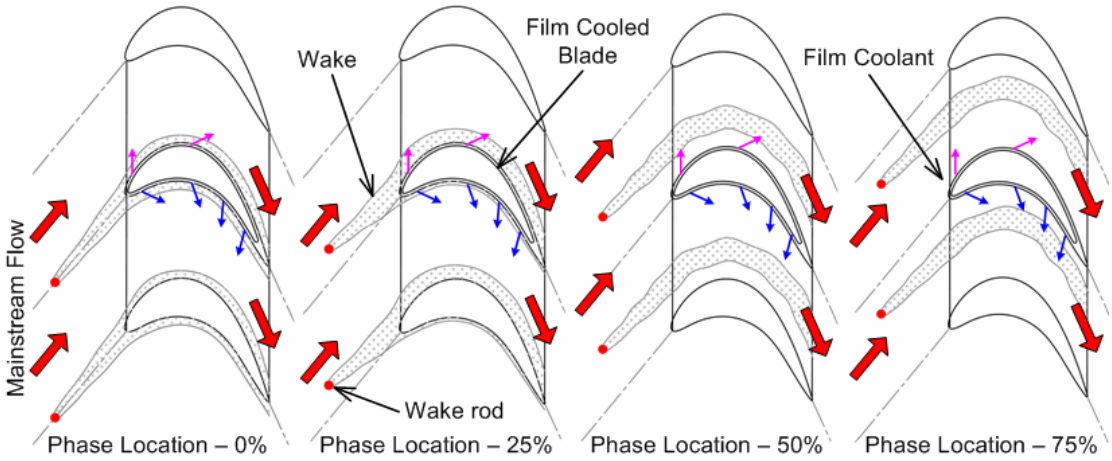

Fig. 3.4 Wake rod phase position and conceptual view of wake effect on test blade

3.2 Mach Number and Local Blowing Ratio Distribution on the Blade Surface

Figure 3.5 shows the Mach number distributions at three span locations - 50%, 75% and 94% without the presence of wake rods and film cooling holes. The Mach numbers were calculated from the pressure ratio, which was obtained by normalizing the blade inlet total pressure with the static pressure over the blade surface. The static pressure at the respective locations was measured using pressure taps instrumented on a separate blade without film cooling. The inlet total pressure was measured using a pitot tube placed 6.3cm upstream of the center blade. The pressures were recorded with a 48-channel Scanivalve System coupled with LabView software. LabView discarded all data that fell outside the initial mean ±1.5 standard deviation. It then recorded the mean value of the screened data. Every pressure measurement was repeated at least three times to reduce data uncertainty and verify data repeatability. The pressure side Mach number distributions for all three span locations are more or less similar. There is a gradual decrease in Mach number till $x/C_x \sim 0.6$ after which there is a sharp rise. On the suction side, the Mach number distribution shows a steady increase till $x/C_x \sim 0.65$, beyond which it starts falling. The point of inflection on the suction side corresponds to the throat region where the mainstream reaches its maximum velocity. The interaction of the mainstream and tip leakage vortex can be clearly observed from this plot, with an appreciable reduction of Mach number for the 94% span case in the first half of the blade axial chord.

Figure 3.6 shows the Mach number distribution under the influence of stationary wakes at four phase locations. Data is shown for the same three blade span locations. It is interesting to find that the midspan region is most affected by the upstream

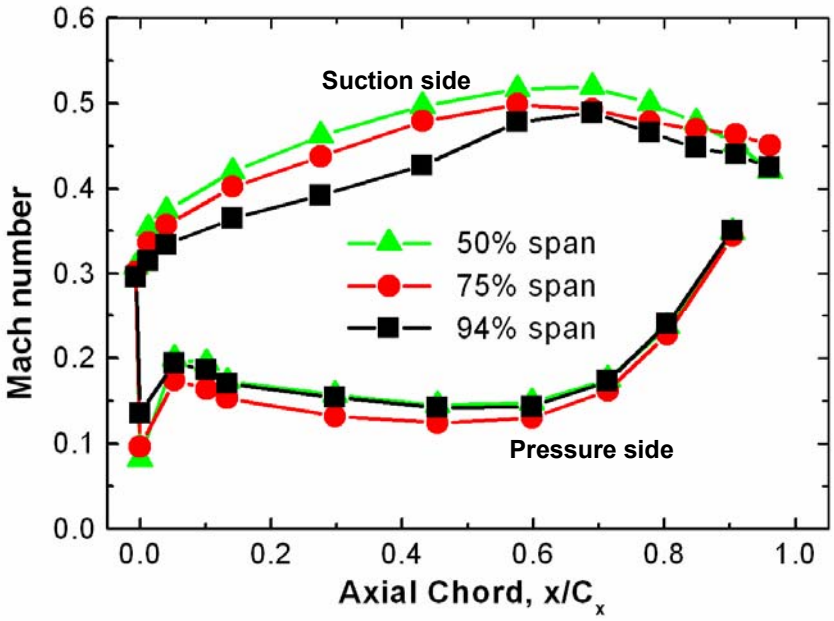

Fig. 3.5 Mach number distributions without upstream wake

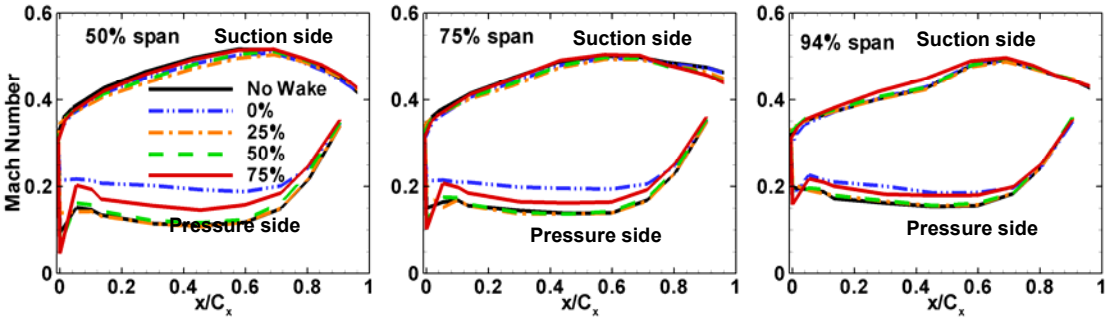

Fig. 3.6 Mach number distributions under the influence of upstream wake rods

rods followed by 75% and 94% span locations. This is indicative of the fact that the strong endwall vortices and tip leakage vortices override any small disturbance created by the wake rods. In the midspan region, where the influence of endwall vortices is negligible, the effect of wake rods become apparent. It has to be noted that the pressure measurements were carried out on a blade without cooling holes. With the presence of film cooling, the boundary layer attached to the blade surface is disturbed. This is particularly true at higher blowing ratios. In general, on the pressure side, the wake rods at phase 0% show the highest influence on the Mach number distribution followed by phase 75%. The other two wake rod phases show little or no effect. On the suction side, rod phase 25% followed by rod phase 0% shows the highest influence in the midspan region. This agrees well with the conceptual wake paths depicted in Fig. 3.4. On the suction side near tip region (75% and 94% blade span), the wake rod effect on Mach number is not substantial as the tip leakage flow is predominant.

Experiments were performed with five different average blowing ratios (M) of 0.4, 0.6, 0.9, 1.2 and 1.5. As mentioned earlier, the coolant was injected from only one side of the blade. The holes on the other side, which was not being tested, were sealed. The average blowing ratio was defined as $M = \rho_c V_c / \rho_m V_m$, where V_m is mainstream velocity at 50% of the blade span in the hole row location. In the current study, the density of coolant and mainstream is the same; the blowing ratio is reduced to a velocity ratio. By knowing the local mainstream velocity, total coolant mass flow rate required by a cavity was pre-determined for each average blowing ratio and was set using a dedicated rotameter connected to the coolant loop for each cavity. The coolant velocity V_c was calculated based on the round cross section area of the cylindrical part of a film cooling hole. The actual or local blowing ratio $M_{local} = \rho_{c,local} V_{c,local} / \rho_{m,local} V_{m,local}$ for the

holes in a hole row can vary due to the pressure variation in the coolant cavity and on the outer surface of the blade along its span. To check the coolant distribution, the local blowing ratio was examined. The discharge coefficients C_D was calculated and the mass flow rate from each hole was determined. The local blowing ratio distribution on the suction side or pressure side was quite uniform. The coolant mass flow rate for the holes in a cavity was found relatively evenly distributed.

3.3 Film-Cooling Effectiveness on the Blade Surface

The film cooling effectiveness distributions on the blade surface were measured at five blowing ratios and four wake rod positions using pressure sensitive paint. During the film cooling effectiveness test, the coolant was only allowed to eject from one side of the blade surface (either pressure side (PS) or suction side (SS)). All the holes on the side of interest were open while the holes on the other side were sealed. As shown in Fig. 3.7, camera was placed at two locations to capture the film cooling effectiveness distribution on the whole pressure surface, three locations to capture it on the suction surface. The effectiveness data obtained at each individual camera position was projected onto a radial plane passing through the axial chord of the blade and combined to form a complete picture for pressure side or suction side. In the contour plots, the abscissa and the ordinate were normalized with the axial chord length and the blade height, respectively.

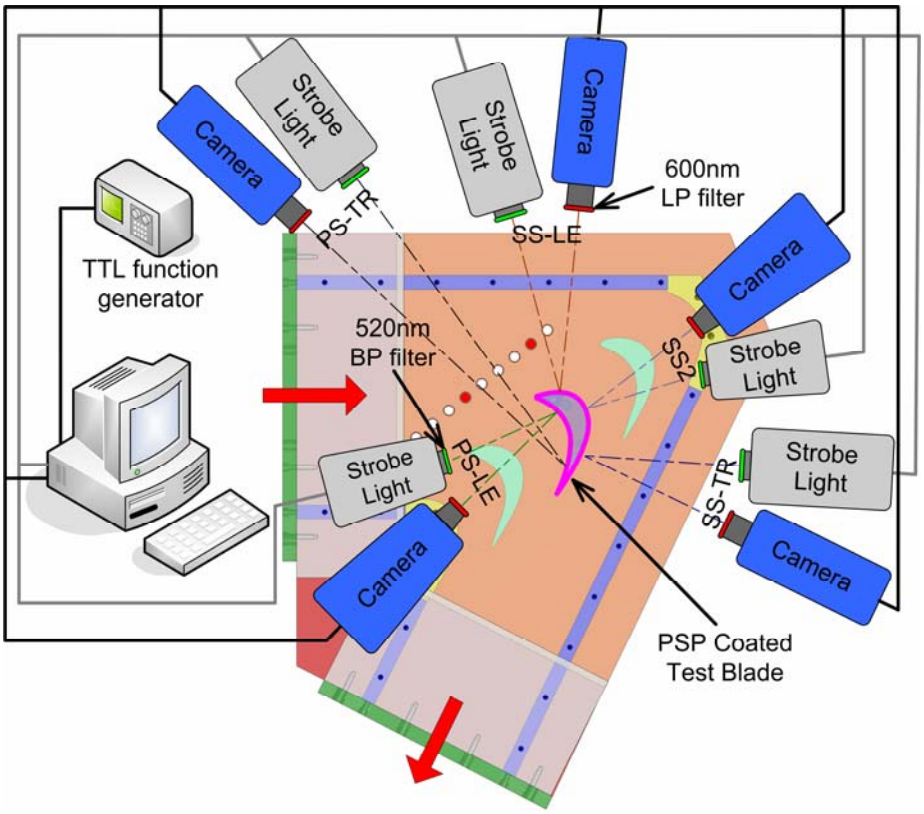

Fig. 3.7 Optical setup for PSP film cooling measurement on blade surface

3.3.1 Effectiveness on Film Cooled Blade with Axial Shaped Holes

To examine of effect of upstream wake, film cooling effectiveness distribution on the blade surface without presence of upstream wake was taken as the baseline case. Figure 3.8 shows the film cooling effectiveness distribution on the pressure side or suction side of Blade 1 (with axial shaped holes) of baseline case. Although these film cooling holes were oriented in axial direction, the coolant jets are re-directed by the mainstream. The tip leakage flow drives the coolant upward towards the tip on the pressure side near the tip region, while the pressure side horse vortex and corner vortex drag the coolant to the hub on the pressure side near the hub region. Starting at $x/C_x \sim 0.3$ on the suction side, the coolant is swept towards the midspan by the spiraling motion of the passage vortex near the hub and the tip leakage vortex near the tip. It is well known that the passage vortex drifts from the pressure-side leading edge towards the suction-side trailing edge of the adjacent blade and climbs on to the suction surface with an upwash motion. The tip leakage vortex, however, creates a downwash motion on the suction surface. These vortices acting on the suction surface result in a well defined converged coolant trace toward the midspan and attribute to the two unprotected triangular zones near the tip and hub. The effects of secondary vortices on effectiveness distribution were also observed in by Mhetras et al. [17] and Narzary et al. [18]. Compared with pressure side film cooling, the coolant trace on the suction side is longer and effectiveness level is higher. The suction side convex surface produces favorable pressure gradient and flow acceleration, making it easier for coolant to stay close to the suction surface. On the contrary, coolant jets tend to separate from the concave

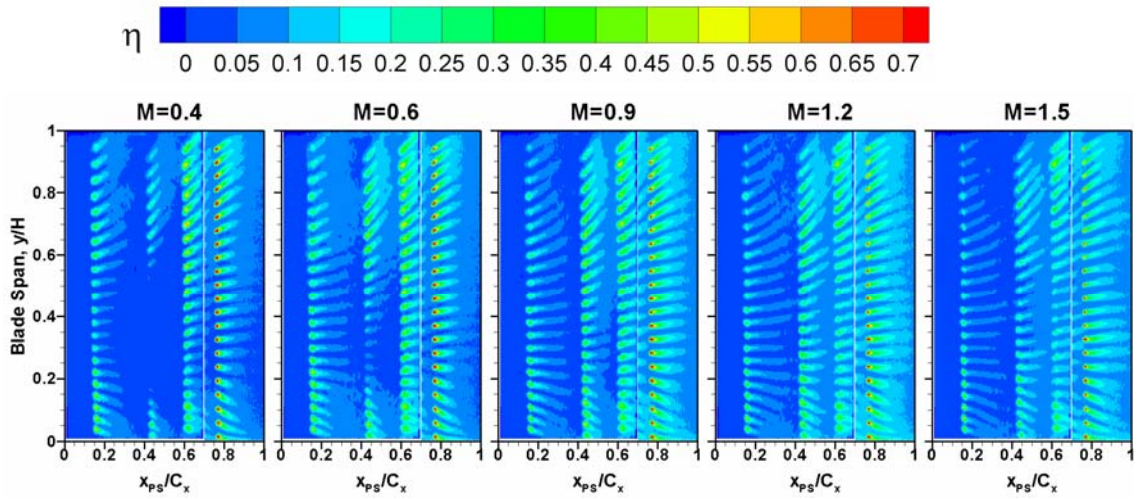

(a) Pressure Side

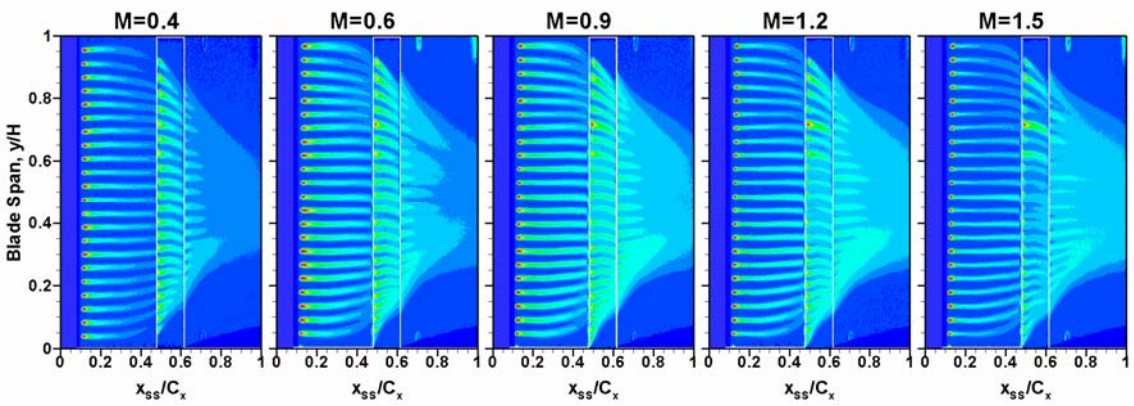

(b) Suction Side

Fig. 3.8 Film cooling effectiveness distribution for varying blowing ratios without wake on Blade 1 (with axial shaped holes)

pressure surface. Therefore, in general, the film coverage on the suction surface is better than that on the pressure surface. However, the film cooling effectiveness distribution on the pressure side is fairly uniform with the multiple rows of film cooling hole design, particularly at higher blowing ratios.

As shown in Fig. 3.8, the film cooling effectiveness from PS1 row is the lower than the other PS rows (except PS2 at low M) and the coolant from PS1 row barely reaches PS2 row. Due to the big curvature coupled with the flow deacceleration, the coolant jets from PS1 row tend to lift off from the surface, resulting in poor film coverage. The highest effectiveness from PS1 row is achieved at M=0.6. As the jet momentum increases with blowing ratio, the coolant penetrates the freestream and mix with the freestream, therefore very limited coolant protection remains on the surface. For the downstream PS rows (PS2, PS3 and PS4), the film cooling effectiveness increases when the blowing ratio increases from M=0.4 to M=1.2. The film cooling effectiveness magnitude are comparable for M=0.9 and M=1.2. Further increasing the blowing ratio to M=1.5, the effectiveness magnitude from the PS rows drops due to jet liftoff. The coolant no longer stays attached to the surface. In general, the effectiveness in the downstream is better than that in the upstream at moderate and high blowing ratios (M=0.9. 1.2 and 1.5) because more coolant from upstream is carried over to downstream. In addition, the flow acceleration and reduced curvature in the downstream region are also favorable to the elevated effectiveness. At low blowing ratio M=0.4, the pressure inside the cavity may not be high enough to drive the coolant to eject through the holes, therefore, the coolant jets are not observed from some of the PS2 holes.

Immediately downstream of SS1 row, the highest effectiveness occurs at M=0.6. The effectiveness near the holes drops when the blowing ratio is greater than M=0.6.

The higher jet momentum causes the jet penetration and the mixing with the freestream is enhanced. This leads to a thinner coolant trace and lower magnitude in effectiveness. The coolant from SS1 row extends beyond SS2 row. This leads to an elevated effectiveness downstream of SS2 row. The highest effectiveness immediately downstream of SS2 row is achieved at M=0.9. Because of the convex curvature on the suction side, the dispersed coolant re-attached to the surface. This leads to widened coolant traces in the downstream of both SS1 row and SS2 row. When the blowing ratio increases, more coolant will be convected downstream and covers a wider area on the surface.

The spanwise averaged effectiveness versus normalized axial chord length for the no wake case on Blade 1 is presented in Fig. 3.9. The sharp peaks in the plot correspond to the row locations. On the whole, film cooling effectiveness on the pressure side decays faster than that on the suction side because jet lift-off from the concave surface. In general, blowing ratio M=0.6 gives the highest film cooling effectiveness for the first rows (PS1 or SS1); while M=0.9 offers highest effectiveness for the other rows immediately downstream of film cooling holes. Due to the jet lift off, the effectiveness in these near hole regions are lower for higher blowing ratios. However, further downstream of film cooling holes, higher blowing ratios provide higher effectiveness because more coolant is convected back to the surface.

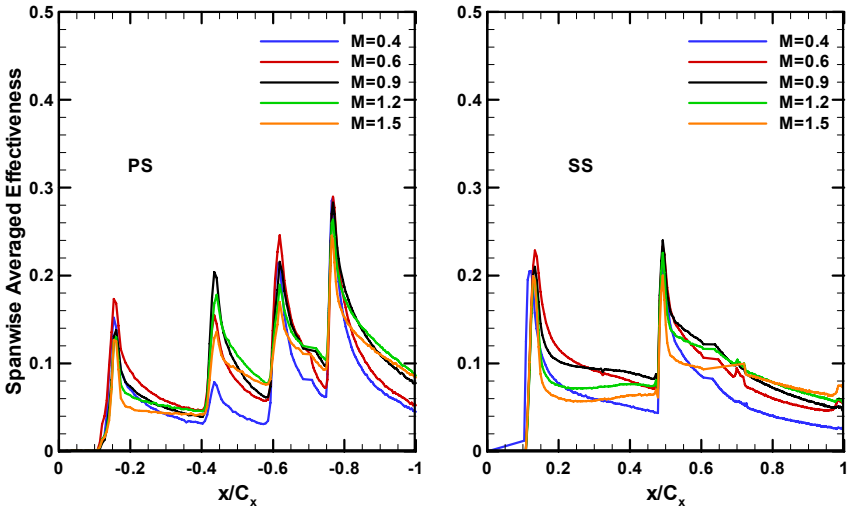

Fig. 3.9 Spanwise averaged effectiveness for the case of no wake on Blade 1 (with axial shaped holes)

To understand the nature of influence exerted by the wake rods at each phase location, the effectiveness distribution for M=0.9 at four wake rod phases are presented in Fig. 3.10. Compared with the case of no wake, the wake produced by the rods reduces the film cooling effectiveness. The mixing between the coolant and mainstream is enhanced by the wakes. The wake rod positions at 0% and 25% exhibits the more adverse effect on film-cooling effectiveness. A conceptual view of the wake paths shown in Fig. 3.4 for 0% and 25% attests to this fact. Vortex shedding from the wake rods brings additional turbulence in the mainstream resulting in more mixing of the mainstream with the coolant, thereby, the coolant trace is shortened. The wake rods at phase 0% show more degradation of coolant trace on the pressure side. The downstream propagation of the wake is evident from the short coolant traces near the PS4 row. On the suction side, it appears that the 25% wake rod location has a relatively higher impact. The wake propagation along the suction surface can be gauged by the coolant trace degradation near the trailing edge. An interesting observation can be made by looking at the suction side effectiveness contours. It appears that the secondary vortices shield the coolant from SS2 row holes to some extent from the incoming mainstream, as a result, the coolant traces close to the tip and hub regions propagate downstream in comparison to those near the midspan region.

Figure 3.11 shows the effectiveness distribution on Blade 1 at rod phase location 0% for varying blowing ratios. It can be seen that the effectiveness on pressure side dramatically decreases at this rod location for all the blowing ratios. The enhanced mainstream turbulence produced by the wakes rapidly mixes the coolant with mainstream when the coolant ejects from the holes. The pressure surface is barely protected by the film cooling at this rod phase location. The effectiveness on the suction

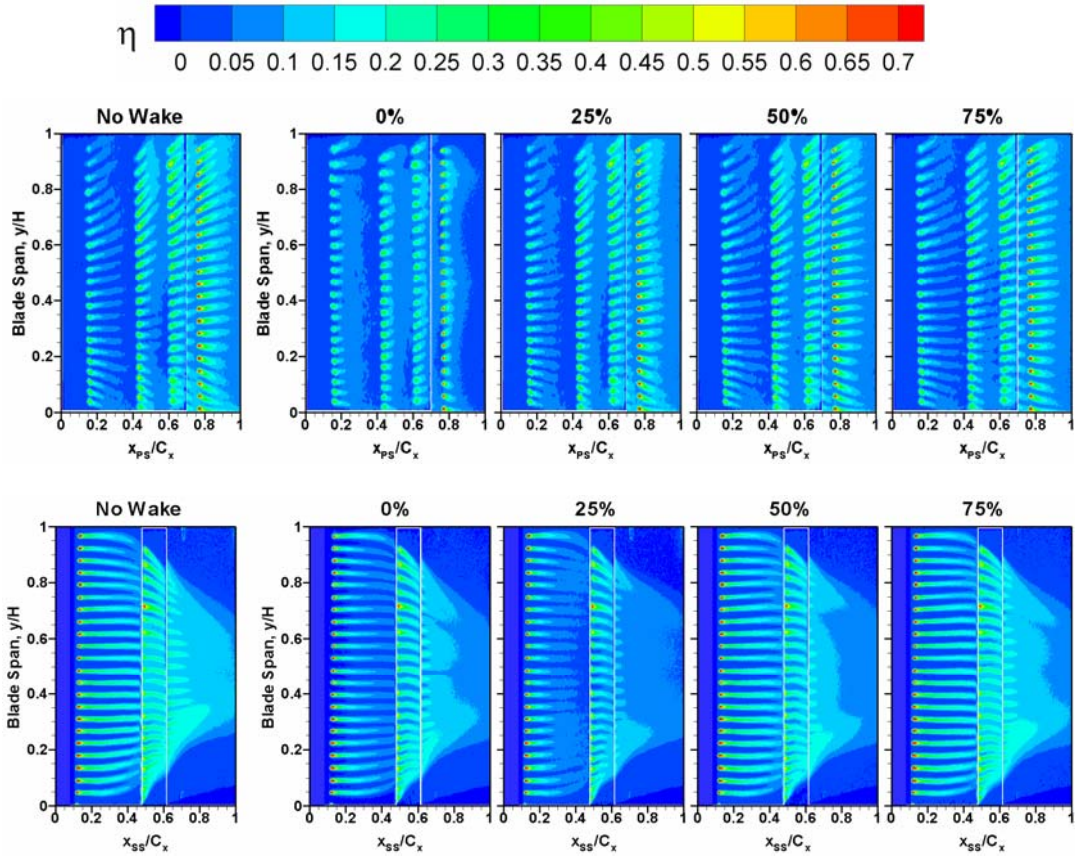

Fig. 3.10 Film cooling effectiveness distribution on Blade 1 for M=0.9 at varying wake rod phases

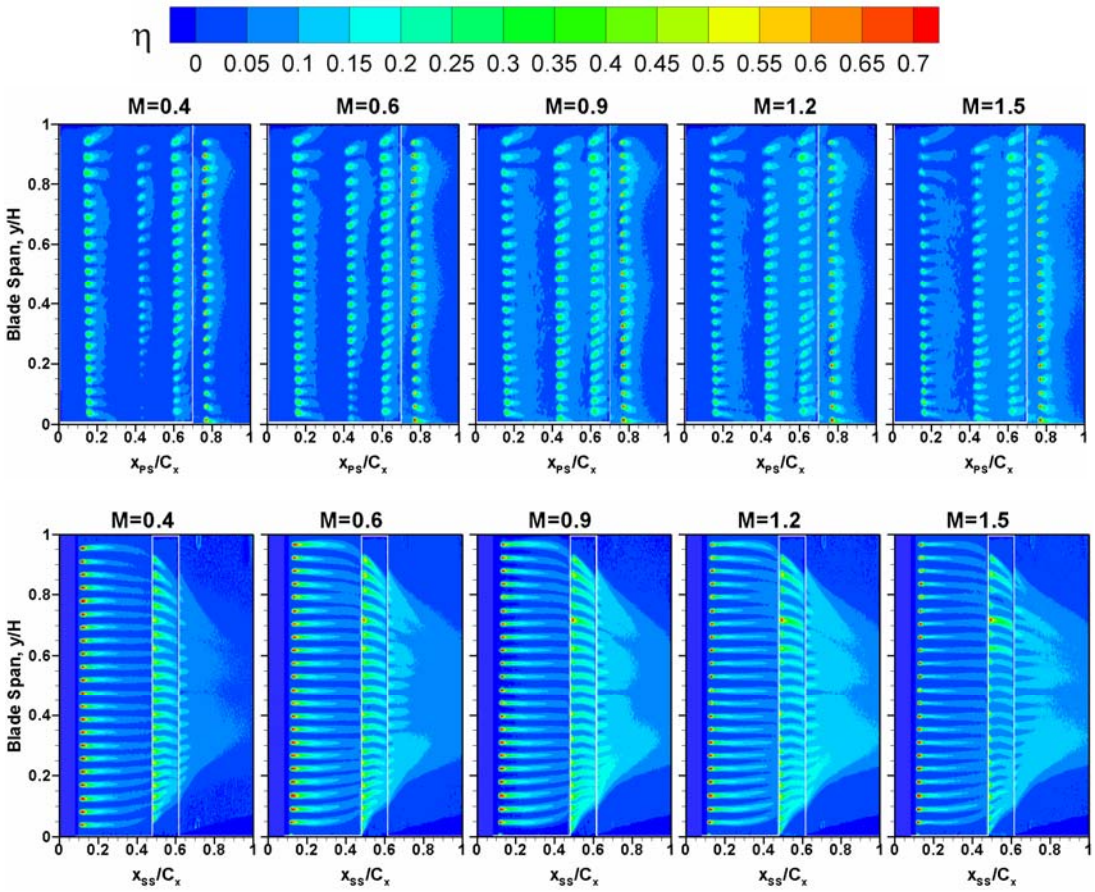

Fig. 3.11 Effectiveness distribution Blade 1 at wake rod phase 0%

side also decreases. The coolant trace becomes shorter and effectiveness level becomes lower. However, the damage on suction side is not as sever as on the pressure side.

Figure 3.12 shows the effectiveness distribution on Blade 1 at rod phase location 25%. On the suction side, as can be seen, not only the elevated effectiveness is reduced, but also the coolant trace is much narrowed and shortened at this rod phase location. The coolant has mixed with mainstream before it reaches SS2 row. Similar to the case of no wake, the best effectiveness is achieved at M=0.6 immediately downstream of SS1 row; blowing ratio M=1.5 gives better coverage further downstream of SS2 rows near the trailing edge. As shown in Fig. 3.8, the secondary flow is predominant in tip region and hub region. The wake effect is more pronounced in the midspan region. On the pressure side, the adverse effect of wake rod still observable, but not as bad as that at phase 0%.

Figure 3.13 shows the wake rods effect on the spanwise averaged effectiveness for varying blowing ratios. Wake rod phase at 0% has the maximum detrimental effect on pressure side film cooling. The film cooling effectiveness for the other wake rod phases is comparable. For the suction side film cooling, the 25%, followed by 0%, shows the largest effect. The effectiveness at the other two rod phase locations (50% and 75%) are comparable to the case of no wake.

The blowing ratio effect on the spanwise averaged film cooling effectiveness at different wake rod phases are presented in Fig. 3.14. In general, M=0.4 provides the lowest effectiveness for either pressure side film cooling or suction side film cooling. For pressure side film cooling, the impact of blowing ratio is reduced at wake rod phase 0%. As aforementioned for the case of no wake, the film cooling effectiveness immediately downstream of the holes is reduced at high blowing ratios (M=1.2 and

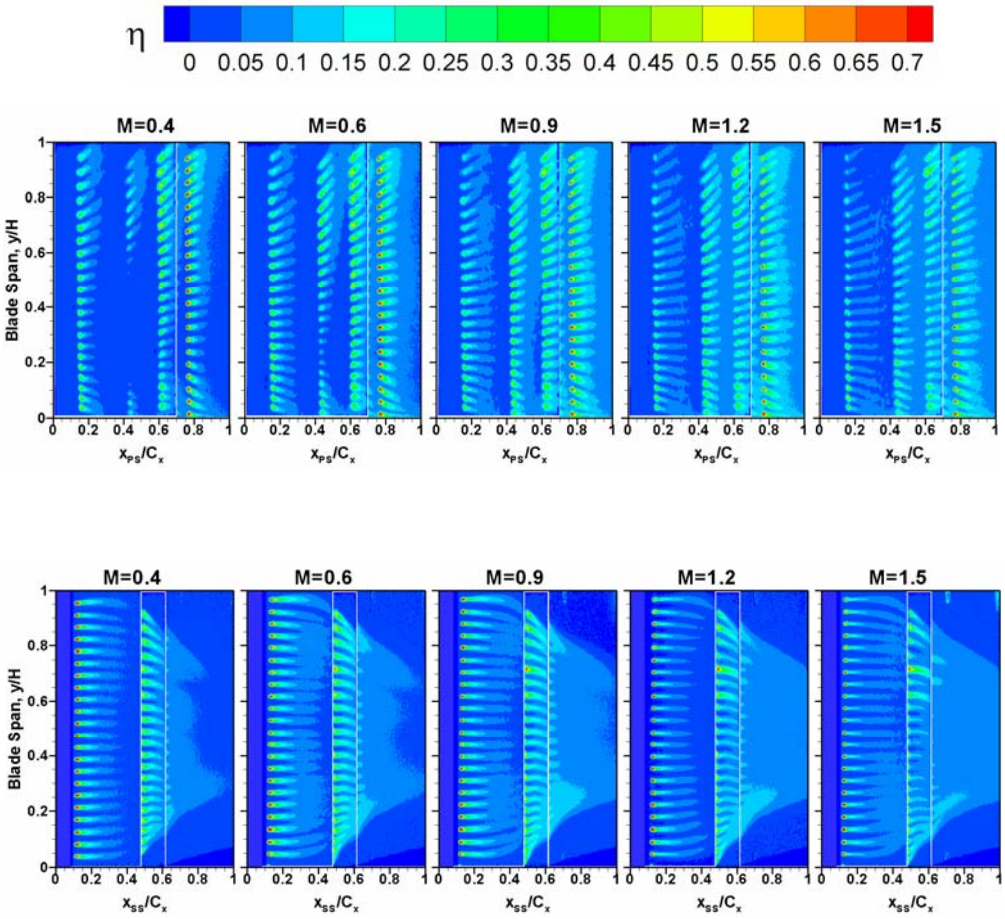

Fig. 3.12 Effectiveness distribution on Blade1 at wake rod phase 25%

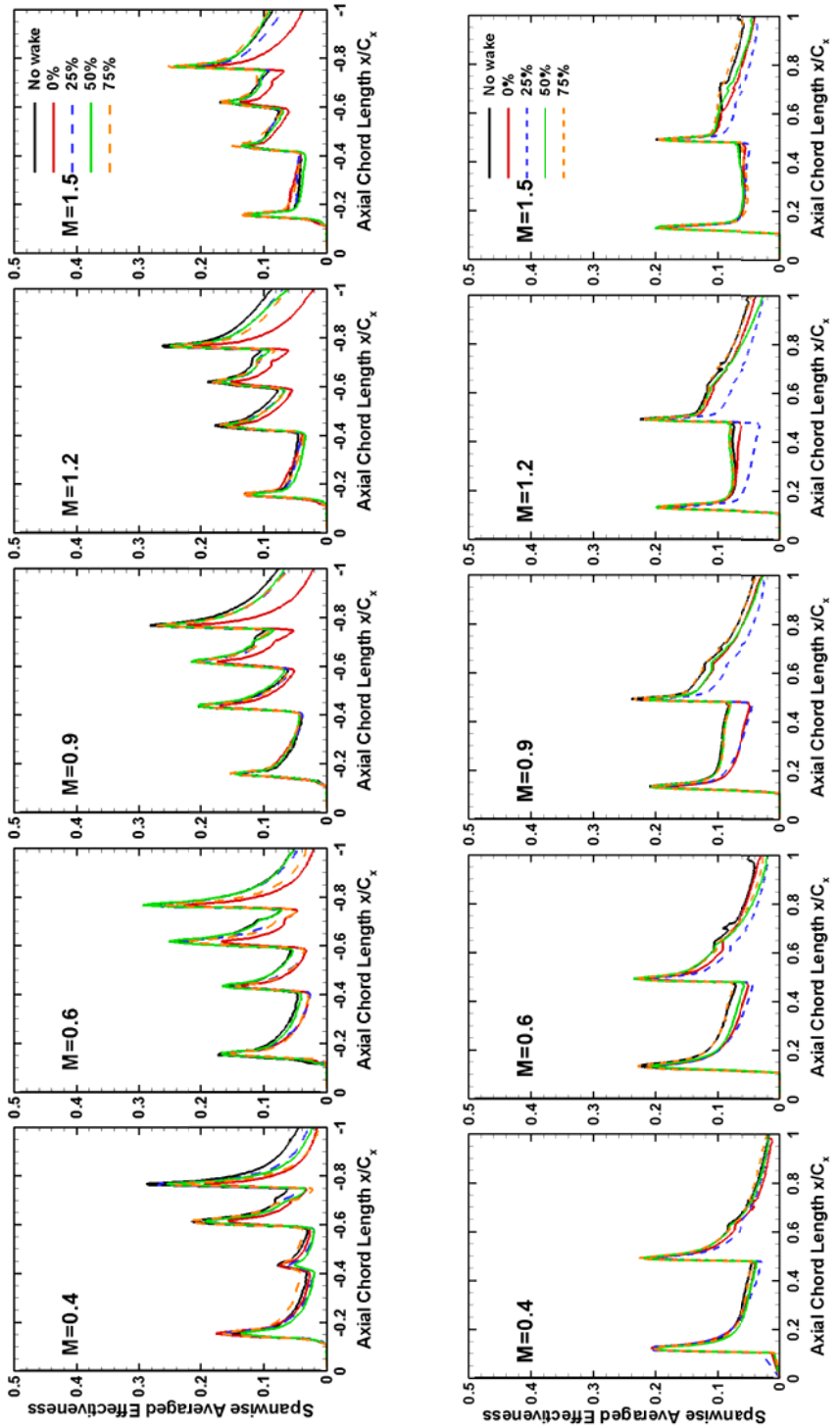

Fig. 3.13 Spanwise averaged film cooling effectiveness on Blade 1 (wake rod effect)

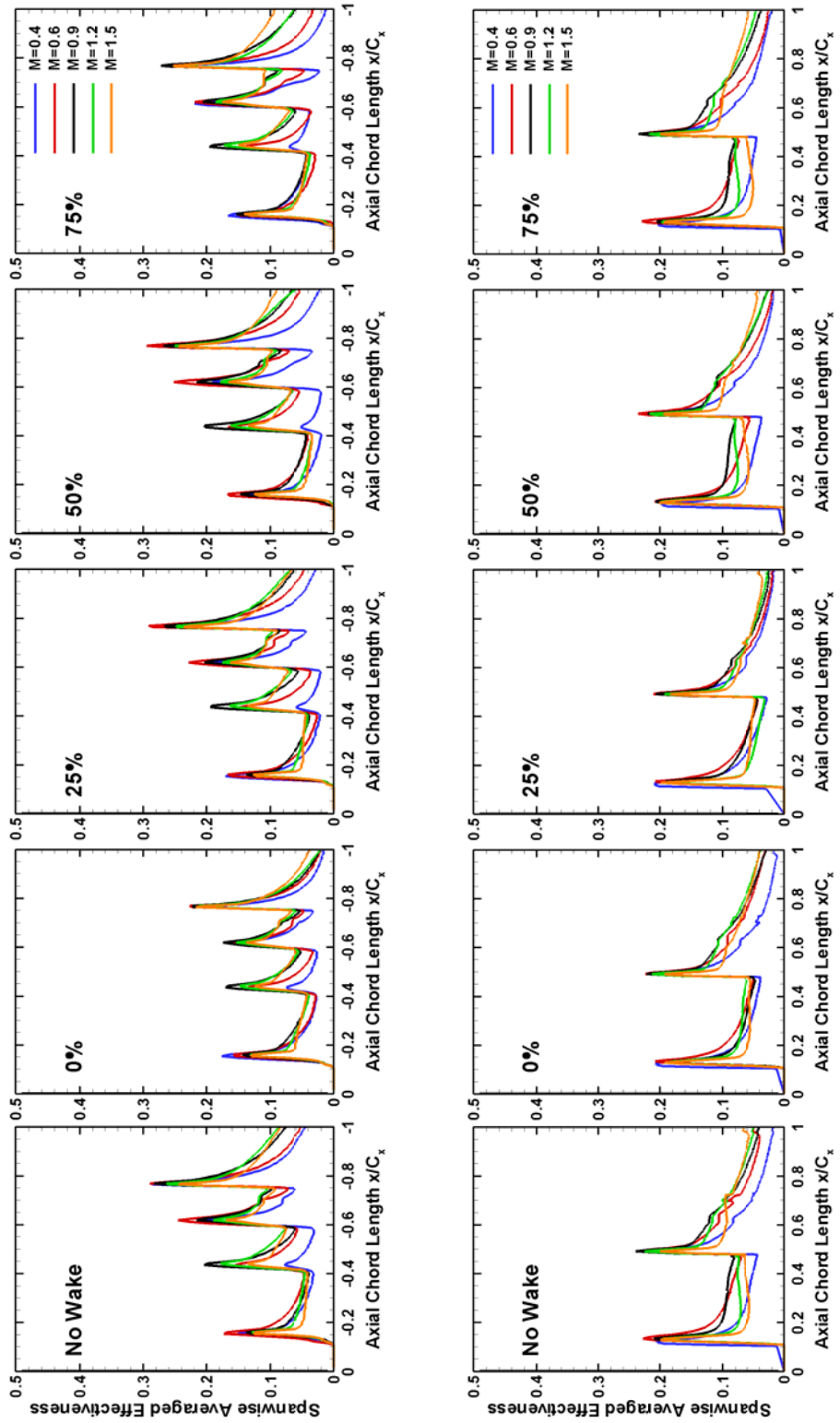

Fig. 3.14 Spanwise averaged film cooling effectiveness on Blade 1 (blowing ratio effect)

M=1.5) due to increased jet momentum. Further downstream of the holes, the high blowing ratio presents higher effectiveness because more coolant is dispersed and convected back to the surface. The effectiveness decays faster with *x/Cx* for pressure side film cooling that suction side film cooling as the coolant tends to lift off from the concave pressure surface. A sharp drop for the suction side film cooling appears for wake rod phase 25%.

3.3.2 Effectiveness on Film Cooled Blade with Compound Angle Shaped Holes

Figure 3.15 shows the effectiveness distribution on the Blade 2 surface (with compound angle shaped holes) for the case of no wake. Compared with Blade 1 (with axial shaped holes), some common characteristics of film cooling is observed.

1. The detrimental effect of the secondary flow on film-cooling effectiveness distribution is clearly observed near the endwall and blade tip. Starting at $x/C_x \sim 0.3$ on the suction side, the spiraling motion of the passage vortex near the hub surface and the tip leakage vortex draws the coolant towards the blade midspan. These vortices acting on the suction surface result in a well defined converged coolant trace toward the midspan. On the pressure side, the corner vortices drive the coolant to hub region. This leads to downward coolant traces. However, the tip leakages draw the coolant to the blade tip. In the midspan region on the pressure side, the coolant basically follow the mainstream flow and is deflected to the axial direction.
2. The film coverage on the suction surface is better than that on the pressure surface, although there are more rows of cooling holes on the pressure side. The coolant traces on the suction side are much longer than that on the pressure surface. The

peak of effectiveness for the suction side film cooling is also higher than pressure side film cooling.

3. The coolant accumulation from the upstream film holes is observed with an elevated film cooling effectiveness in the downstream. This is true for film cooling effectiveness on both pressure side and suction side.

Compared with Fig. 3.8, it is clearly seen that effectiveness from the compound angle shaped holes (Blade 2) is much higher than the axial shaped holes (Blade 1), particularly at higher blowing ratios. The film cooling effectiveness increases with the increase of blowing ratio for either pressure side coolant injection or suction side coolant injection. Jet lift-off is not observed even for the highest blowing ratio M=1.5. However, for the axial shaped hole cooled blade (Blade 1), optimal blowing ratio exists, beyond which the film cooling effectiveness drops because of jet liftoff. As indicated in Table 3.3, the compound angled shaped holes have a larger exit cross-sectional area than the axial shaped hole. Therefore, the coolant jet momentum is further reduced. The coolant jets are more likely suppressed by the mainstream and stay close to the surface. This is more noticeable for the film cooling effectiveness distribution on the suction side. In addition, the coolant jet more spreads out from the compound angle holes by the mainstream. The film coverage area increases.

The comparison of spanwise averaged effectiveness for the axial shaped holes and the compound angle shaped holes is shown in Fig. 3.16 for the case of no wake. Usually, the coolant jets from compound angle shaped holes are deflected by the mainstream, and cover a wider surface area. Whereas the coolant jets from axial shaped hole follow the mainstream directions and the jet coverage is confined to the axial direction. Therefore, in general, the compound angle shaped holes perform better than

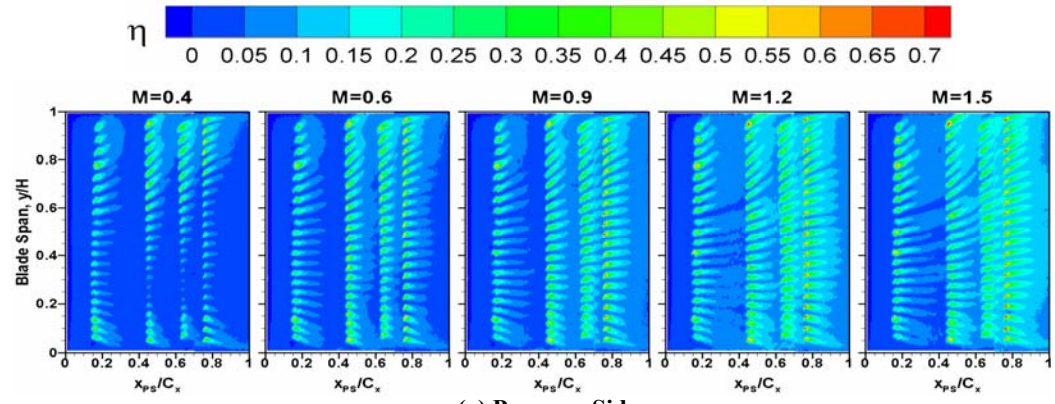

(a) Pressure Side

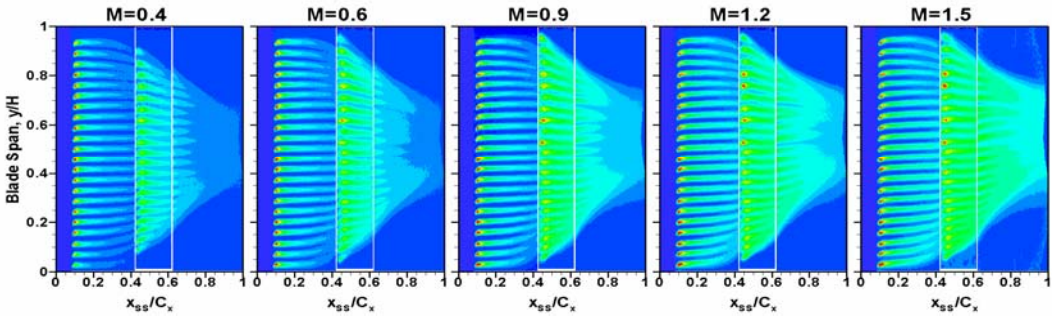

(b) Suction Side

Fig. 3.15 Film cooling effectiveness distribution on Blade 2 for varying blowing ratios without wake

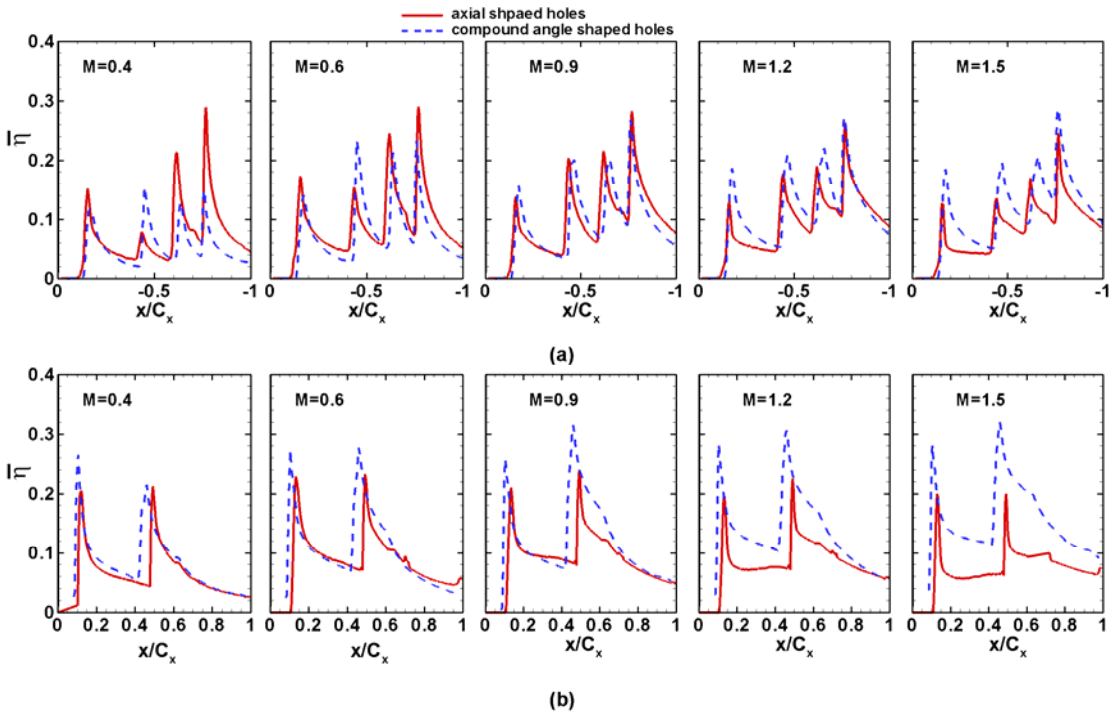

Fig. 3.16 Comparison of spanwise averaged film cooling effectiveness for axial shaped holes (Blade 1) and compound angled shaped holes (Blade 2).

axial shaped holes. In addition, the compound angle holes have larger exit area. The jet momentum from those compound angle shaped holes is further reduced. Coolant is more easily to stay close to the surface with the reduced jet momentum. On the pressure side, the compound angle shaped holes and axial shaped holes show comparable effectiveness for the moderate blowing ratio M=0.6 and M=0.9. At higher blowing ratio M=1.2 and M=1.5, the compound angle holes shows better effectiveness. On the suction side, a clear rise in effectiveness is observed for compound angled shaped holes. As the blowing ratio increases, the advantage of compound angled shaped hole becomes more evident. However, the compound angle shaped holes might cause higher heat transfer coefficients and losses due to coolant jets deflection by mainstream, as compared to the axial shaped holes.

The spanwise averaged effectiveness for the compound angle shaped holes for the no wake case is presented in Fig. 3.17. The effectiveness increases with blowing ratio for either pressure side or suction side. There is no optimal blowing ratio observed in the range considered. Overall, the effectiveness levels on the suction side are higher than that on the pressure side for a particular blowing ratio, as seen from the contour maps.

The effect of wake rods is also examined on Blade 2. Similar to the case for axial shaped hole, the wake produced by the rods reduces the film cooling effectiveness. The mixing between the coolant and mainstream is enhanced by the wakes. The wake rod positions at 0% and 25% exhibits the more pronounced influence on film-cooling effectiveness. The effect of wake rod on Blade 2 film cooling is presented in terms of spanwise averaged effectiveness in Fig. 3.18 and Fig. 3.19. Figure 3.18 shows the effect of blowing ratio. The film cooling effectiveness increases when blowing ratio increases

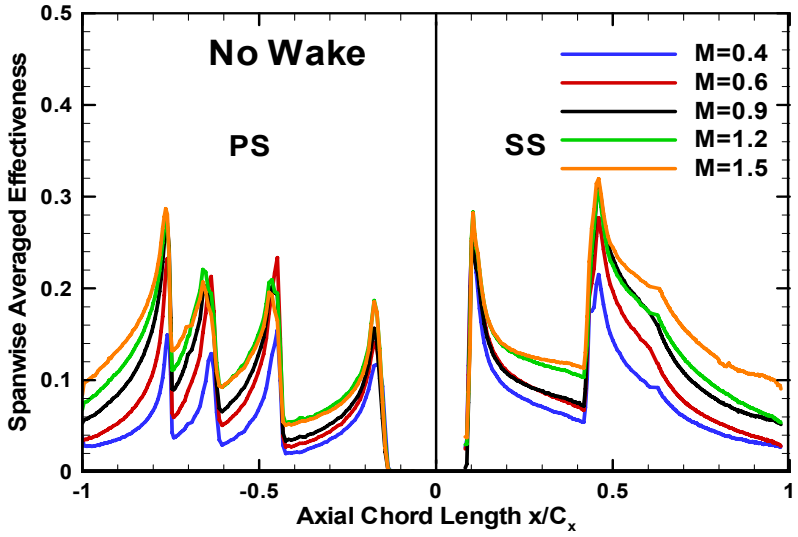

Fig. 3.17 Spanwise averaged effectiveness for the case of no wake

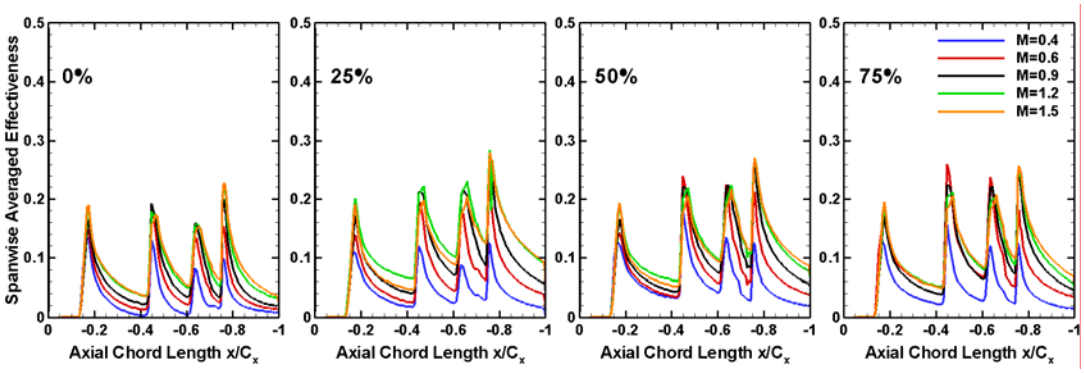

(a) Pressure Side

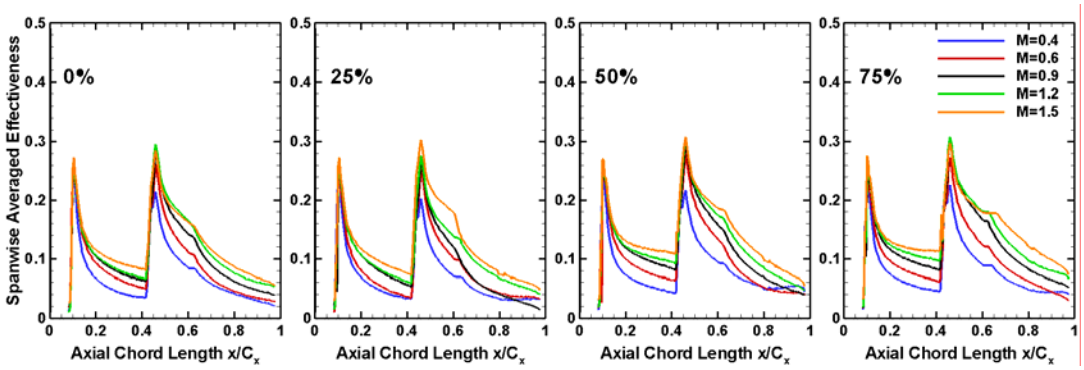

(b) Suction Side

Fig. 3.18 Spanwise averaged film cooling effectiveness on Blade 2(blowing ratio effect)

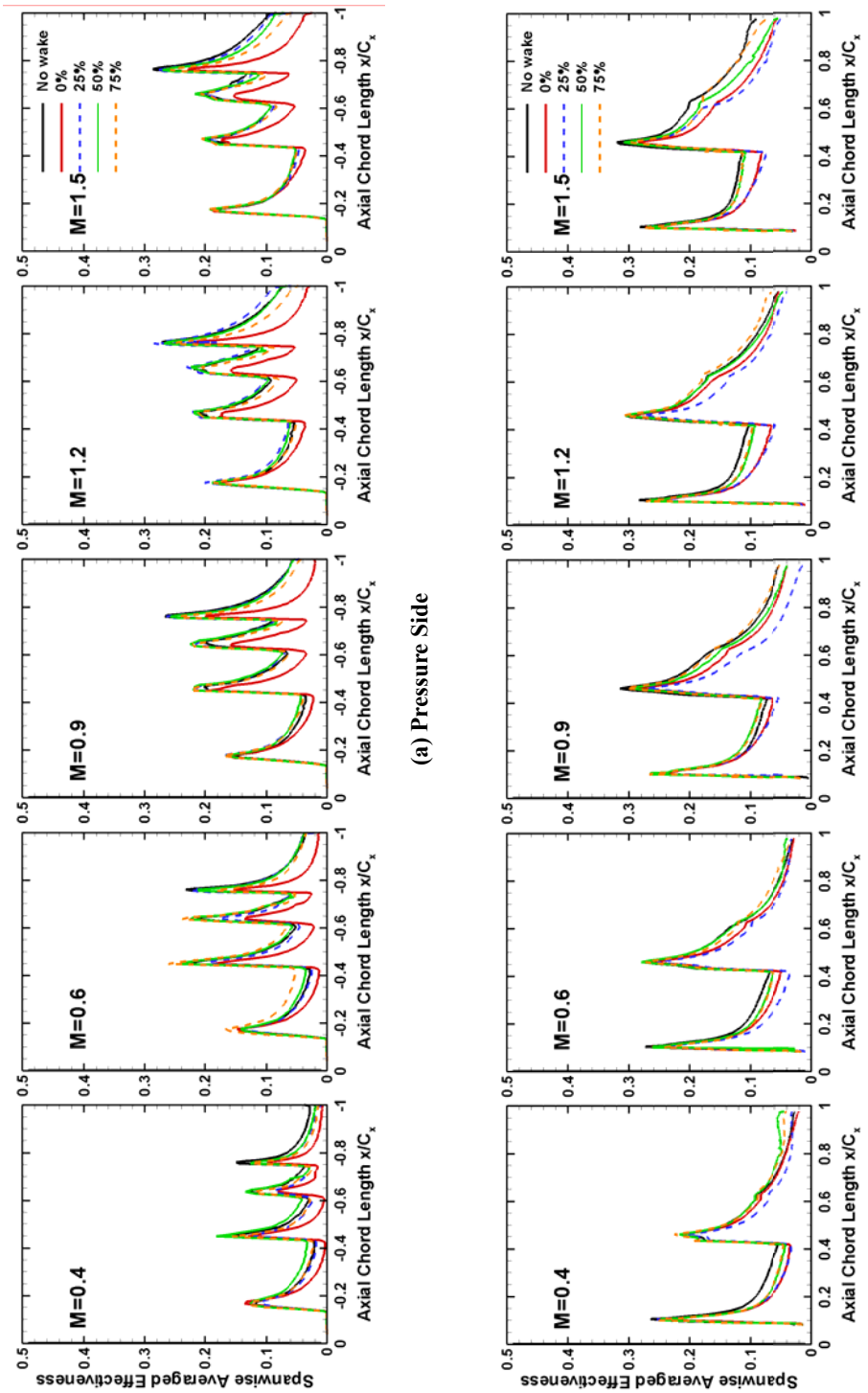

(a) Pressure Side

(b) Suction Side

Fig. 3.19 Spanwise averaged film cooling effectiveness on Blade 2 (wake Rod effects)

for either pressure side or suction side for all the wake rod position. The effectiveness trend pretty much follows that of the no-wake case. Figure 3.19 shows, for a given blowing ratio, the lowest effectiveness occurs at rod phase 0% for pressure surface, 25% for the suction surface.

3.4 Conclusions

Experimental tests were performed on high pressure turbine rotor blades with axial angle shaped holes and compound angle shaped holes. The shaped holes featured a 10° expansion in the lateral direction and an additional 10° in the forward direction. The coolant was issued from either pressure side film cooling holes or suction side film cooling holes. The effect of blowing ratios and the presence of stationary, upstream wakes are examined. Some of the main highlights from the present study are presented below:

1. Pressure sensitive paint (PSP) technique enables us to clearly visualize the impact of the passage vortex, corner vortex and tip-leakage vortex on coolant film trace distribution over the blade surface. Accurate effectiveness data is obtained on the heavily film cooled blade surface.
2. The suction side gains better film effectiveness than the pressure side. The suction side convex surface and favorable pressure gradient help the coolant stay closer to the surface; while the coolant jets tends to lift off the concave pressure surface. Even with more rows of film cooling holes, the effectiveness on the pressure side is still lower than on the suction side.
3. The tip leakage vortex and passage vortex have severe detrimental effect on the suction side film cooling. The strong mixing sweeps the coolant away from the

suction surface and resulted two unprotected triangular zone near the trailing edge.

4. An upstream wake can have a severe detrimental effect on film coverage depending on the wake rod phase locations. Wake phase locations of 0% and 25% significantly decrease the film cooling effectiveness magnitudes. Wakes from 50% and 75% phase locations do not attach to the blade surfaces and hence the adverse impact is reduced.
5. The tip leakages vortices and endwall vortices are predominant at near tip and near hub region. The upstream wake effect on suction side is more observable at midspan region.
6. Comparison between the compound angle shaped hole and axial shaped hole designs show higher effectiveness values for compound angle shaped holes on either pressure side or suction side, particularly, at higher blowing ratios.
7. For the axial shaped holes, the moderate blowing ratio (M=0.6 and M=0.9) shows better film cooling effectiveness on either pressure side or suction side immediately downstream of the film cooling holes. Further downstream of the film cooling holes, high blowing ratios provide wider film coverage. For the axial shaped holes, optimal blowing ratios exists, beyond with effectiveness decreases.
8. Film cooling effectiveness from the compound angle shaped holes increases with blowing ratio on either surface of the blade. There is no optimal blowing ratio observed in the range of study (M=0.4~1.5).

4. UPSTREAM VORTEX EFFECTS ON TURBINE BLADE PLATFORM FILM COOLING WITH TYPICAL STATOR-ROTOR PURGE FLOW

4.1 Experimental Facilities

Test for the platform purge flow cooling was done in the same five-blade cascade as that for blade film cooling test in Section 3. The mainstream flow conditions were set same as in blade film cooling test. Detailed cascade configurations and flow conditions can be found in Section 3. Figure 4.1 schematically shows the five-blade linear cascade with the platform test section cooled the purge flow. The definition of the coordinate, which will be used in the discussion, is presented in Fig. 4.1(b). C_x is the axial chord length of the blade, while x and x' are the axial distance measured from the blade leading edge and the slot upstream edge, respectively.

A new labyrinth-like seal, which is a typical rotor stator seal in real gas turbine engine**,** is used to simulate the stator-rotor purge slot. The seal covers two passages of the linear cascade. Figure 4.2 shows the seal configurations and two delta wing geometries. The seal consists of two parts, an upstream (stator) part with round teeth and a downstream (rotor) part with sharp teeth. The two parts match together and result in a throat width (s) of 0.19cm at the purge slot exit as indicated in Fig. 4.2(b) and Fig. 4.2(c). The upstream part, with a radius of 0.1cm, breaks at 1.64cm upstream of blade leading on the platform. The downstream part is inclined 20° to the mainstream. The junction of inclined slot and the flat platform is located 0.62cm of leading edge. Therefore, the total breakout width (b) of the slot is 1.02cm. Other dimensions can be found in Fig. 4.2. A coolant plenum is attached underneath the purge slot. The coolant enters the plenum and travels through the seal before being expelled to the mainstream.

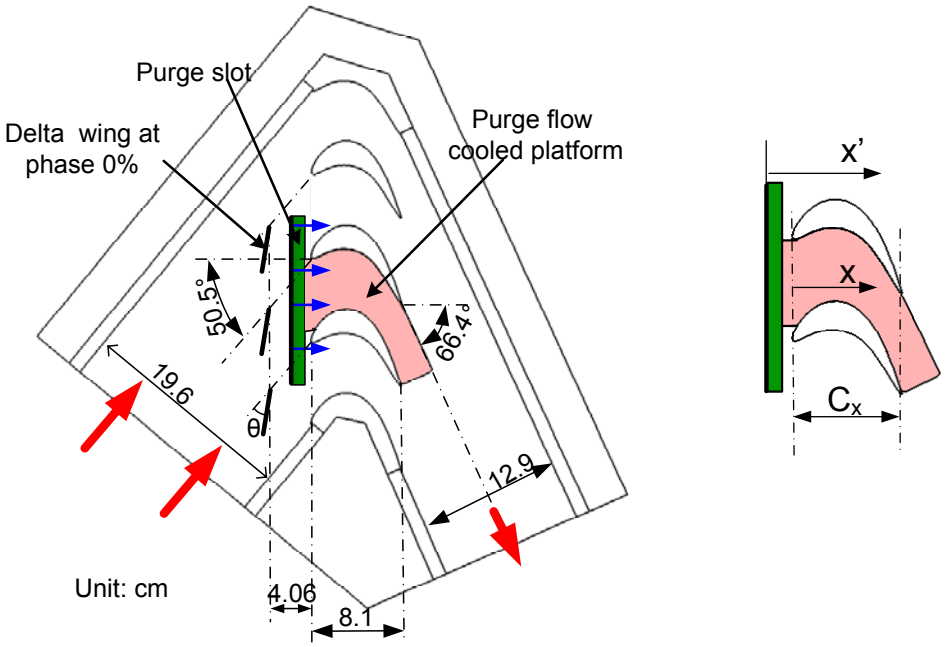

(a)

Fig. 4.1 (a) Schematic of cascade blade platform with upstream delta wing and purge slot (b) Definition of platform coordinates

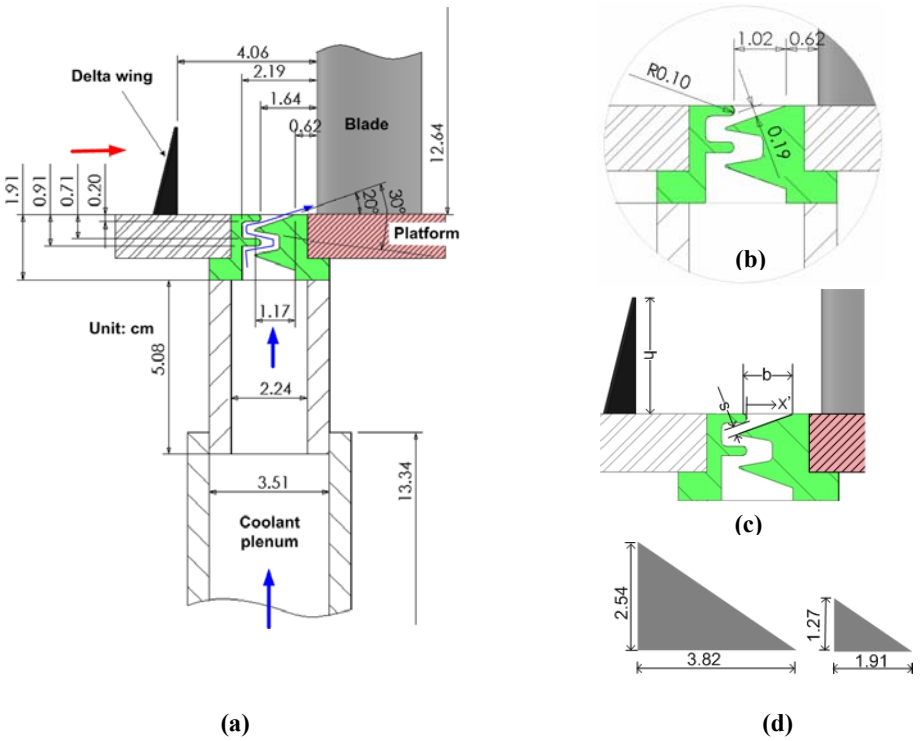

Fig. 4.2 (a) Detail of a typical labyrinth-like stator rotor seal (b) Detail view of the seal (c) Notations of the seal (d)Two delta wing geometries

Five pressure taps are instrumented on the side wall the plenum to examine the pressure. Uniform pressure distribution was found inside the plenum during the film cooling test. The coolant purge flow rate is generally considered as a percentage of the mainstream mass flow rate. Four coolant mass flow rates (MFR) are considered in this study – 0.25%, 0.5%, 0.75% and 1.0% of mainstream flow rate. The corresponding blowing ratios M, defined as the ratio of coolant mass flux ($\rho_c V_c$) to mainstream mass flux ($\rho_m V_m$), are 0.17, 0.33, 0.50 and 0.67. The coolant velocity at throat of seal (based on s) is used in the blowing ratio calculation. The mainstream velocity is measured at cascade inlet.

Wright et al. [51] demonstrated that the vortex generated by delta wing can be used to simulate the passage vortex. Depending on the upstream vane configuration, the passage vortex generated by upstream vane varies in term of size and strength. Changing the delta wing size and attack angle will alter the vortex size and strength. In this study, two sets of delta wings are selected to model the different size and strength of vane passage vortices. Figure 4.2(d) shows the dimensions of the delta wings. One set of delta wings have a height of 20% of cascade height (h=0.2H) with a width of 1.5 times of the delta wing height. The other set of delta wings were scaled down to the half size of the first set, i.e., the height is 10% of the cascade height (h=0.1H). The delta wings were located at a distance equivalent to 50% of axial chord upstream of the blades. They were periodically placed at four equally spaced locations. Figure 4.3 shows the locations of the delta wings relative to the blade leading edge. The delta wing edge directly upstream of the leading edge is indicated as the phase 0%. The delta wings shift a quarter of blade pitch along the pitchwise direction and progressively reach phase

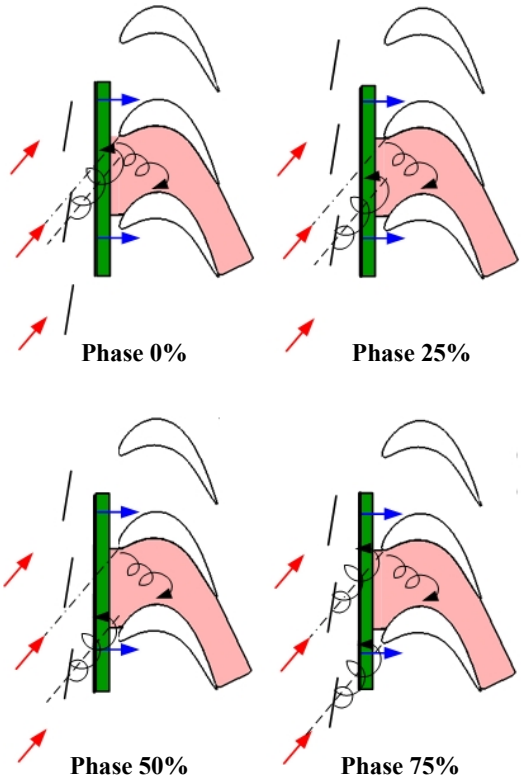

Fig. 4.3 Delta wing phase positions in reference of blade leading edge

position 25%, 50%, and 75%. For a given size of delta wing, the vortex strength is determined by the mainstream attack angle (θ) to the delta wing. Two attack angles, 30° and 45°, were considered in the study to vary the strength of passage vortex. Figure 4.3 also conceptually shows the vortices generated by the upstream delta wings and the passage vortex generated in the downstream local blade passage.

4.2 Results and Discussion

4.2.1 Film Cooling Effectiveness Distribution

Prior to presenting the film effectiveness data, the pressure and Mach number distribution were examined and shown in Fig. 4.4. The pressure distribution on the platform was represented by ratio of local static pressure and inlet total pressure. The local static pressure was measured by PSP while the inlet total pressure was measured by pitot tube upstream of the cascade inlet. Several pressure taps were put on the platform along the three curves to calibration PSP data. The pressure and Mach number data along three curves on the platform was extracted and compared with pressure tap measurement. One curve was offset of the blade pressure side by 10% of pitch length, the other was offset of suction side by 10%. The third curve was along the mid-passage. Pressure distribution on the blade surface along the midspan measured by pressure taps is also presented for comparison. On the contour plots, the black line upstream of the blade leading edge indicates the junction of the inclined purge slot and the flat platform. It can be seen from the contour plot that the static pressure near the pressure side is higher than that near the suction side. This is driving force of blade work as well as the passage cross flow. From the leading edge to the trailing edge, the pressure gradually decreases; the mainstream flow is accelerated; Mach number increases. The pressure

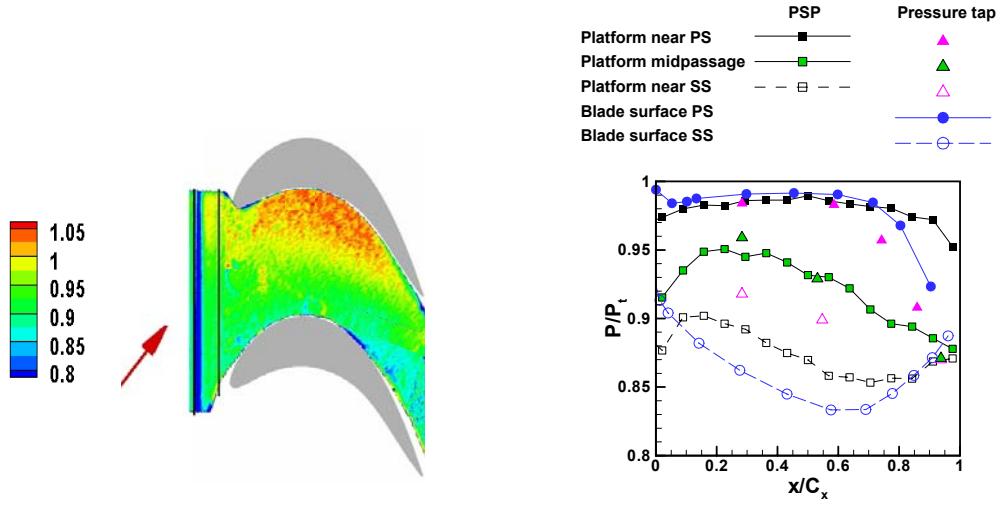

(a) Pressure distribution

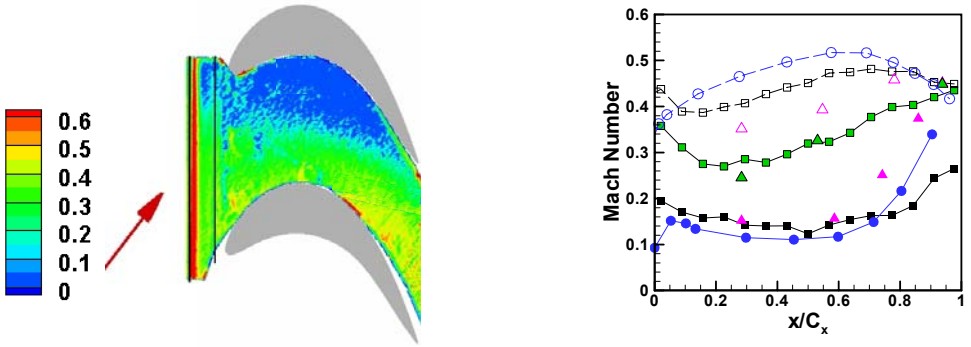

(b) Mach number distribution

Fig. 4.4 Pressure and Mach number distribution without coolant injection

distribution along the slot exit is non-uniform with higher pressure existing near the blade leading edge. This non-uniform outer pressure affects coolant mass flow distribution along the slot, particularly, when the coolant flow rate is low. It can be seen from the line plots that the PSP data matched well with pressure tap data; the maximum deviation is less than 6%. Near the pressure side, the pressure is very close to the pressure on the blade midspan. However, near the suction side, the pressure is higher than that on the blade surface at midspan location. This results in a reduced driving force (pressure differential between pressure side and suction side) near the platform. It can be seen from Fig. 4.4(b), the velocity near the suction side on the platform is lower than the freestream velocity.

The test cases that have been performed are listed in Table 4.1. However, not all the film cooling effectiveness distribution is presented. Results are selected to aid the discussion and understand the purge flow cooling. To study the effect of vane passage vortex simulated by the delta wings, the film cooling effectiveness without presence of the delta wings was taken as baseline case. Fig. 4.5 shows the detailed film cooling distributions on the blade platform with no upstream vane influence. The film effectiveness distributions are shown for four coolant flow ratios MFR=0.25%, 0.5%, 0.75% and 1.0%, corresponding to the blowing ratio M=0.17, 0.33, 0.50 and 0.67, respectively. To clearly show the effectiveness distribution in the inclined slot and the flat platform, the contours are plotted at two difference scales. At the lowest flow rate of MFR = 0.25%, the coolant ejection from the slot is non-uniform. The high outer pressure near the leading edge of the blade prohibits the coolant exiting from this region. As the coolant mass flow rate increases, the pressure inside the coolant plenum

Table 4.1 Test Cases

Upstream vane effect	Vortex generator Delta wing	Phase position	Purge flow rate
None (baseline)	--	--	0.25%, 0.5% 0.75%, 1.0%
Passage vortex	h=0.1H, θ=30°	0%, 25% 50%, 75%	0.25%, 0.5% 0.75%, 1.0%
	h=0.1H, θ=45°	0%, 25% 50%, 75%	0.25%, 0.5% 0.75%, 1.0%
	h=0.2H, θ=30°	0%, 25% 50%, 75%	0.25%, 0.5% 0.75%, 1.0%
	h=0.2H, θ=45°	0%, 25% 50%, 75%	0.25%, 0.5% 0.75%, 1.0%

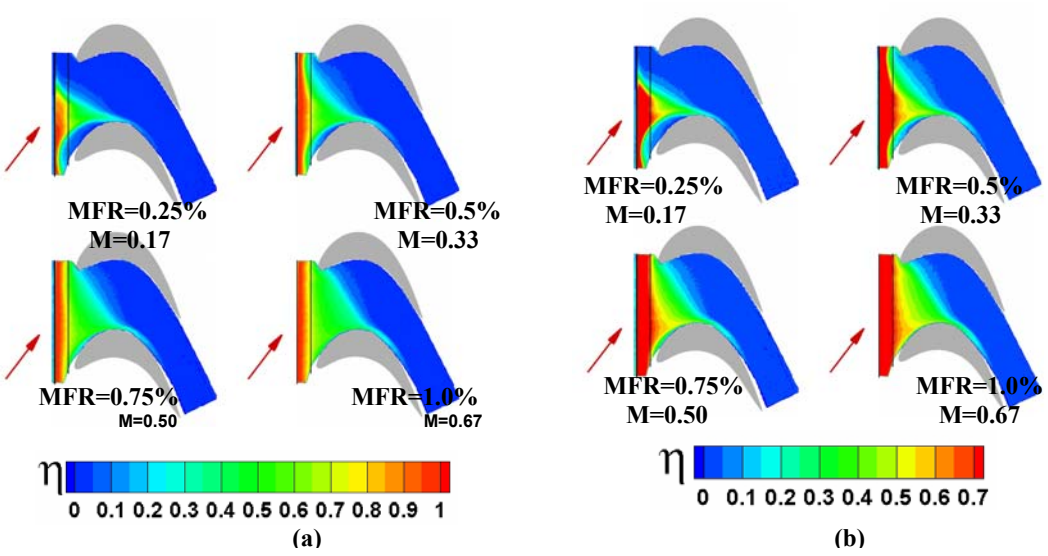

Fig. 4.5 Film cooling effectiveness at various coolant injection rates (baseline) (a) scale 0~1.0, (b) scale 0~0.7

increases. The coolant ejection becomes more uniform. It can be observed at MFR=0.5%~1.0%, the effectiveness at the slot exit is close to unity. The 20° inclination of slot keeps coolant close to the surface where exhibits high effectiveness. However, the mainstream and coolant mixing takes place in the inclined slot before the coolant reaches the flat platform. Therefore, the effectiveness in the inclined portion gradually decreases. At the junction of inclined slot and the flat platform, the effectiveness for MFR=0.75% and 1.0% drops to about 0.7. To better visualize the film cooling effectiveness downstream of the junction, the effectiveness distribution is presented Fig. 4.5(b) with smaller scale. The pressure difference between the pressure side and the suction side induces cross flow in the passage. The flow is driven from pressure side to suction. The coolant is swept from the pressure side to the suction side. At low coolant mass flow rate (MFR=0.25% and 0.5%), the coolant is taken away from the surface by the horseshoe vortex, so film cooling effectiveness in the leading edge region is close to zero. The effect of horseshoe vortex even extends to the inclined slot and results in a decreased effectiveness in the slot. When the coolant mass flow ratio increases, the strength of the horseshoes vortex is reduced by the purge flow. With less mixing with mainstream, the leading edge region gains some film coverage at MFR=0.75% and 1.0%. Inside the blade passage, the coolant is skewed to the suction side by the cross flow. The cross flow also drives the pressure side leg of the horseshoes vortex moves to the suction side, and forms passage vortex. The strong passage vortex caused violent mixing between the coolant and mainstream. The film effectiveness quickly dies out. The passage vortex acts like a barrier, beyond which the coolant vanishes. Increasing the coolant flow rate weakens the effect of the passage vortex, and thus film coverage

extends a little to the downstream. However, from MFR=0.75% to MFR=1.0%, the increment of film coverage is limited. At the lowest flow rate of MFR = 0.25%, a large portion of the passage is left unprotected. Doubling coolant mass flow rate from 0.5% to 1.0% of the mainstream flow yields only marginal improvement in film coverage. The coolant covers partial area of the upstream passage, while a large portion of the downstream half of the passage remains unprotected. The film protection on the platform is minimal after the mid-chord. From the studies [46-48], it can be conjectured that the film coverage would increase if the MFR were further increased. This is accompanied at the cost of large amount of coolant consumption. It may be an efficient way to cool the platform by combining the upstream purge flow cooling with discrete-hole film cooling strategically arranged on the downstream of the platform. This research will continue on platform film cooling with combined upstream purge flow and downstream discrete hole film cooling.

To create the vortex, the delta wings were periodically placed upstream of the stator-rotor seal. Because the exact size and strength of the passage vortex leaving the vane passage, corresponding to the present blade geometry, is not known, it is vital to consider a range of possibilities. Four delta wing configurations were generated by varying two sizes of delta wings (h=0.1H and h=0.2H) at two flow attack angles (θ=30° and θ=45°). For each delta wing configuration (given size and attack angle θ), four phase position along the pitchwise direction are used to simulate the advancement vane passage vortex. The influence of upstream vane passage vortex is presented in Fig. 4.6 and Fig. 4.7 with MFR=0.75%. A generalization of the following discussion can be applied to the other coolant mass flow rates in the range of current study. Figure 4.6

shows the film cooling effectiveness distribution at MFR=0.75% under the influence of delta wing h=0.2H. Compared with MFR=0.75% in Fig. 4.5, the area with elevated film effectiveness decreases for all the phases in the presence of upstream delta wings. The effectiveness pattern are similar when delta wings are placed at the same phase position for θ=30° and θ=45°. The area of coolant coverage does not extend as deep into the passage when the delta wing is placed upstream of the blades except at phase position 25%. As the vortex passes over the seal, the coolant lifts off the platform, and mixes with the mainstream. Therefore, it does not remain attached to the surface and results in a lower effectiveness. A better understanding of the interaction of delta wing generated vortex with downstream flow may be achieved from Fig. 4.3. At phase 0%, the vortex is close to the pressure side leading edge, so the effectiveness near the leading edge region of pressure side is reduced. At phase 25%, the upstream vortex reaches the center of the passage. It competes with passage vortex generated by the blades passage. The strength of local blade passage vortex reduced. So the coolant is more spread out to the downstream. Therefore at phase 25% the film coverage is slight larger than the case with no delta wings. At phase 50%, the upstream vortex is close to suction side leading edge. It interacts with suction leg horse vortex, and caused more mixing, therefore, the suction side leading edge is less protected. This is more evident at θ=45°. At phase 75%, the upstream vortex is more or less directed to the leading of the blade. As a result, the film effectiveness in the leading edge region reduces due to interaction of upstream vortex with horseshoe vortex reduces.

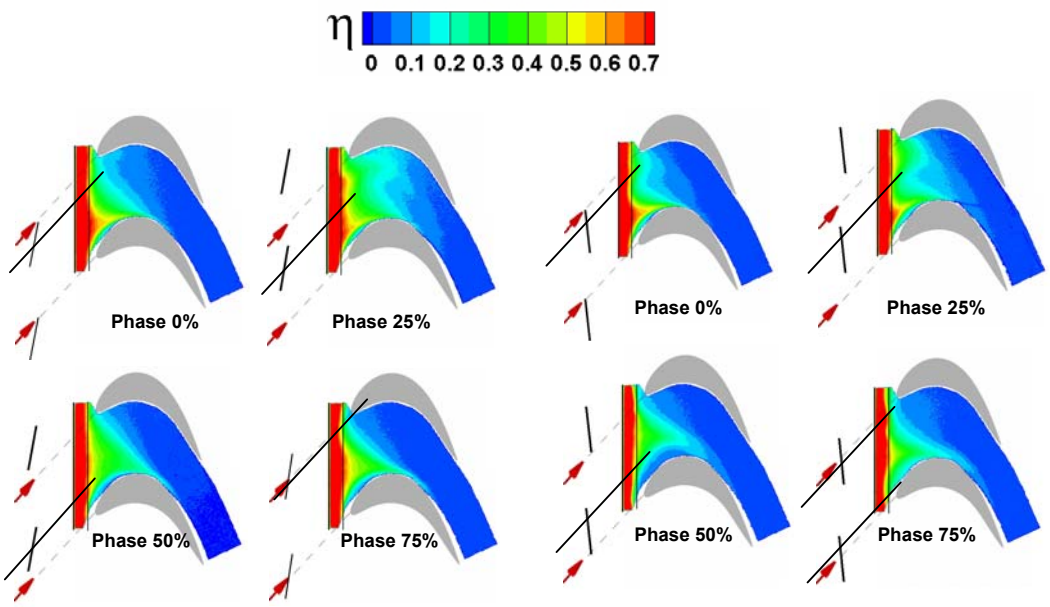

Fig. 4.6 Film cooling effectiveness at various phase location at MFR=0.75% with delta wing h=0.2H

In general, the upstream vortex causes more turbulence mixing and is detrimental to the slot purge cooling. With a larger attack angle, the vortex strength for θ=45° is larger than that for θ=30°. Therefore, the adverse effect of upstream vane passage vortex is more evident for θ=45°.

Fig. 4.7 shows the impact of the vortex created by upstream delta wing h=0.1H at MFR=0.75%. The delta wing dimension is scaled down to half of the previous one. With the smaller size of delta wing, both the size and strength of the vortex generated by this delta wing (h=0.1H) reduce. The upstream vortex alters the effectiveness distribution pattern. The impact of local passage vortex is dominant. When the coolant meets the local blade passage vortex, it is wiped off and disappears in the mainstream. Although θ=45° shows slightly more effect, the difference in effectiveness from the two attack angles is small. The vortex created by delta wing is directed to the passage at phase 0% and 25%, compared with baseline case, the effectiveness pattern is altered. The upstream vortex is close to the blade surface at phase 50% and 75%, and interacts with horseshoes vortex. However, the enhanced mixing doesn't lift the coolant off the surface completely, there is still some coolant coverage left the near the leading edge region. Comparing with Fig. 4.6, it can be seen that upstream vortex from h=0.1H has less impact on the downstream film cooling effectiveness.

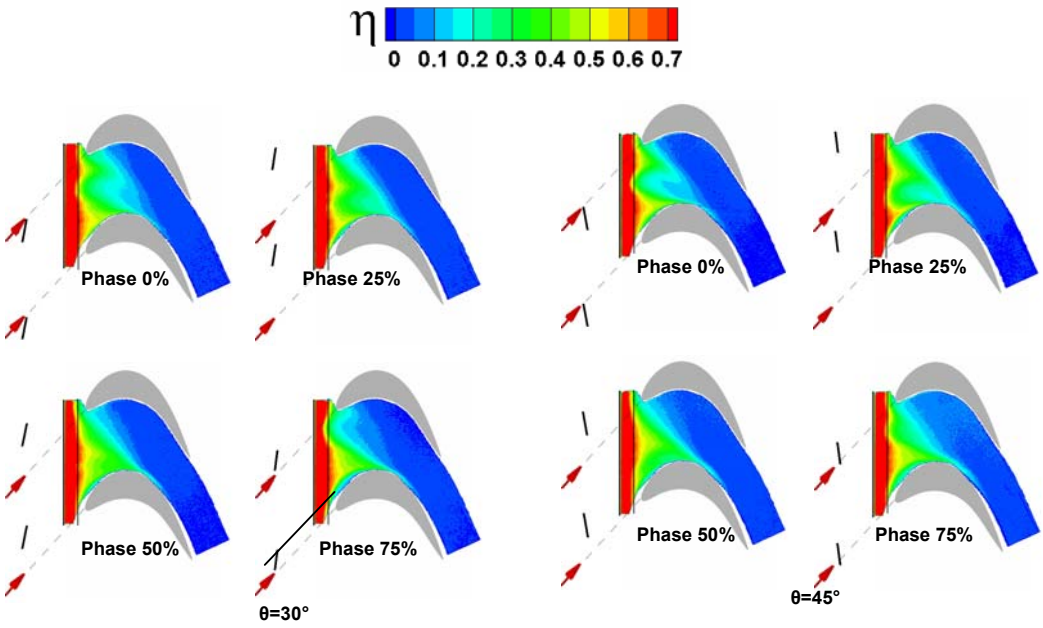

Fig. 4.7 Film cooling effectiveness at various phase location at MFR=0.75% with delta wing h=0.1H

4.2.2 Laterally Averaged Film Cooling Effectiveness

More general comparisons of all the cases studied can be made by comparing the laterally averaged film cooling effectiveness versus axial chord. The arrows in the line plots (if any) indicate the location of slot exit and dashed lines indicate the blade leading edge. Fig. 4.8 shows the laterally averaged effectiveness for the baseline case (no delta wings). It can be seen from Fig 4.8(a), the higher coolant mass flow rate shows higher effectiveness. The averaged effectiveness at slot exit is about unity except MFR=0.25%, at which the coolant ejection is not uniform. The coolant quickly mixes with mainstream out of the slot exit and the effectiveness drops rapidly. The laterally averaged effectiveness reduces to about 0.54 for MFR=1.0% at the blade leading edge. It is even lower for the other coolant flow rates. Inside the blade passage, the coolant is further dissipated into mainstream. $\overline{\eta}$ becomes negligible (<0.1) for all MFRs when x/Cx > 0.4. This indicates the passage vortex meets the blade suction surface around x/Cx=0.4 and starts climbing up to the suction surface of the blade. The coolant is lifted off by the passage vortex. The film protection vanishes downstream of the passage vortex. The blade surface film cooling study in previous section showed the coolant on the blade suction surface is swept towards to blade midspan when x/Cx>0.4. This is consistent with the current findings. The platform is partially covered by the purge coolant when x/Cx<0.4, beyond which the platform is left unprotected. Figure 4.8(b) shows $\overline{\eta}$ vs x'/Ms, where x'=0 is defined at the slot exit (upstream edge of the seal). The correlations for the tangential slot and discrete hole film cooling on flat plate [82] are also presented in the plot for comparison. The experimental data is close to tangential slot correlation near the slot exit. Further downstream, $\overline{\eta}$ for platform purge

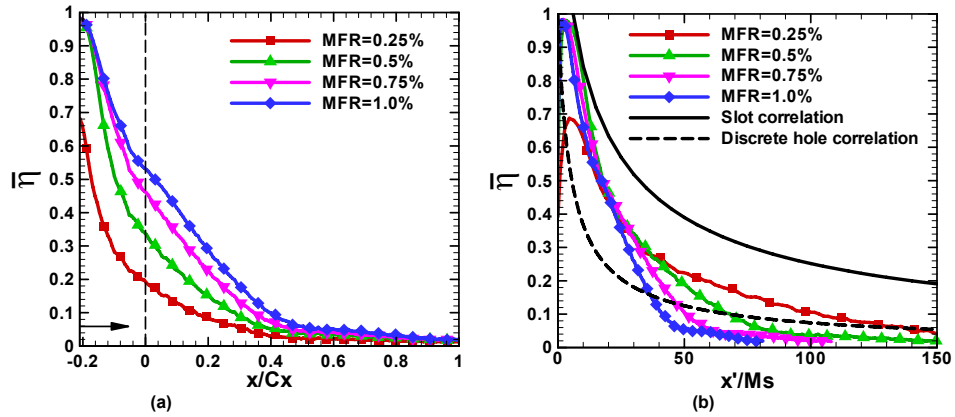

Fig. 4.8 Laterally averaged effectiveness for baseline case (a) effectiveness vs x/Cx (b) effectiveness vs x'/Ms

slot cooling is much lower than the tangential slot correlation. The passage induced secondary flow enhances mixing between the coolant and the mainstream. $\overline{\eta}$ on the platform decreases rapidly. Comparing with discrete film cooling, $\overline{\eta}$ from experiment is higher than the correlation downstream of slot exit. Further downstream, the $\overline{\eta}$ is lower than the discrete hole correlation on flat plate. There is little coolant remaining on the platform downstream of passage vortex.

The influence of upstream vortex generated by delta wings at different phase positions is shown in Fig. 4.9 – Fig. 4.12. The upstream vortex induced additional turbulence and enhances the coolant and mainstream interaction. For all delta wing configurations, the averaged effectiveness decreases with presence of delta wings prior to the blade passage. In side the blade passages, the effect of upstream vortex is also detrimental except for delta wing h=0.2H at θ=30° and phase 25%. It seems with this configuration, the delta wing generated vortex is directed into the blade passage and competes with blade passage vortex. The strength of blade passage vortex reduces and the mixing between the coolant and the mainstream also reduces. The coolant is more spreaded out. Therefore, for this particular case, the effectiveness in the blade passage is slightly higher than the baseline case. The delta configuration h=0.2H, θ=45° has the largest detrimental effect on effectiveness. The averaged effectiveness has the largest phase dependency for h=0.2H, θ=30°. Although the local film effectiveness distribution

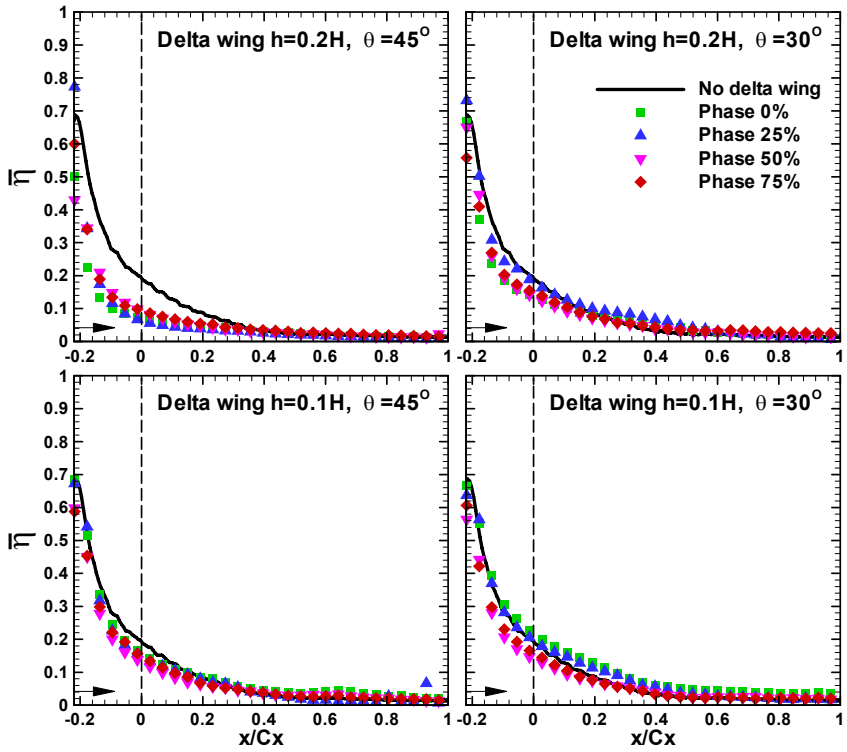

Fig. 4.9 Film cooling effectiveness at various delta wing phases at MFR=0.25% (M=0.17)

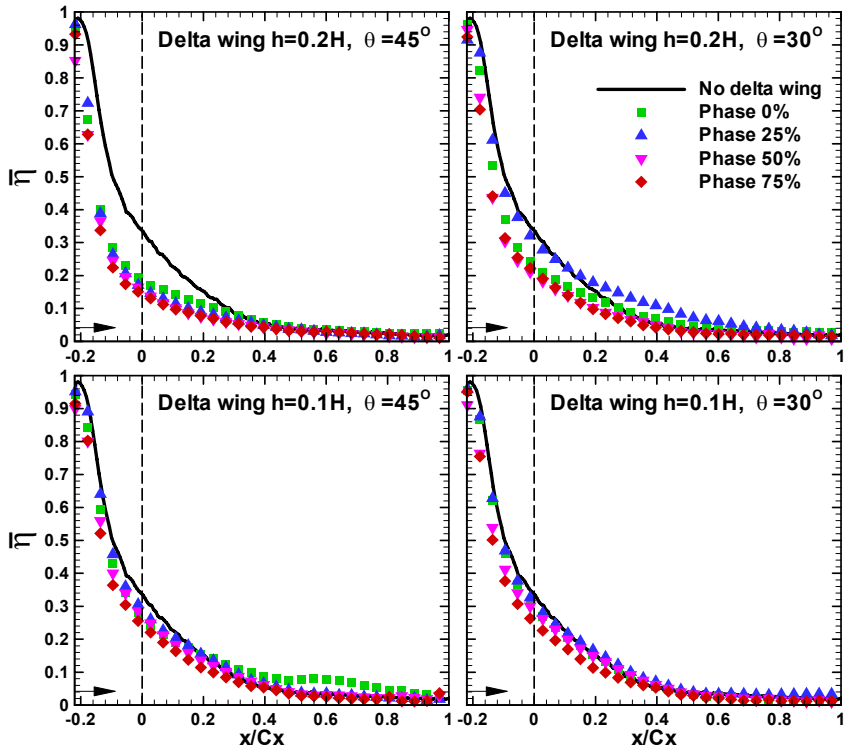

Fig. 4.10 Film cooling effectiveness at various delta wing phases at MFR=0.50% (M=0.33)

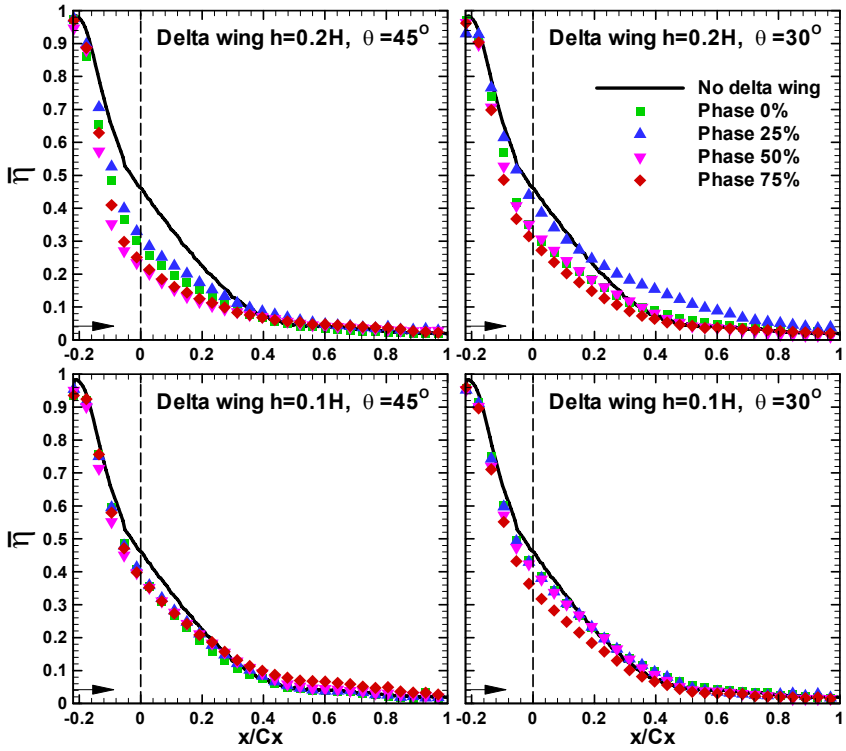

Fig. 4.11 Film cooling effectiveness at various delta wing phases at MFR=0.75% (M=0.50)

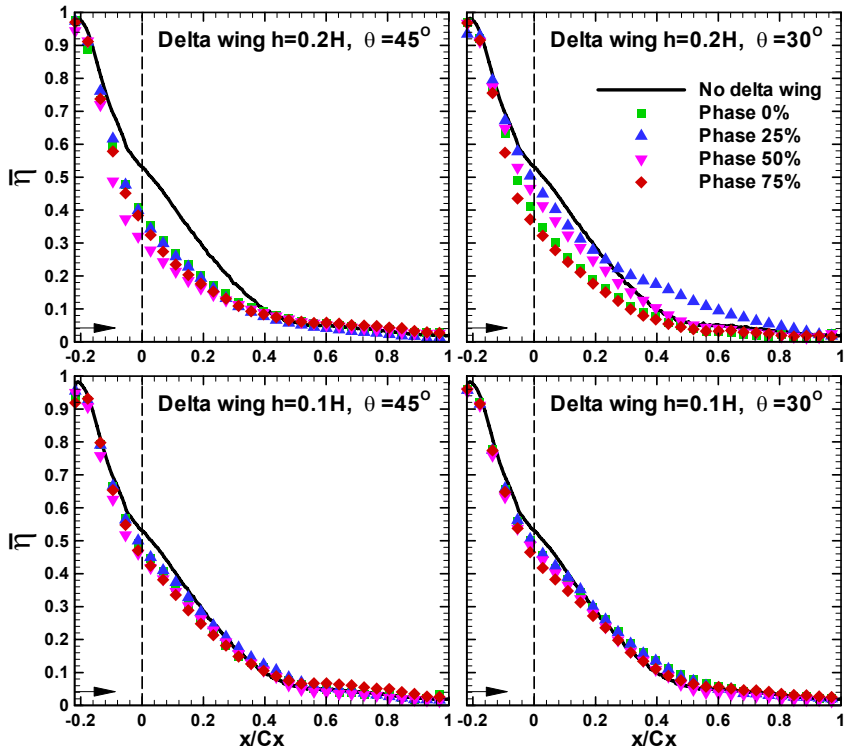

Fig. 4.12 Film cooling effectiveness at various delta wing phases at MFR=1.0% (M=0.67)

is altered at difference phases, the averaged effectiveness from different phases for delta wing h=0.1H are comparable regardless of phase positions. For all the MFRs, the averaged effectiveness decays faster for delta wing h=0.2H with flow attack angle θ=45° that the other delta wing configurations.

Fig. 4.13 and Fig. 4.14 show the effect delta wing configuration on the effectiveness for MFR=0.5% and MFR=1.0%, respectively (the discussion below is valid for MFR=0.25% and MFR=0.75% as well). In general, delta wing h=0.2H shows the more effect than h=0.1H. Attack angle θ=45° has more detrimental effect than θ=30° for delta wing h=0.2H. The effect from different flow attack angles are comparable for delta wing h=0.1H. When x/Cx>0.4, the effect of upstream vortex becomes less noticeable.

To examine the effect of coolant injection ratio, delta wing with the most detrimental is chosen (i.e. h=0.2H, θ=45°). Fig. 4.15 and Fig. 4.16 show effect of coolant mass flow rate. Similar to the case without presence of delta wing, the effectiveness increases with coolant mass flow rate. Examining $\overline{\eta}$ versus x'/ Ms, except at phase 0%, all the data for the other phase positions collapses well. $\overline{\eta}$ is lower than tangential slot correlation and higher than discrete hole correlation near the slot exit. Downstream of the passage, all the coolant are swept away by the passage vortex, so the $\overline{\eta}$ is even lower than discrete hole correlations.

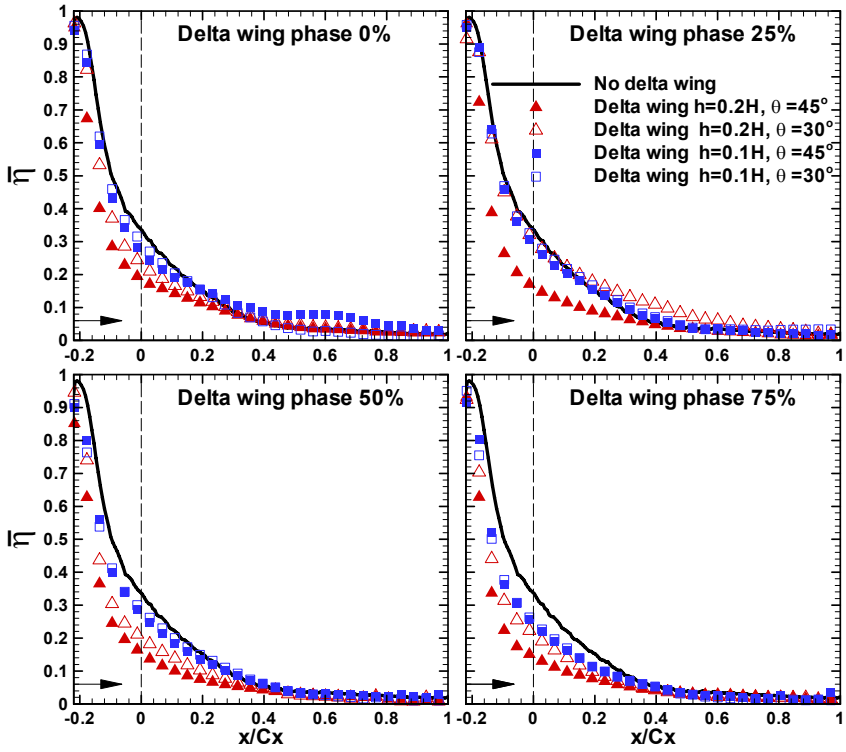

Fig. 4.13 Effect of delta wing configuration on film cooling effectiveness at MFR=0.5% (M=0.33)

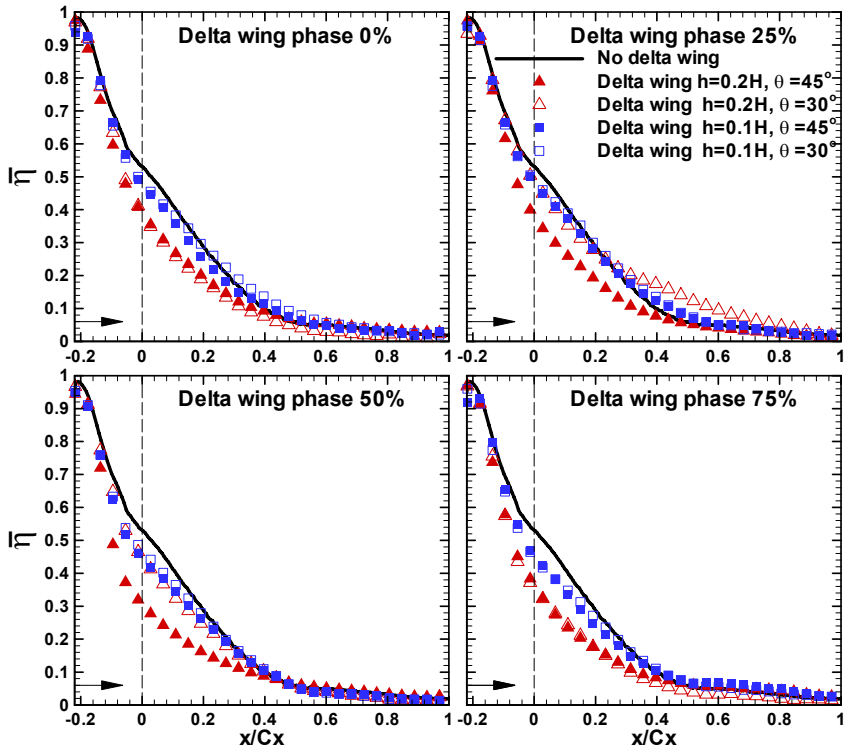

Fig. 4.14 Effect of delta wing configuration on film cooling effectiveness at MFR=1.0% (MFR=0.67)

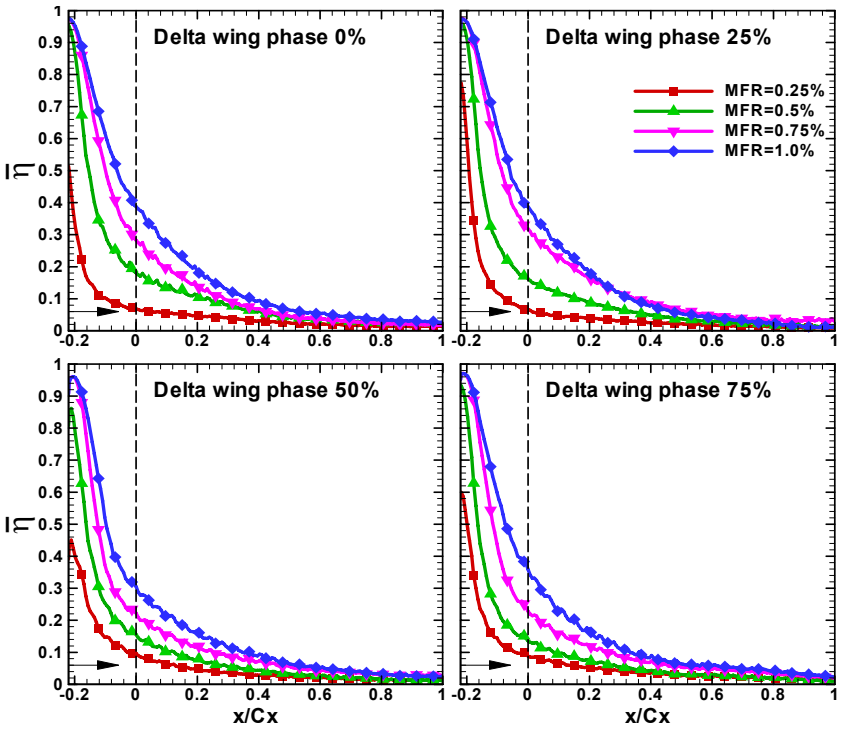

Fig. 4.15 Effect of coolant mass flow rate on film cooling effectiveness for delta wing h=0.2H, θ=45°

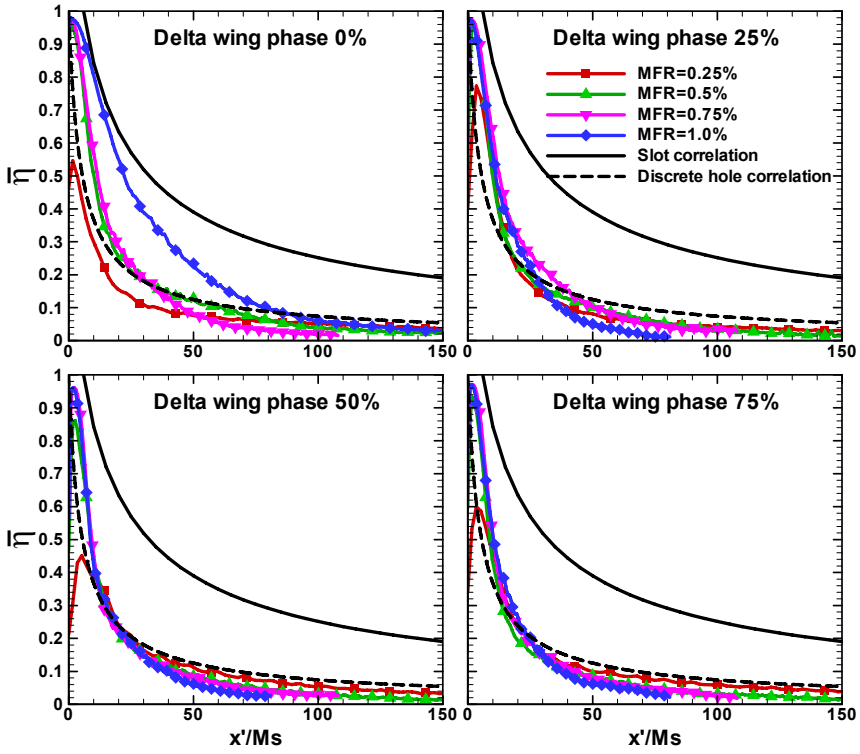

Fig. 4.16 Effect of coolant mass flow rate on film cooling effectiveness for delta wing h=0.2H, θ=45°

4.3 Conclusions

An experimental study was undertaken to measure the film cooling effectiveness on a turbine blade platform within a five-blade linear cascade subject to purge flow from a typical stator-rotor seal. The labyrinth-like seal was located upstream of the blades, and the amount of purge flow through the seal varied from 0.25% to 1.0% of the mainstream flow. Delta wings were used to generate a vortex upstream of the blade passage; this vortex is similar to the passage vortex that would be created as the mainstream flow travels through the vane passage. Pressure sensitive paint was used to measure the film cooling effectiveness. Because the exact strength and structure of the vortex created in the vane passage varies, different size of delta wings combined with different attack angles were considered to show how the effectiveness changes when the upstream vortex structure changes. In general, the film cooling effectiveness increases with increasing coolant mass flow rate. The presence of upstream vane passage vortex is detrimental to the platform slot purge cooling, particularly, in the region between the purge slot and about the first half of platform ($x/Cx<0.4$). The strong mixing between the coolant and blade passage vortex causes effectiveness vanishing downstream of passage vortex. Depending on the phase position, the pattern of the effectiveness distribution alters. The larger delta wings ($h=0.2H$) have more effect on platform film cooling effectiveness than the smaller delta wings ($h=0.1H$). Combined with attack angle $\theta=45°$, delta wings with $h=0.2H$ have the largest adverse effect on film effectiveness. Delta wings $h=0.1H$ show the same level of influence on the film cooling effectiveness at the attack angle 30° and 45°.

5. INFLUENCE OF HOLE SHAPE AND ANGLE ON SHOWERHEAD FILM COOLING

5.1 Experimental Facilities

Test for leading edge film cooling study is done in a low speed wind tunnel. Fig. 5.1 schematically shows the experimental setup. The mainstream flow travels through a nozzle and into the test tunnel. The test section is placed in the wind tunnel. The center of the cylinder is located at 73.7 cm downstream of the nozzle exit. The mainstream flow is adjusted to maintain a Reynolds number of 100,900 (based on the cylinder's diameter). To increase the freestream turbulence of the mainstream flow, a turbulence grid is added at the exit of the nozzle. With the grid, turbulence intensity of 7% with turbulence integral length scale about 1.5cm is measured near the cylinder. Fig. 5.1(a) also shows the position of excitation light and camera for PSP measurement. A close view of the test section is shown in Fig. 5.1(b). The turbine blade leading edge is modeled as a blunt body with a semicylinder and an afterbody. The semicylinder, made of Stereolithography (SLA), can be detached from the afterbody when changing film cooling hole configuration. The semi-cylinder has a diameter of 7.62 cm, height of 25.4 cm, and a wall thickness of 0.64 cm. The hollow semicylinder serves as a coolant plenum. Coolant flow travels through an orifice flow meter and enters the cylinder from bottom. The coolant is discharged to mainstream through the film cooling holes. Definition of coordinate can also be found in Fig. 5.1(b). The coordinate is used to present the effectiveness data.

Two film cooling designs are considered: a heavily film cooled leading edge feathered with seven rows of film cooling holes, and a moderate case with three rows.

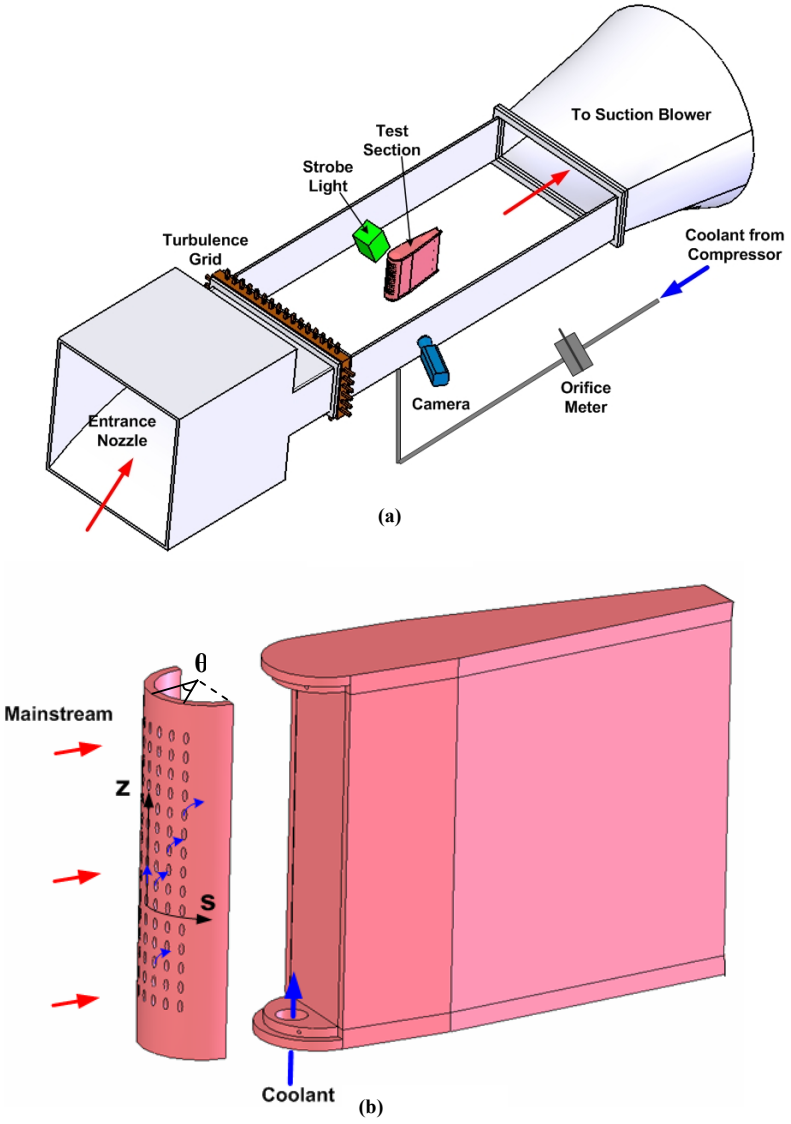

Fig. 5.1 (a) Test facilities (b) test section

Four different film cooling hole configurations are applied for each design: radial angle cylindrical holes, compound angle cylindrical holes, radial angle shaped holes and compound angle shaped holes. In total, eight leading edge film cooled models are investigated. Fig. 5.2 shows the seven-row film-hole configurations. The seven rows are located at 0° (stagnation line), ±15°, ±30° and ±45°. For the radial angle holes (either cylindrical holes or shaped holes), the holes are oriented in the radial (spanwise) direction and orthogonal to the local mainstream direction. While for the compound angle holes, each row oriented at different angles with respect to the local mainstream due the constraint of space. As shown in Fig. 5.2(b) and Fig. 5.2(d), the holes are oriented (β) at 90°, 75°, 67.5°, and 60° to the local mainstream direction for the row 0°, ±15°, ±30° and ±45°, respectively. Fig. 5.3 shows the three-row film-hole configurations. The three rows of holes are located at 0° (stagnation line) and ±30° on either side of cylinder. The holes at ±30° are oriented at 67.5° to the local mainstream direction in the compound angle design. The stagnation row is always angled to the radial (spanwise) direction. For both seven-row and three-row designs, each row has 15 holes with a p/d of 4. Fig. 5.4 shows hole orientations and the shaped hole angles. All these holes were angle (α) at 25° to the model surface and arranged inline pattern. The shaped holes are laidback fanshaped holes with lateral expansion (γ) of 5° from the hole centerline, and additional 5° forward expansion (δ) to the surface. The metering part of the shaped holes has the same diameter (d=0.32cm) as the cylindrical holes. The expansion of shaped holes starts in the middle of hole. This results in a area ratio about 2 between the expanded cross section at the hole exit and the metering part. Details of holes dimension can be found in Table 5.1.

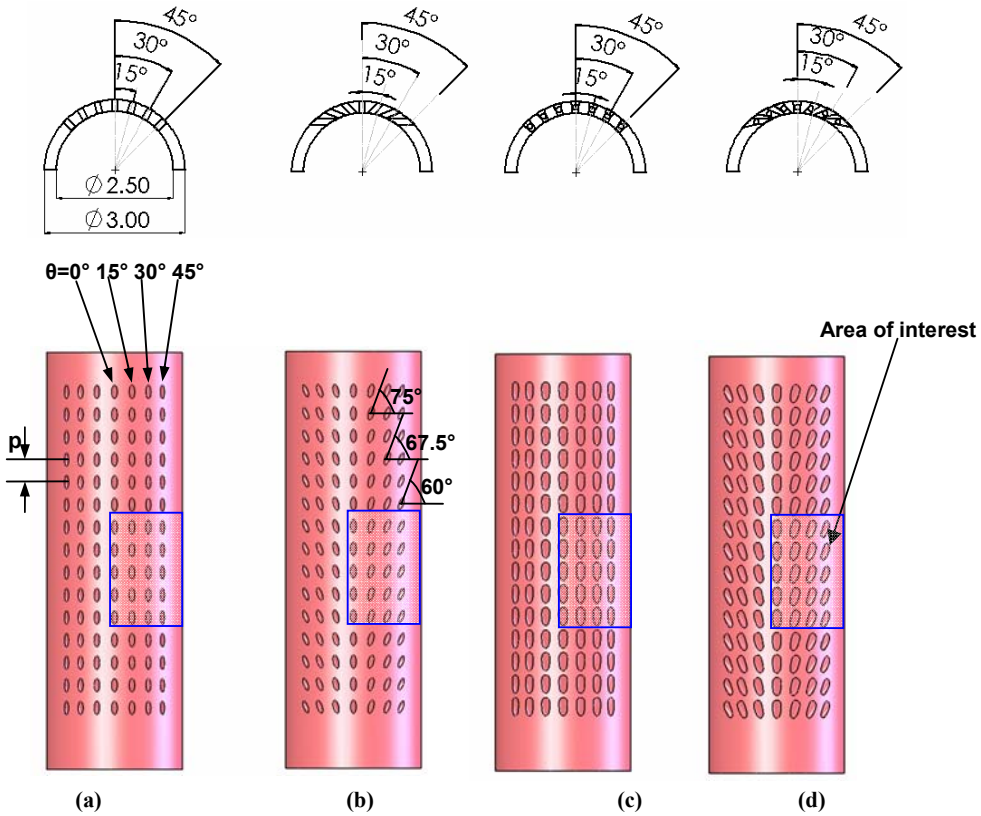

Fig. 5.2 Seven-row film cooled leading edge models (a) radial angle cylindrical holes (b) compound angle cylindrical holes (c) radial angle shaped holes (d) compound angle shaped holes

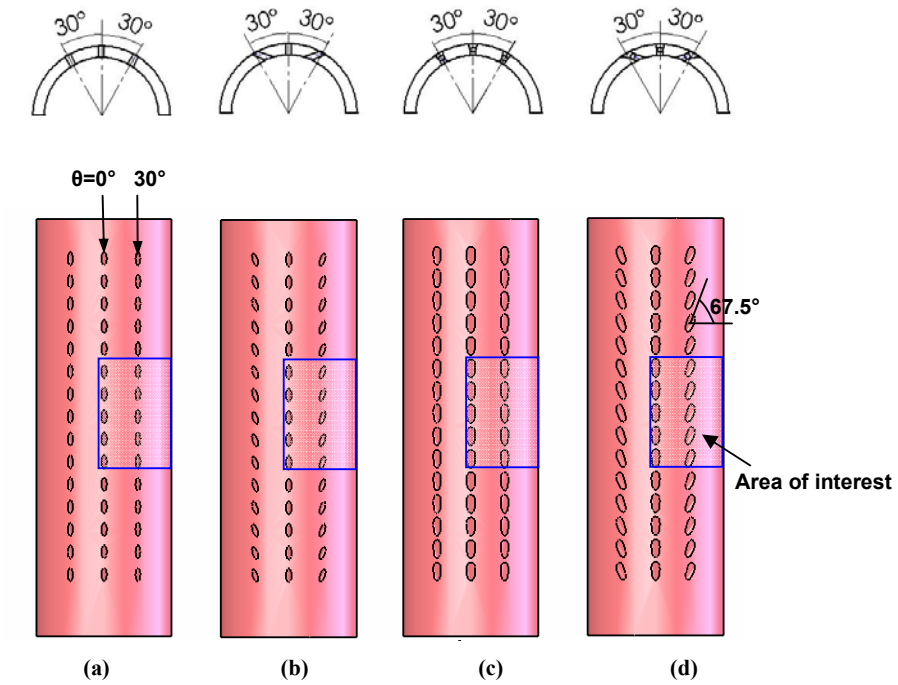

Fig. 5.3 Three-row film cooled leading edge models (a) radial angle cylindrical holes (b) compound angle cylindrical holes (c) radial angle shaped holes (d) compound angle shaped holes

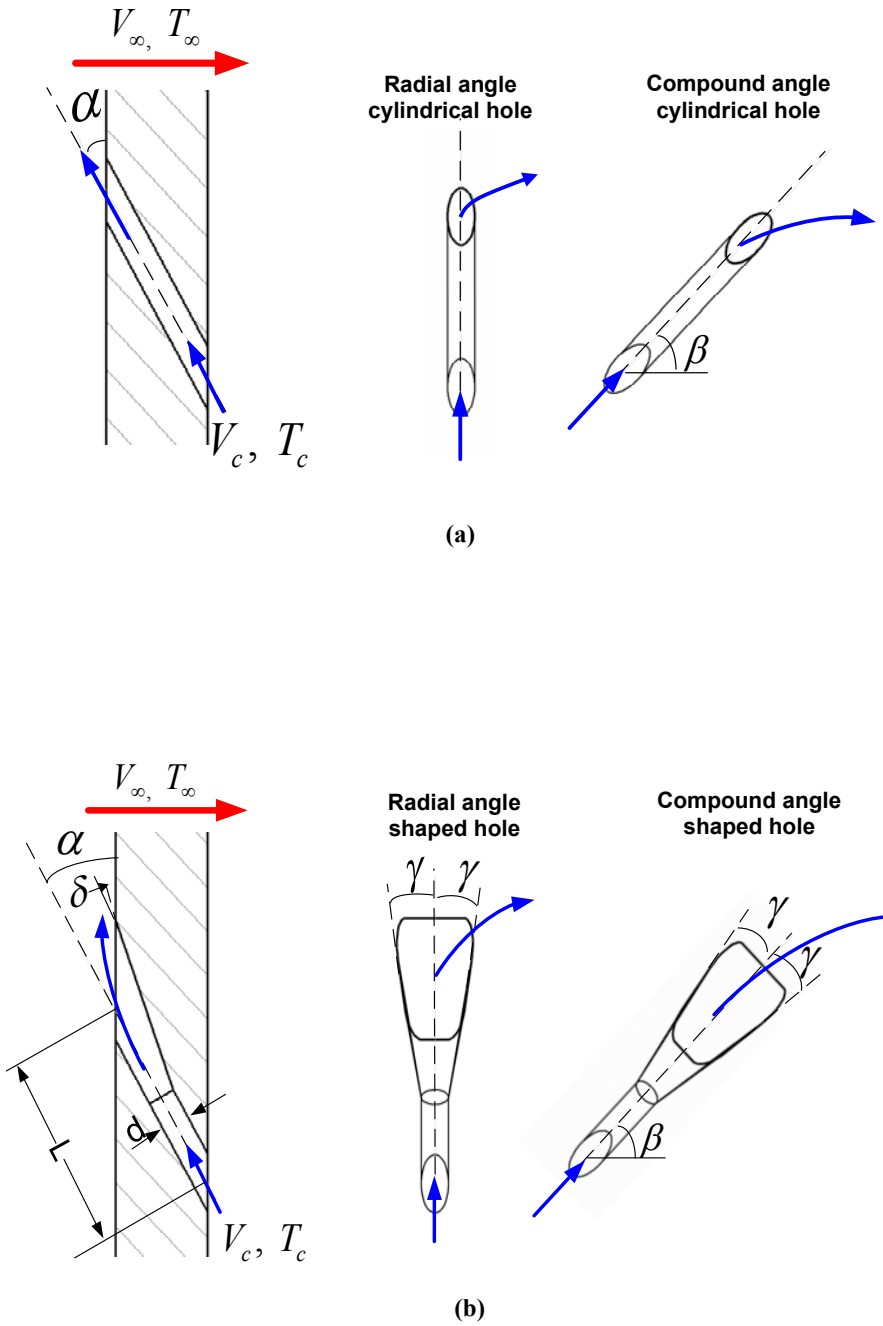

Fig. 5.4 Definition of hole shape and orientations (a) cylindrical hole (b) shaped hole

Table 5.1 Film Cooling Hole Configurations

Design 1 (Seven-row)				
Hole configurations	cylindrical holes		shaped holes	
	Radial angle	Compound angle	Radial angle	Compound angle
Hole diameter (d, cm)	0.3715	0.3715	0.3715	0.3715
Diameter ratio (D/d)	24	24	24	24
Hole to hole spacing (p/d)	4d	4d	4d	4d
Ratio of hole length to diameter (L/d)	4.73	4.73~5.46	4.73	4.73~5.46
Lateral expansion angle (γ, °)	0	0	5	5
Forward expansion angle (δ, °)	0	0	5	5
Angle to surface (α, °)	25	25	25	25
Streamwise angles (β, °)	90	90/75/ 67.5/60	90	90/75/ 67.5/60
Ratio of hole breakout area to metering cross-section area	1.0	1.0	1.9	1.9/1.94/1.98/2.1
Design 2 (Three-row)				
Hole configurations	cylindrical holes		shaped holes	
	Radial angle	Compound angle	Radial angle	Compound angle
Hole diameter (d, cm)	0.3715	0.3715	0.3715	0.3715
Diameter ratio (D/d)	24	24	24	24
Hole to hole spacing (p/d)	4d	4d	4d	4d
Ratio of hole length to diameter (L/d)	4.73	4.73~5.46	4.73	4.73~5.46
Lateral expansion angle (γ, °)	0	0	5	5
Forward expansion angle (δ, °)	0	0	5	5
Angle to surface (α, °)	25	25	25	25
Streamwise angles (β, °)	90	90/67.5	90	90/67.5
Ratio of hole breakout area to metering cross-section area	1.0	1.0	1.9	1.9/1.98

5.2 Results and Discussion

Due to the geometric symmetry and flow symmetry, only one-side midspan portion of cylinder was painted with PSP as indicated in Fig. 5.2 and Fig. 5.3. During the test, five averaged blowing ratios were examined ranging from M=0.5 to M=2.0. The driving force for the coolant to eject through the holes is pressure differential between the internal (coolant plenum) total pressure and external static pressure. The higher the pressure differential, the more the coolant ejects from the holes. Figure 5.5 schematically shows the coolant mass flow rate distribution. It is reasonable to assume that internal total pressure is constant in the midspan region of the cylinder for a given average blowing ratio. This assumption won't cause significant error in the calculation of discharge coefficients. However, the external static pressure along the curved surface varies with the biggest static pressure existing on the stagnation line. From stagnation to downstream, the surface static pressure gradually decreases and the driving force (the difference between internal pressure and external pressure of the cylinder) the gradually increases. Therefore, the least amount of coolant ejection occurs to the stagnation row. More coolant ejects from the downstream rows. This non-uniform coolant ejection will influence the film cooling effectiveness distribution on the leading edge surface.

The film-cooling effectiveness distribution on the leading edge models for the seven-row design is shown in Fig. 5.6. The white line through the film holes represents the stagnation line. The effectiveness is presented at five average blowing ratios ranging from M=0.5 to M=2.0. Although the film hole configurations are different, some common characteristic can be observed. Near the stagnation, the mainstream momentum is small, so the coolant jets from stagnation row basically go to radial

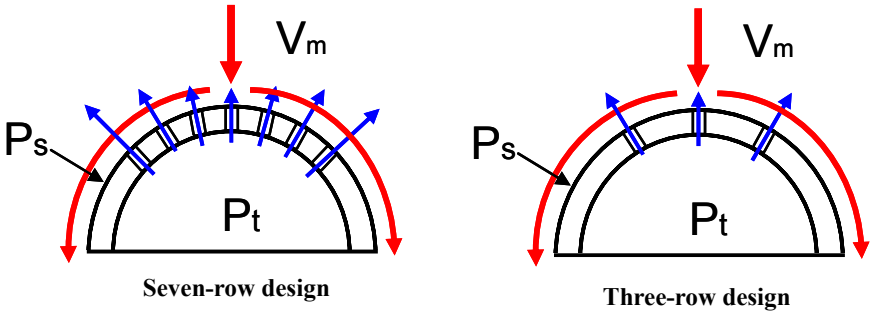

Fig. 5.5 Schematic of local coolant mass flow rate distribution

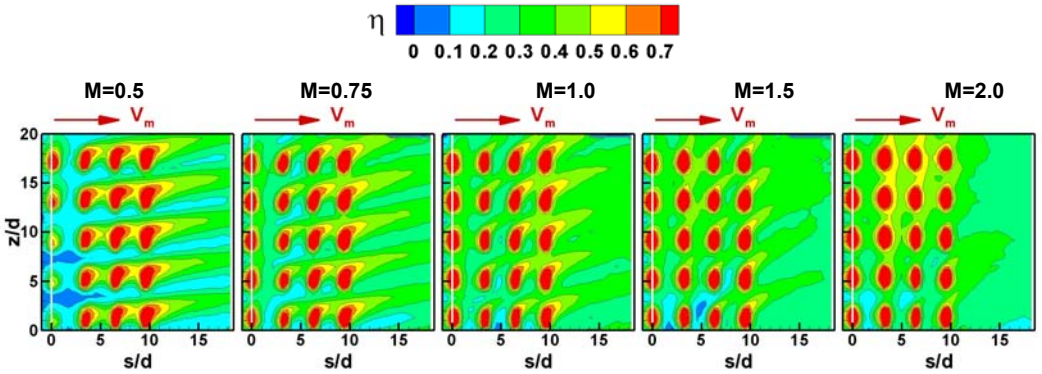

(a) Radial angle cylindrical holes

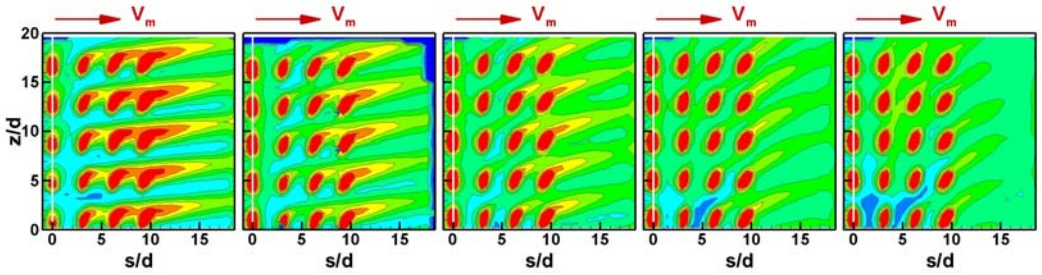

(b) Compound angle cylindrical

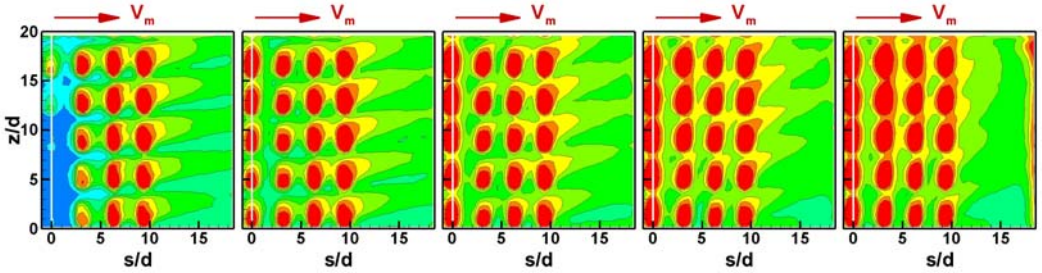

(c) Radial angle shaped holes

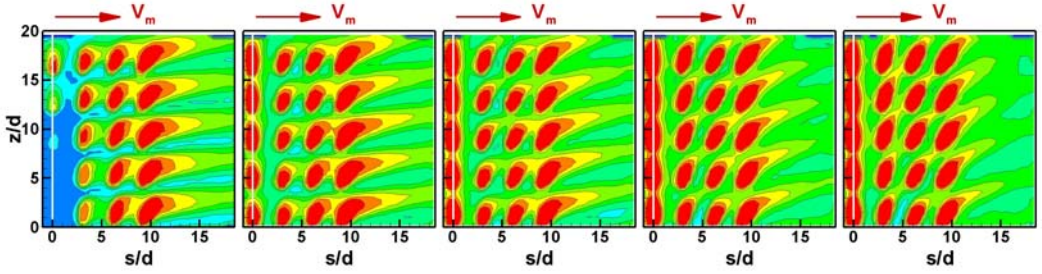

(d) Compound angle shaped holes

Fig. 5.6 Film cooling effectiveness distribution for seven-row design

direction without being deflected. In the downstream region, the mainstream momentum increases. Subjected to the mainstream, the coolant jet is deflected. When the jet momentum increases (i.e. average blowing ratio increases), the deflection decreases. The jets are less deflected at higher average blowing ratio. The jets tend to go to more radial directions at higher average blowing ratio M=1.5 and M=2.0. Therefore, the upper portion of the leading edge model (with larger z/d) gains higher effectiveness due to coolant accumulation; while the effectiveness in the region downstream of film cooling holes (s/d>10) is reduced compared with lower average blowing ratios. At lower average blowing ratio M=0.5 to M=1.0, the coolant jets are more deflected to the streamwise direction, so the coolant accumulation effect is evident downstream of film cooling rows. This is featured with a larger downstream area covered by elevated film cooling effectiveness. On the contrary, the coolant accumulation in the radial direction is not significant at these lower average blowing ratios. As the jet momentum increases from M=0.5 to M=2.0, the coolant jets tend to life off the surfaces. The area with elevated effectiveness reduces. In the region near the stagnation (0<s/d<6), the effectiveness seems to increase with increasing of average blowing ratios; Further downstream, (s/d>10) the film effectiveness decreases with increasing of average blowing ratios. Near the stagnation region, the mainstream momentum is small; the jet interaction with mainstream is weak. In addition, the small incline angle (α=25°) helps the coolant remain closer to the surface. More coolant accumulates around the stagnation region with more coolant injection. In the downstream region, the mainstream momentum increases. The interaction (mixing) between the coolant jet and mainstream enhances. The high the jet momentum, the stronger the interaction (mixing)

is. Therefore, the effectiveness decreases when average blowing ratio increases at s/d>10.

The effect of hole angle can be detected by comparing Fig. 5.6(a) and Fig. 5.6(b) with cylindrical holes. For the compound angle holes, the angles of film holes to mainstream reduces (except the stagnation rows), the coolant jets are less deflected. Consequently, the coolant trace with elevated effectiveness become narrower but longer instead of spread-out. The coolant accumulation in the radial direction, compared with radial angle holes, is less significant even at the highest average blowing ratio M=2.0. At lower average blowing ratios (M=0.5 and M=0.75), it seems that the compound angle holes result in higher effectiveness than the radial angle holes. However, at higher average blowing ratios (M=1.5 and M=2.0), the effectiveness from compound angles cylindrical holes seems lower than that from radial angle cylindrical holes. This is largely due to the less jet spread-out with the compound angle holes.

Fig. 5.6(c) shows the effectiveness distribution for radial angle shaped holes. Compared with the cylindrical holes (both radial angle and compound angle), the effectiveness for the shaped holes significantly increases except stagnation row at M=0.5. The jet momentum reduces due to hole expansion for the shaped holes. With lower jet momentum, the coolant tends to stay closer to the surface and offers better film protection. The advantage of the shaped holes becomes more evident at higher average blowing ratios. Similar to the radial angle cylindrical holes, the streamwise coolant accumulation is more noticeable at lower average blowing ratios; the spanwise (radial) coolant accumulation is more evident at higher average blowing ratios. The film effectiveness between the hole row ($0<s/d<10$) increases with increasing of average

blowing ratio. This is consistent with the observation from the radial angle cylindrical holes. However, further downstream, (s/d>10), the effectiveness for the radial angle shaped hole doesn't decrease monotonically with increasing of average blowing ratios. The best film coverage is obtained at about M=1.0. At lowest average blowing ratio M=0.5, the pressure inside the cylinder is low. The high outer pressure in the stagnation region prohibits coolant ejecting from these stagnation holes. More coolant is directed to the downstream holes.

Fig. 5.6(d) shows the effectiveness distribution for the compound angle shaped holes. Compared with it radial angle counterpart, the coolant trace with elevated effectiveness for the compound angle shaped holes becomes narrower and longer. This is similar to the observation for the cylindrical holes at different angles. At higher average blowing ratios M=1.5 and M=2.0, the effectiveness reduces because the coolant jets less spreads out. The area between the holes (in radial direction) is less protected. At lower average blowing ratios M=0.5 to M=1.0, the compound angle shaped holes seems offers better effectiveness than radial angle shaped holes for the region s/d>10.

Fig 5.7 and Fig. 5.8 are the spanwise averaged effectiveness for the seven-row models. The data are presented in terms of s/d and θ (angles to the stagnations line), which are depicted in the bottom and top x-axes, respectively. The peak of the effectiveness corresponds to the location of film cooling rows. Fig. 5.7 shows influence of average blowing ratio on film cooling effectiveness. The film cooling effectiveness near the stagnation region (s/d<6 or θ<30°) increases with increasing of average blowing ratios. Further downstream (s/d>10 or θ>45°), the trend reversed. With multiple rows of film cooling design, the coolant accumulation effect can be detected from the

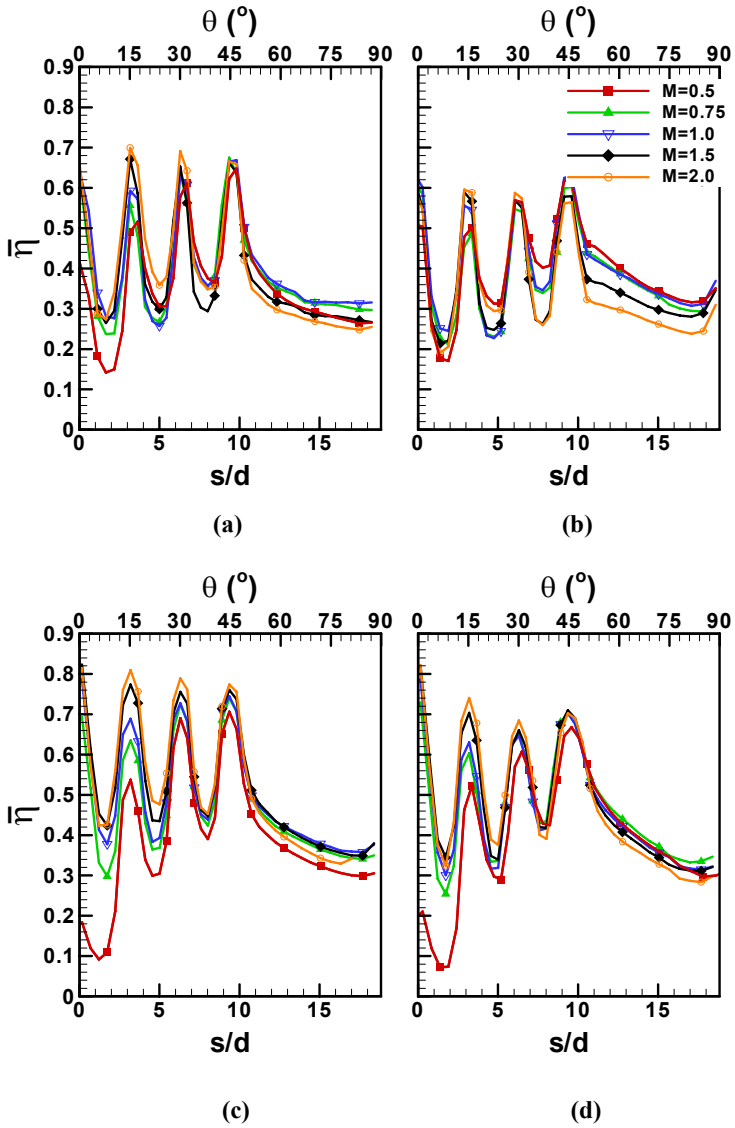

Fig. 5.7 Effect of blowing ratio on spanwise averaged film effectiveness (seven-row design)
(a) radial angle cylindrical holes (b) compound angle cylindrical holes
(c) radial angle shaped holes (d) compound angle shaped holes

elevated effectiveness in the downstream region. The effectiveness variation with averaged blowing ratio is relatively small for the shaped holes, particularly, for the compound angle shaped holes.

Fig. 5.8 shows the effect of hole configurations on film cooling effectiveness. For the stagnation rows, the holes are all angle to the radial direction, therefore, the lines for the same hole shape fall together. In general the shaped holes (red line) give better effectiveness than the cylindrical holes (black line) except at very low average blowing ratio M=0.5. Between the hole rows (0<s/d<10), the radial holes (both cylindrical hole and shaped holes) offer higher effectiveness than their compound angle counterparts. Downstream of film holes (s/d>10), the compound angle holes offer higher effectiveness at lower average blowing ratios (M=0.5 and M=0.75). At higher average blowing ratios (M=1.5 and M=2.0), the effectiveness from the radial angle shaped holes is slightly higher than compound angle shaped holes; the compound angle cylindrical higher than the radial angle cylindrical holes.

Fig. 5.9 shows the film cooling effectiveness distribution for the three-row film cooling design. It can be seen that effectiveness level dramatically decreases with less number of film cooling holes. However, some characteristics observed in seven-row design also take place in the three row design. When the average blowing ratios increase, the effectiveness in the stagnation region (between the film rows) increases; it decreases in the downstream (s/d>7) region. The mainstream momentum is small in the stagnation region; the jet interaction with mainstream is limited. More coolant is accumulated in this region and convected to downstream with more coolant injection. Further downstream, the mainstream momentum increases. The interaction between the

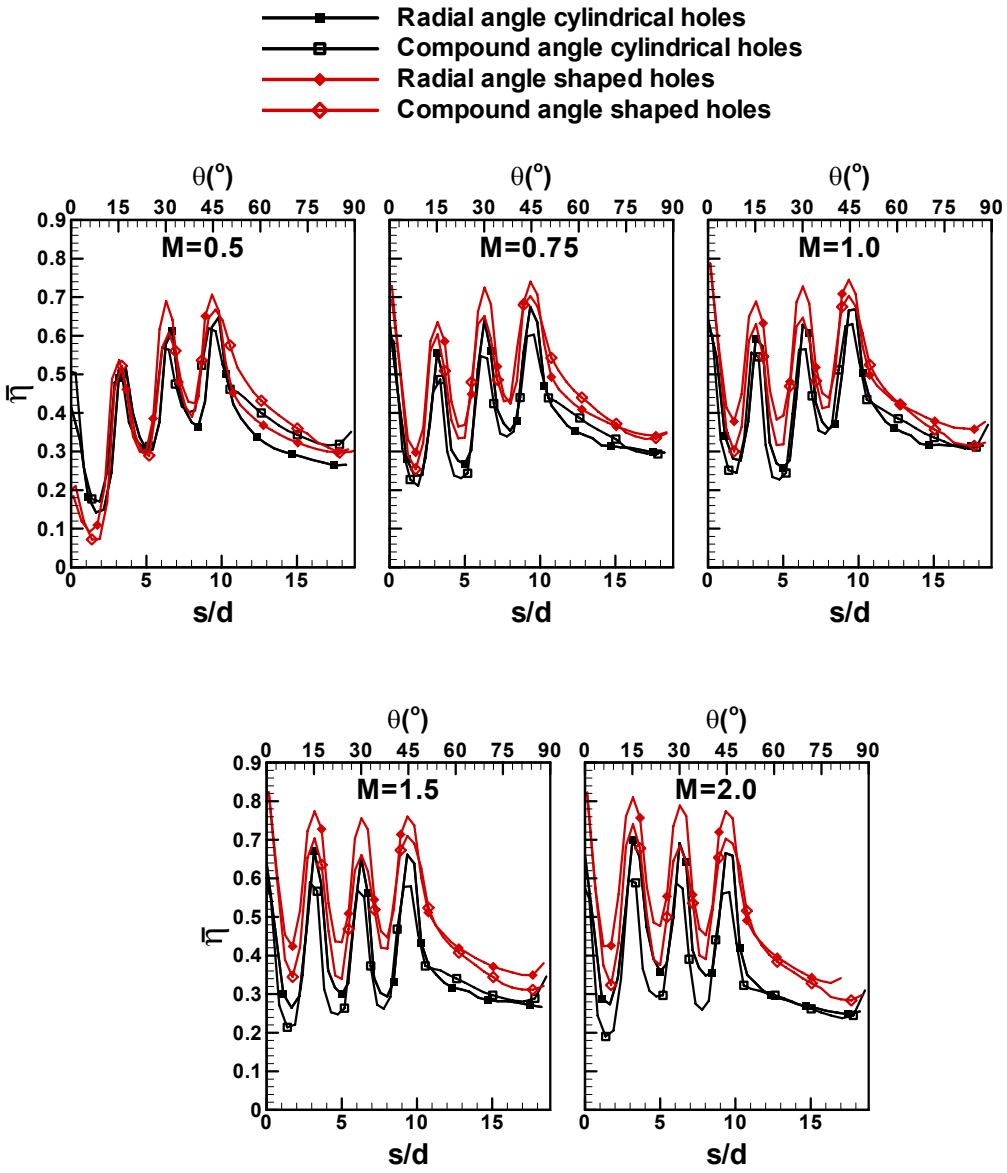

Fig. 5.8 Effect of hole configuration on spanwise averaged film effectiveness (seven-row design)

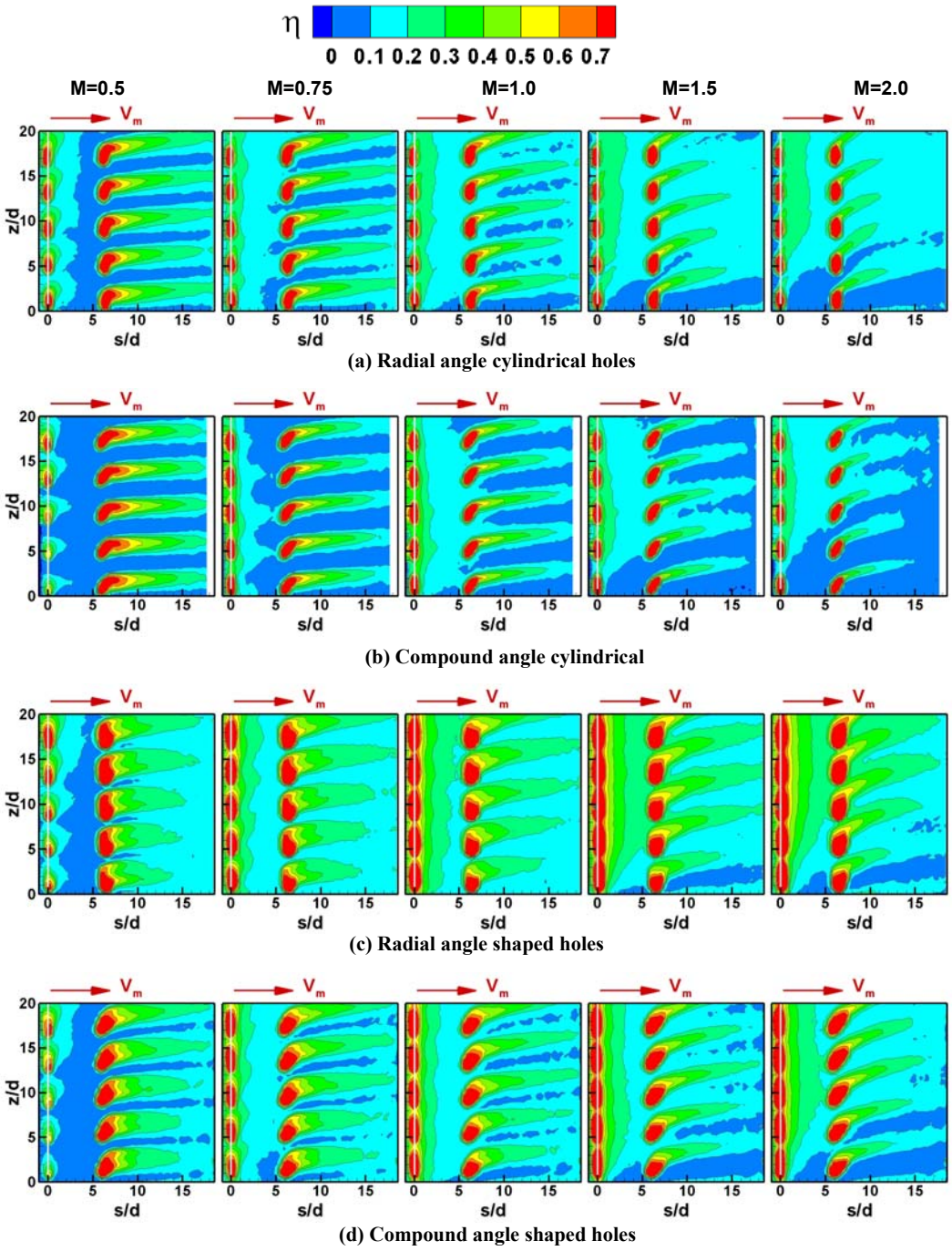

(a) Radial angle cylindrical holes

(b) Compound angle cylindrical

(c) Radial angle shaped holes

(d) Compound angle shaped holes

Fig. 5.9 Film cooling effectiveness distribution for three-row design

coolant and the jet is enhanced. When the jet momentum increases, the jets are less deflected by the mainstream, and tend to penetrate the mainstream. Therefore, the effectiveness on the surface reduces. For the same hole geometry (either cylindrical hole or shaped hole), it can been seen that the coolant jets from compound angle holes are narrower than that from radial angle holes. The jets less spread out and film coverage reduces. When compared with the cylindrical holes, the superiority of shaped holes in film coverage is obvious, particularly at higher average blowing ratios.

Figure 5.10 shows the average blowing ratio effect on spanwise averaged effectiveness for the three-row design. When the average blowing ratio increases, the effectiveness in the area between the stagnation row and downstream row ($s/d<5$) increases for all these hole configurations. However, the trend reverses further downstream ($s/d>7$). The effectiveness for the shaped holes is relatively insensitive to average blowing ratio variation in this region ($s/d>7$), particularly for the radial angle shaped holes.

The comparison of spanwise averaged film cooling effectiveness from different hole configurations is shown in Fig. 5.11**.** The radial angle shaped holes give best film cooling effectiveness. The evidence is more observable at higher averaged blowing ratios. In general, the shaped holes give better effectiveness than cylindrical holes; the radial angle holes give better effectiveness than compound angle holes.

Fig. 5.12 shows the area averaged film cooling effectiveness. The abscissa is coolant mass consumption normalized with the case of seven-row at M=1. The seven-row design produces better effectiveness than the three-row at similar coolant consumption. The area averaged effectiveness from the radial angle holes is higher than

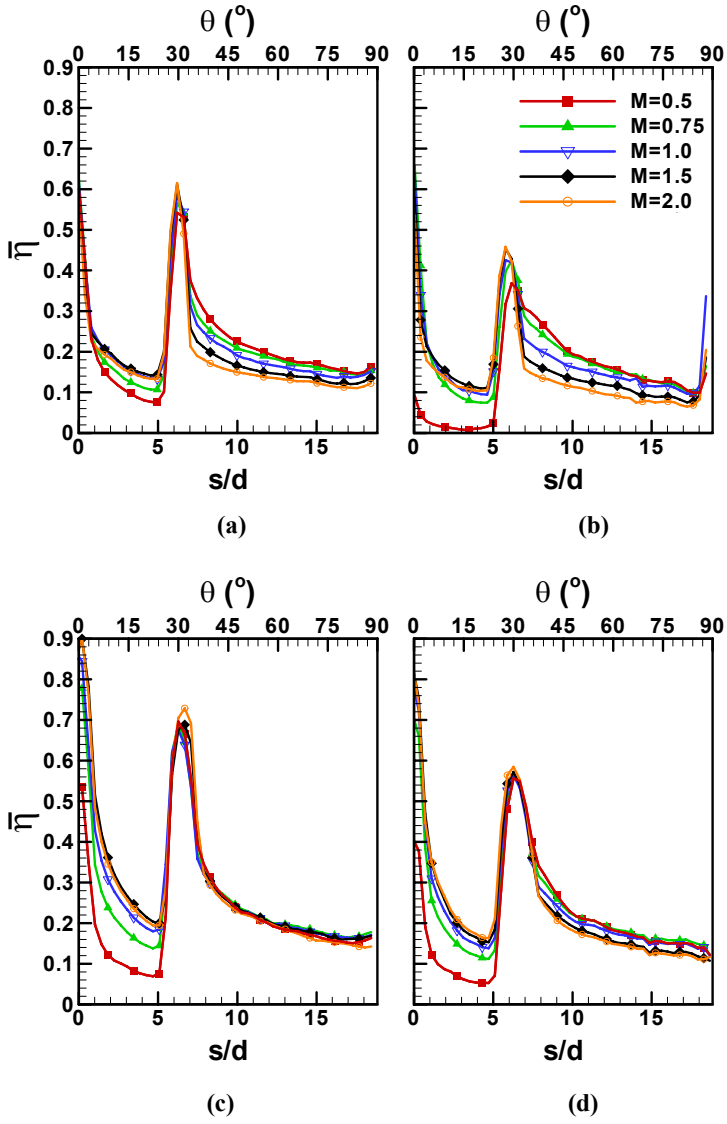

Fig.5.10 Effect of blowing ratio on spanwise averaged film effectiveness (three-row design)
(a) radial angle cylindrical holes (b) compound angle cylindrical holes
(c) radial angle shaped holes (d) compound angle shaped holes

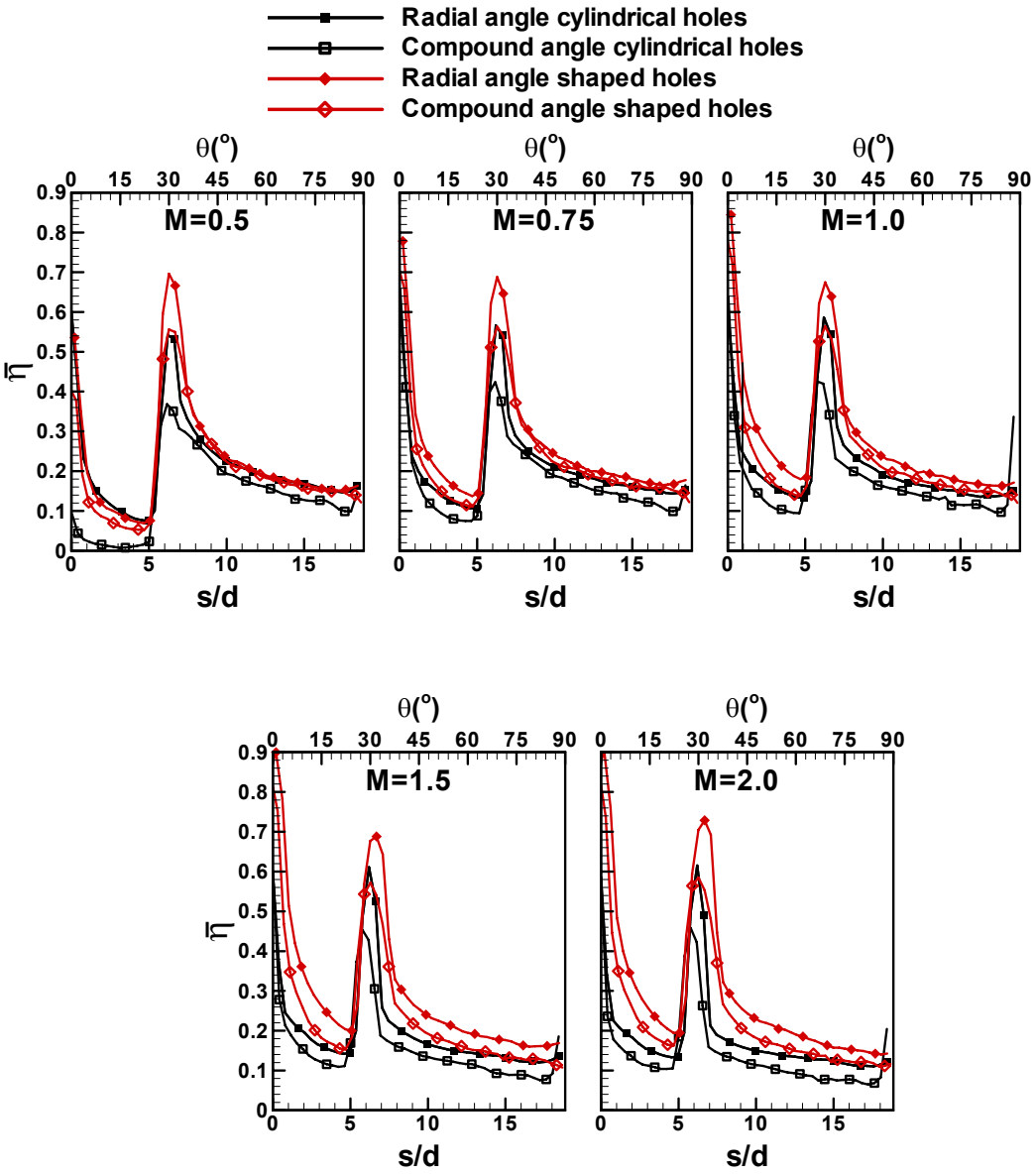

Fig. 5.11 Effect of hole configuration on spanwise averaged film effectiveness (three-row design)

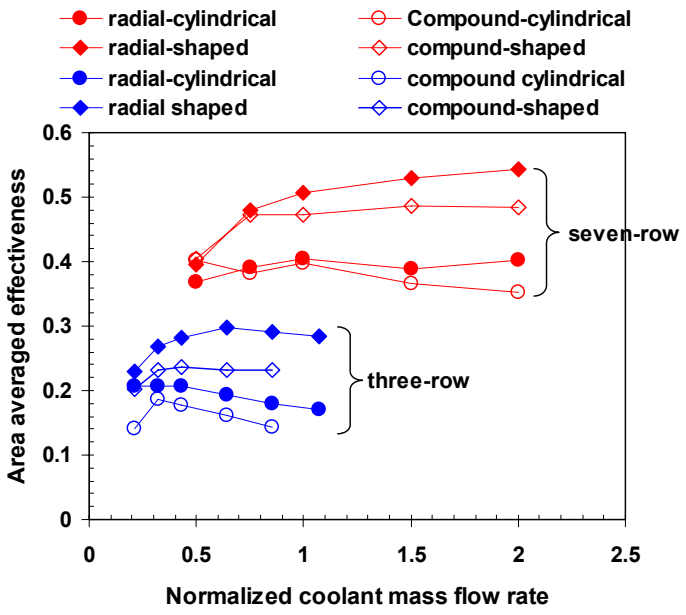

Fig. 5.12 Area averaged effectiveness

the compound angle holes, the shaped holes is higher than the cylindrical holes for both seven-row and three-row designs. The radial angle shaped holes give best film effectiveness among the four configurations.

5.3 Conclusions

Two leading edge film cooling designs were investigated — a heavily film cooled leading edge with seven rows of film holes and a moderately film cooled model with three rows of film holes. For each design, four different film cooling hole configurations were studied. Pressure Sensitive Paint (PSP) experiments were performed to measure the film cooling effectiveness on leading edge models. PSP is the superior method for determining the film cooling effectiveness, especially for the surfaces with heavily distributed film holes. Because PSP relies on the mass transfer rather than heat transfer, inherent problems associated with heat transfer methods are avoided. Main finding from the study are:

1. The film cooling effectiveness for the seven-row design is much higher than that for the three-row design at the same average blowing ratio or at same amount of coolant consumption. Because of large row-to-row spacing, the film accumulation is relatively insignificant for the three-row models. While the jets accumulation enhances for the seven-row models; the superposition of the coolant jets leads to elevated effectiveness level.

   In general, the shaped holes offer higher effectiveness than cylindrical hole at intermediate and high average blowing ratios (M=0.75~2.0) for both the three-row and seven-row designs. The advantage of shaped holes is more evident at higher average blowing ratios (M=1.5 and 2.0). Due to increased breakout area,

the jet momentum from the shaped holes is reduced. Therefore, the coolant jets stay closer to the surface, and result in a higher effectiveness.

2. Compared with compound angle holes, the coolant jets from radial angle holes are more deflected by the mainstream and cover a wider surface area,. For the three-row model, the radial angle holes provide higher effectiveness than its compound angle counterparts. For seven row model, similar behavior is observed at higher average blowing ratios (M=1.0~2.0).

3. For both three-row and seven-row designs, the effectiveness increases with increasing of average blowing ratios in the stagnation region. In the downstream region, the enhanced interaction (mixing) between coolant jets and mainstream cause effectiveness decrease when average blowing ratio increases.

6. EXPERIMENTAL INVESTIGATION OF TRAILING EDGE SLOT FILM COOLING

6.1 Experimental Setup

Fig. 6.1 schematically shows the test facilities and optical setup. The low speed wind tunnel used in leading edge film cooling study is used for this study. The details of wind tunnel setup can be referred to Section 5. For optical access, the side wall of the wind tunnel was made of plexiglass. A CCD camera and a strobe light (excitation light) for the PSP test were placed close to the sidewall. Fig. 6.2(a) shows the schematic of the test section with sidewall removed to expose the interior of the test section. A turbine blade was modeled as a semicylinder followed by a symmetric afterbody. The current study was focused on film cooling on pressure side cutback trailing edge region. The mainstream flow on the suction side has little effect on the pressure side film cooling. A symmetric configuration was chosen because it was easy in fabrication. The trailing portion was tapered with an angle of 6°. The internal cooling design was similar to Lau et al.'s [91]. Lau et al. [91] demonstrated the internal heat transfer on the blade sidewalls was enhanced by 20%-70% with the blockages inserts. In the current design, two impingement plates spaced 3.56 cm apart were inserted into the internal passage. The impingement holes in the two plates, with a diameter of 0.95 cm, were staggered to each other. The cooling air turned to right before passing through the first impingement plates. Coolant jets discharging from the second plate impinged on the internal land of the trailing edge model. The trailing edge model simulated a turbine

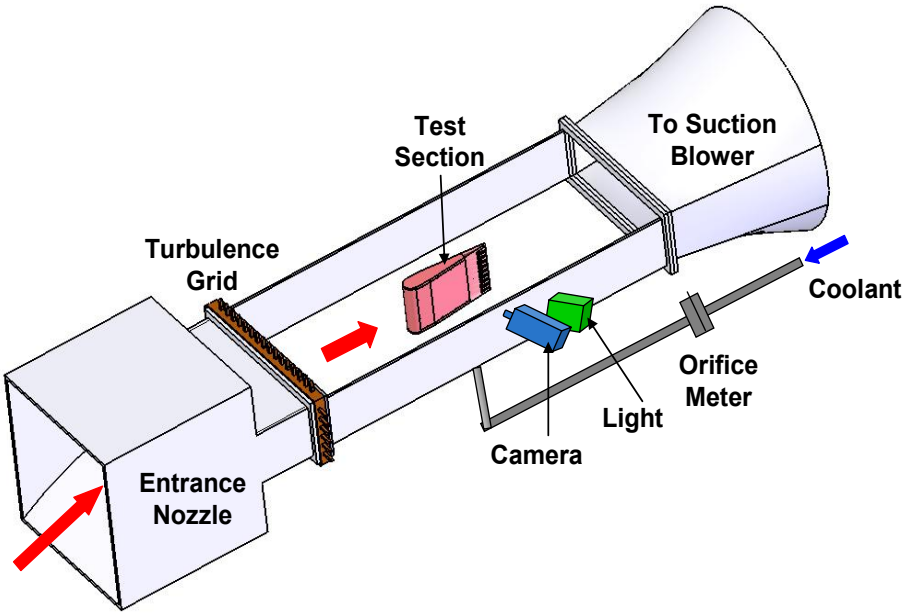

Fig. 6.1 Test facilities and optical setup

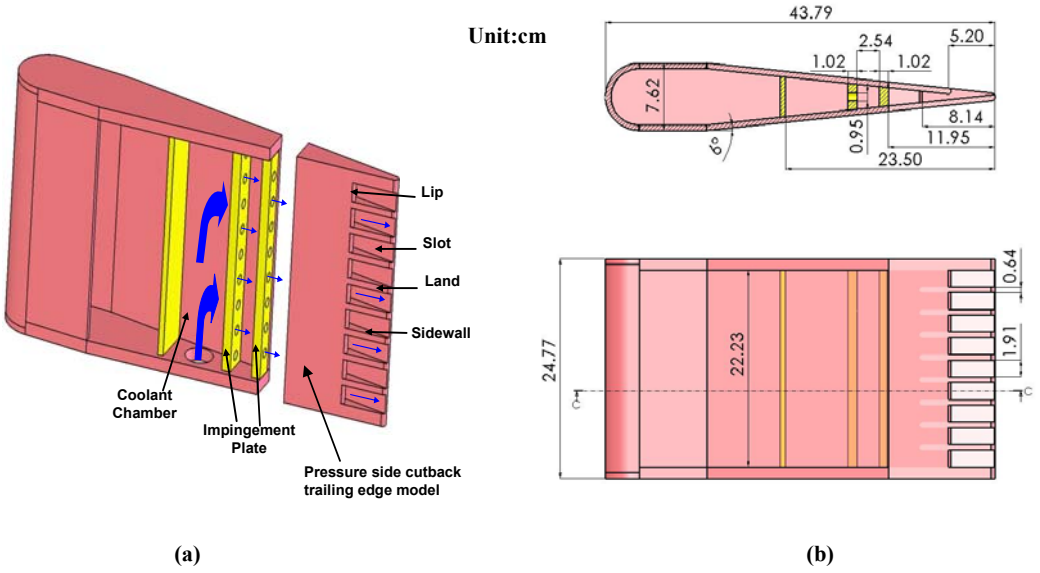

Fig. 6.2 (a) Schematic of test section (b) dimensions of test section

blade trailing edge with pressure side cutback. The cutback trailing edge allows coolant traveling inside the internal cooling passage to discharge through the discrete slots, so that the trailing portion of the blade can be cooled. The notions for the slot are labeled in Fig. 6.2(a); detailed dimensions of the test section can be found in Fig. 6.3(b). To support the trailing edge structure, lands, with width 0.64cm, were periodically placed along the spanwise direction. The land divided the cutback trailing edge into nine discrete slots. Each slot had a width (w) of 1.91cm and length (L) of 5.2cm. Because the lip thickness (t) is an important parameter that affects film cooling effectiveness, three trailing edge configurations with different lip thickness to slot height ratios (t/s) were chosen to study the effect of lip thickness. Fig. 6.3 shows the trailing edge model configurations with t/s of 0.6 (a thin lip), 1.0 (an intermediate thick lip) and 1.4 (a thick lip). The three t/s ratios (0.6, 1.0 and 1.4) were chosen in the range of real turbine blade designs. The configuration with t/s of 1.0 was chosen as a baseline design to evaluate the other designs. In the three designs, the slot height (s) remained constant, i.e. 0.635cm. The ratio t/s was achieved by varying the lip thickness. The geometrical parameters of the slot are also shown in Fig. 6.3.

Tests were done at two different mainstream conditions as shown in Fig. 6.4(a) and Fig. 6.4(b). In the first case, there was no obstruction in the wind tunnel; the flow in the trailing edge portion was slightly decelerated. In the second case, a guide board was inserted in the wind tunnel. The mainstream flow was accelerated about two times from leading edge to the trailing edge. The flow in the second case more resembles the condition in turbine blade cascade environment. For both cases, the mainstream velocity near the trailing edge model was set at 20m/s. The location of pitot tube probes, which

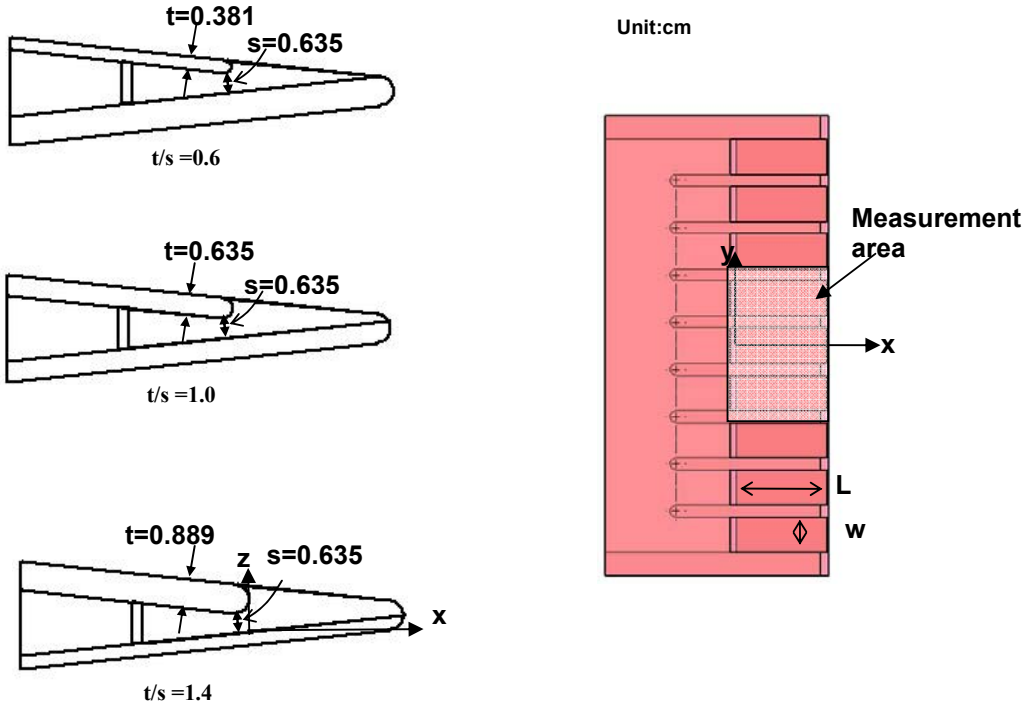

Fig. 6.3 Trailing edge models with geometrical parameters

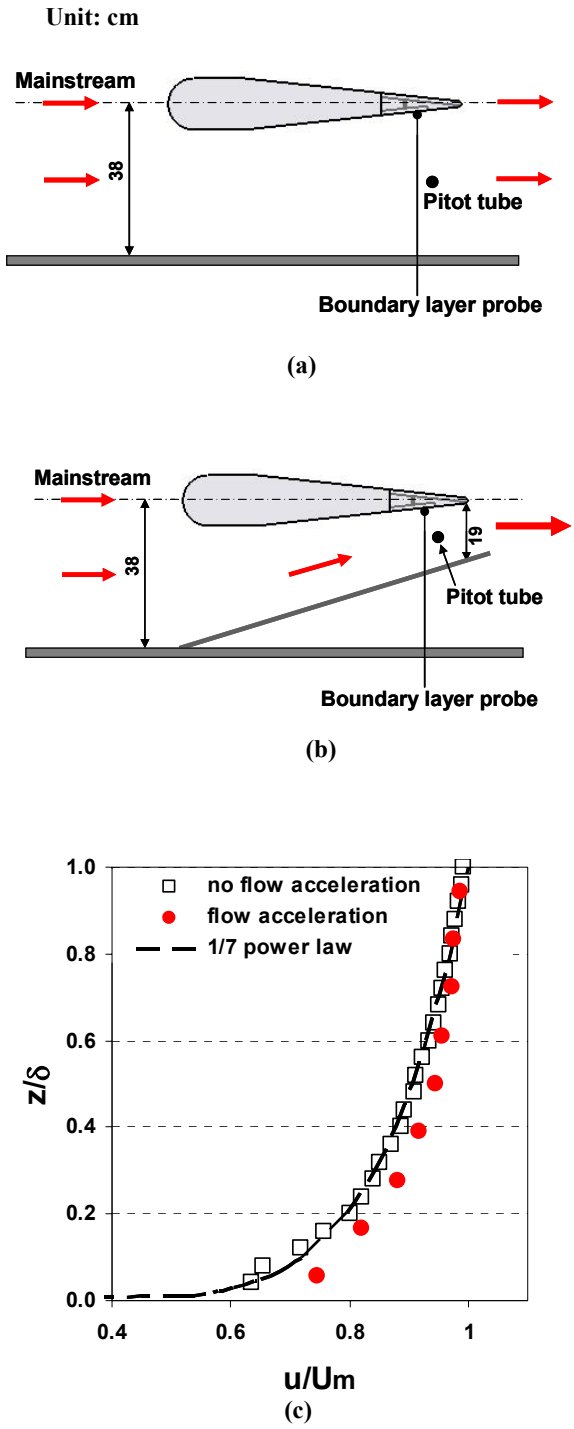

Fig. 6.4 Freestream flow conditions (a) no acceleration (b) with acceleration (c) velocity profile inside boundary layer

measured the mainstream velocity, are indicted in Fig. 6.4. Boundary layer thickness for the two different mainstream flow conditions was measured with a boundary layer probe (total pressure probe). The probe was located 2.5cm upstream of the slot exit. The boundary layer thickness (δ) for the two mainstream conditions was 13mm (case 1) and 8mm (case 2), which corresponded to boundary layer thickness to slot height ratio (δ/s) of 2.1 and 1.3, respectively. In the real engine condition, the δ/s is about 1. So the second case was closer to engine condition. The velocity profile inside the boundary layer was shown in Fig. 6.4(c) and compared with the 1/7 power law.

Table 6.1 shows the test cases for the trailing edge film cooling study. At each mainstream condition, film cooling effectiveness was measured at different blowing ratios. The blowing ratio was defined as the coolant mass flux ratio to mainstream mass flux ratio, i.e., $M=\rho_c V_c/\rho_m V_m$. For the baseline configuration (t/s=1.0), five blowing ratios were tested covered a range of 0.25 to 1.5. For the other two configurations, three typical blowing ratios were tested, i.e. M=0.5, 1.0 and 1.5.

6.2 Results and Discussions

To aid understanding of the film cooling effectiveness data, Fig. 6.5 shows conceptual view of interaction between the mainstream and the coolant. Similar to the wake generated by the blade trailing edge, small wakes (eddies) was created by the lip at the slot exit. The wakes bring additional turbulence and enhance the mixing between the coolant and the mainstream. Thicker lips generate larger wakes. When ejecting from the slots, the coolant also experience expansion in both spanwise (y) and pitchwise (z) direction. Therefore, coolant may also climb over the land to gain film effectives.

Table 6.1 Test Cases for Trailing Edge Slot Film Cooling

	δ/s=2.1	δ/s=1.3
Configuration. 1 (t/s=0.6)	M=0.5, 1.0, 1.5	M=0.5, 1.0, 1.5
Configuration 2 (baseline, t/s=1.0)	M=0.25, 0.5, 0.75, 1.0, 1.25, 1.5	M=0.25, 0.5, 0.75, 1.0, 1.25, 1.5
Configuration. 3 (t/s=1.4)	M=0.5, 1.0, 1.5	M=0.5, 1.0, 1.5

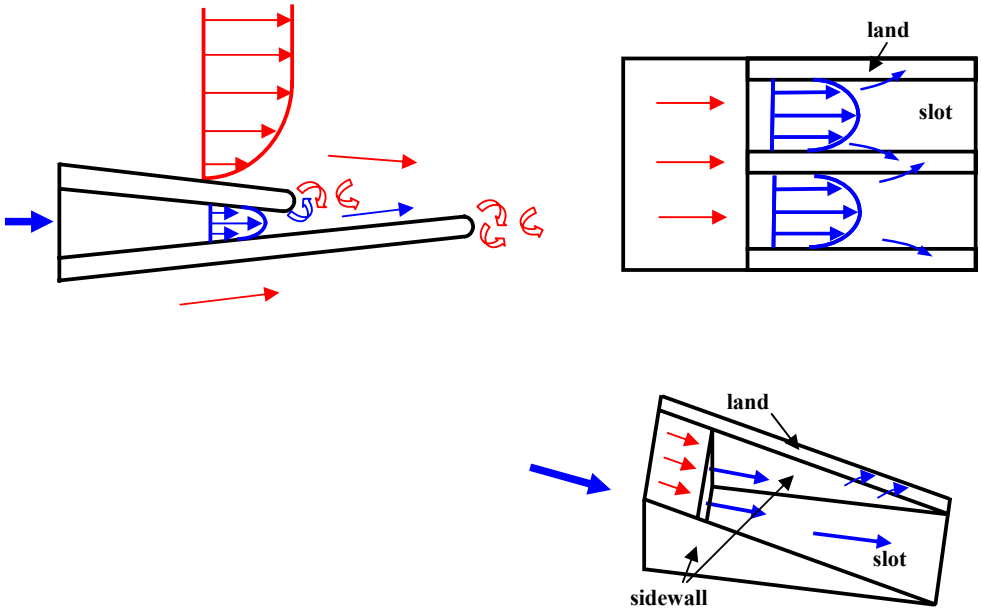

Fig. 6.5 Conceptual view of mainstream and coolant jet interaction

Figure 6.6-6.8 show the effectiveness distribution on the slots, lands, and slot sidewalls. The abscissa and ordinate were normalized with slot height (s). As indicated in Fig. 6.3, the origin of x is the edge of the lip, y the midspan of the mode,l and z the slot height direction. Effectiveness was taken for the middle three slots including the lands, while for the slot sidewalls, only effectiveness on the middle sidewall was measured.

Figure 6.6 shows the effectiveness on the slots and lands for the case of no mainstream acceleration where $\delta/s=2.1$. A wide range of blowing ratios (from M=0.25 to M=1.5) were studied for the baseline configuration (t/s=1.0). Three typical blowing ratios were studies for the other two trailing edge configurations. It can be seen from Fig. 6.6(a) for the baseline configuration (t/s=1.0), the film cooling effectiveness near the slot is quite high, approximately 0.95. Close to the trailing, it slowly decays to 0.85 for the moderate and high blowing ratios (M=0.75 to M=1.5). Even for the smallest blowing ratio M=0.25, good film effectiveness level (about 0.5) at trailing edge is maintained. The film covered area on the slot with elevated film cooling ($\eta>0.9$) becomes larger with increasing of blowing ratios, but not significantly. From M=1.0 to M=1.5, the film effectiveness level and film coverage are comparable. The benefit to the film effectiveness is marginal with large amount of coolant ejection. On the contrary, it will cause more mixing loss (between the coolant and mainstream) and decrease the aerodynamics performance. Therefore, from the aerodynamic point of view, blowing ratio M=1.0 is desired. At lowest blowing ratio M=0.25, the coolant non-uniform distribution along the spanwise direction is observable from the effectiveness distribution on the slots. On the lands, the effectiveness level is much lower than that on the slots. The effectiveness on the lands increases from the slot to the trailing edge

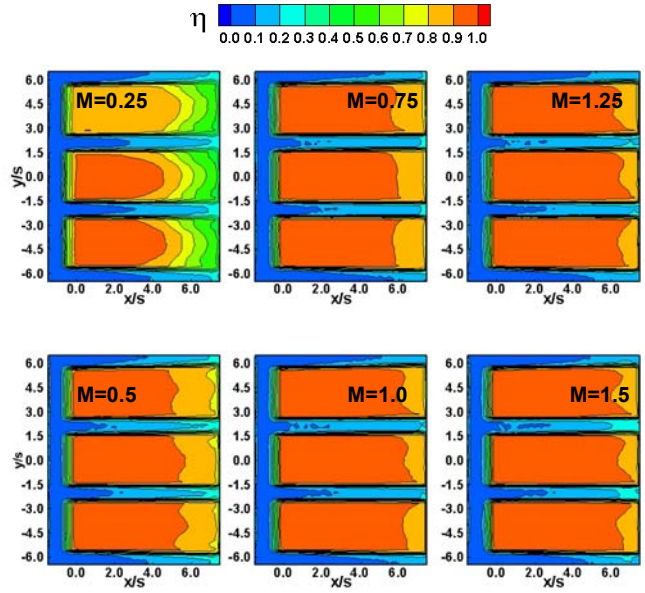

(a) t/s=1.0 (baseline configuration)

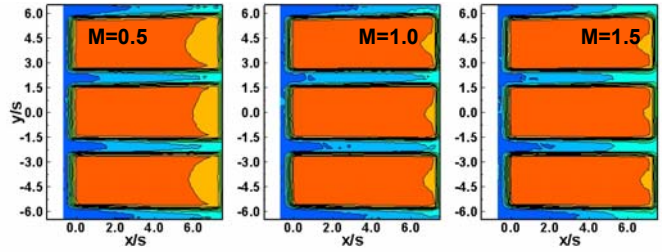

(b) t/s=0.6 (thin lipped)

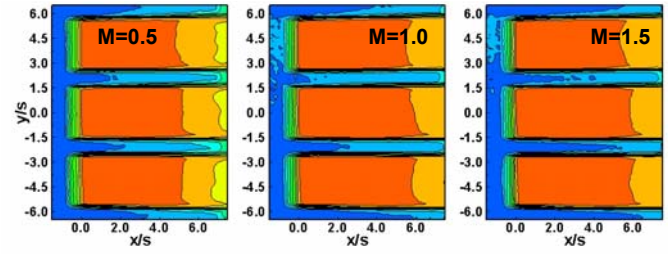

(c) t/s=1.4 (thick lipped)

Fig. 6.6 Film cooling effectiveness distribution on slots and lands without mainstream acceleration (δ/s=2.1)

(along x/s). From the conceptual sketch of Fig. 6.5, coolant expansion is expected to be stronger in the downstream region as the height of lands reduces. Therefore, downstream region of the lands gains more coolant protection than upstream region.

Fig. 6.6(b) and Fig. 6.6(c) shows effectiveness on the slots and lands for the configuration of thin-lip (t/s=0.6) and thick-lip (t/s=1.4), respectively. Compared with Fig. 6.6(a), it can be seen that the effectiveness on the slot for the thin-lip (t/s=0.6) is higher, while for the thick-lip (t/s=1.4) is lower. Consequently, the effectiveness on the land increases for the thin-lip, decreases for the thick-lip. As depicted in Fig. 6.5, the lip creates wakes. The wakes result in additional mixing between the mainstream and coolant and reduce the film cooling effectiveness. The wakes associated with the thin lips are relatively small in size and weak in strength, so the mixing it incurring is also weak. Therefore, the effectiveness for the thin lips is usually higher for thinner lips. It is expected the slots with sharp edge (like knife edge) will give best film effectiveness due to minimized wakes. However, the lip thickness is limited by the structural integrity in blade designs. It can not be infinite small like a knife edge. Similarly to the baseline configuration, the film effectiveness on the slots for these two configurations increases with increasing of blowing ratios, but insignificantly. On the lands, the effectiveness in the downstream region is higher than that in the upstream region.

Fig. 6.7 shows the film cooling effectiveness on the slot sidewall for the case of no mainstream acceleration (i.e. $\delta/s=2.1$). For the baseline case t/s=1 in Fig. 6.7(a), there is a big increase in effectiveness from M=0.25 to M=0.5. However, from M=0.5 to M=1.5, the increase in effectiveness is relatively small. The jet expansion can be clearly seen by the existence of effectiveness where $z/s>1$ (larger than slot height). As the

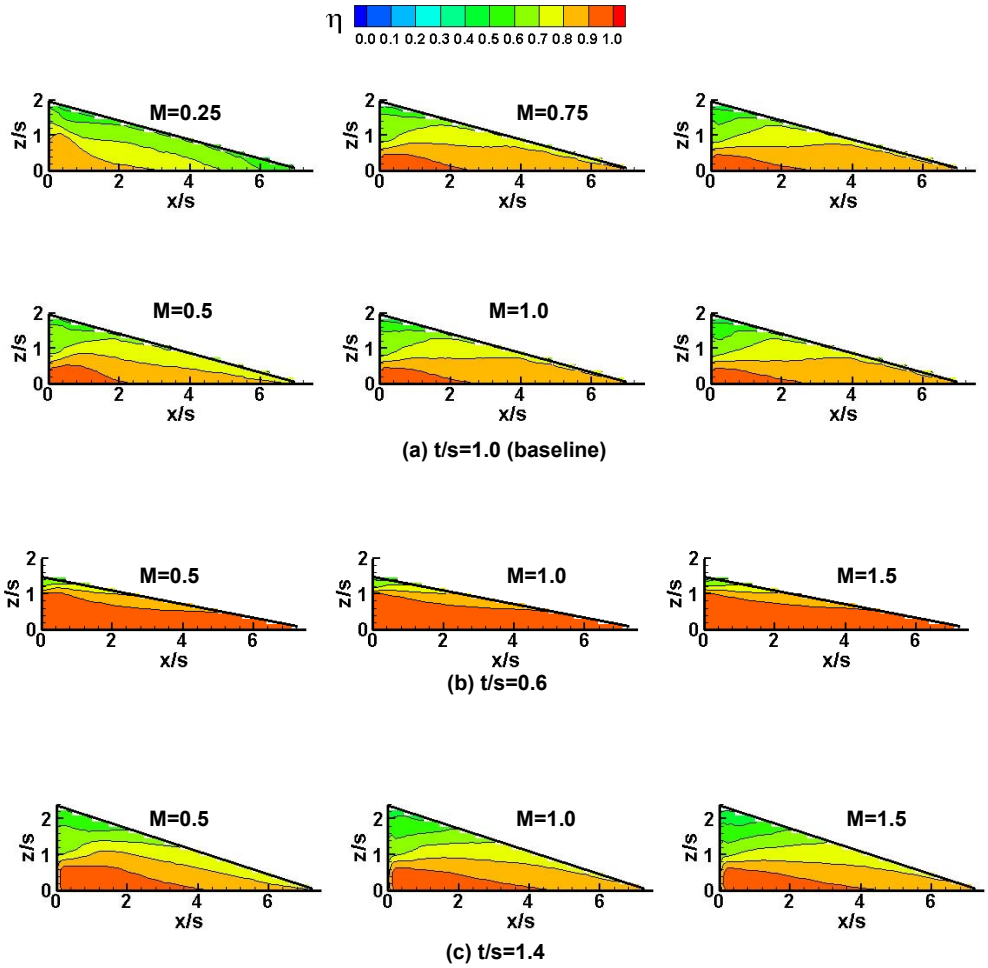

Fig. 6.7 Film cooling effectiveness distribution on slot sidewalls without mainstream acceleration (δ/s=2.1)

sidewalls tapers down, it is anticipated that the coolant is less confined in the channel. It expands and crosses over the lands. That's why the effectiveness on the land gradually increases with x/s. The advantage of thin-lip is shown in Fig. 6.7(b) again. At t/s=0.6, the coverage with elevated effectiveness (η>0.9) is extended all the way to the trailing edge. Compared with Fig 6.7(a) for t/s=1, the area with elevated effectiveness for t/s=1.4 seems extending further to downstream region.

Figure 6.8 shows the effectiveness distribution on the slots and lands for the case of mainstream accelerated where δ/s=1.3. The effect of blowing ratio and lip thickness under this flow condition is similar to the condition without mainstream acceleration as discussed earlier for Fig. 6.6. The discussion of Fig. 6.8 will be focused on the effect of boundary layer thickness by comparing with Fig. 6.6. For all the three configurations, the effectiveness level near the slot is about the same as the condition δ/s=2.1. The difference resulted from the boundary layer thickness is observed in the downstream region close to the trailing edge. For the baseline configuration (t/s=1.0), the effectiveness on the slot near trailing edge increases at low blowing ratios M=0.25 and M=0.5. When the blowing ratios further increase, the effectiveness in this region slightly decreases. Figure 6.8(b) shows the effectiveness distribution for the configuration of t/s=0.6. Compared with Fig. 6.6(b), the effectiveness reduces at M=0.5 and increases at M=1.0 and M=1.5 on the trailing portion of the slot. This trend is similar to that observed for baseline configuration of t/s=1.0. However, for the thick lip t/s=1.4, the effectiveness on the slot trailing portion reduces for all the three blowing ratios with the thinner boundary layer. As shown in Fig. 6.4(c), the velocity gradient inside the thin boundary layer is larger than that in thicker boundary layer. This results

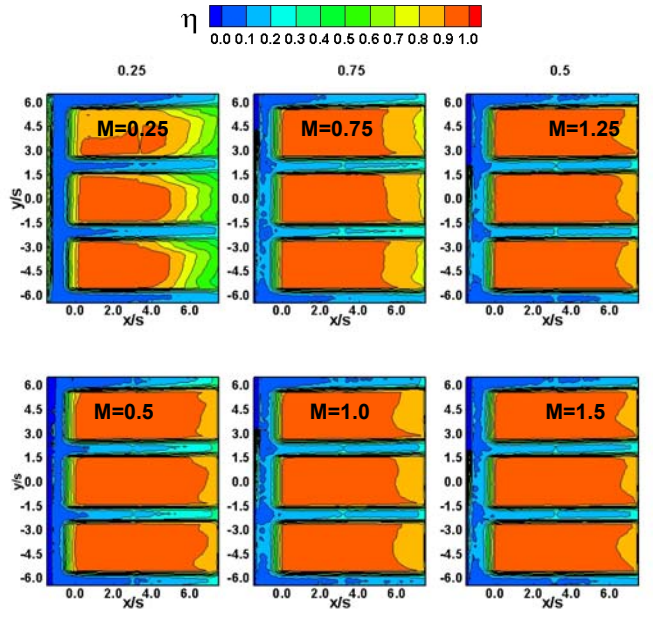

(a) Configuration t/s=1.0

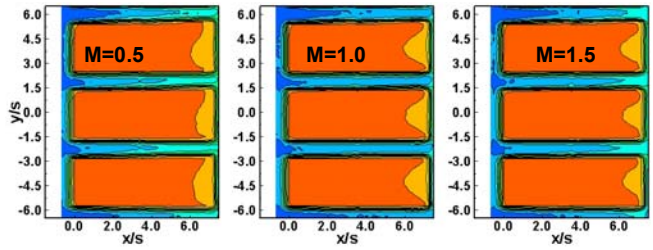

(b) Configuration t/s=0.6

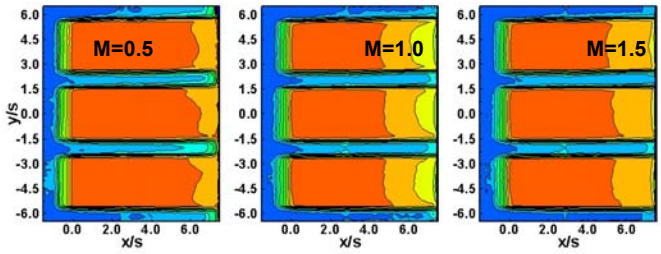

(c) Configuration t/s=1.4

Fig. 6.8 Film Cooling effectiveness distribution on slots and lands with mainstream acceleration (δ/s=1.3)

in more shear mixing. Therefore the mainstream and coolant mixing enhances and effectiveness reduces with thinner boundary layer.

Figure 6.9 shows the laterally averaged effectiveness on the slot, land and slot sidewall for the baseline case (t/s=1.0) at δ/s=2.1. In general, the effectiveness increases with increasing of blowing ratios. On the slot surface, the effectiveness level at the slot exit (x/d < 4) is about the same for all blowing ratio except M=0.25. Further downstream, the effectiveness for the lower blowing ratios decays faster. However, from M=0.5 to M=1.5, the difference in effectiveness at the trailing edge (x/s≈7.5) is less than 10%. On the sidewall, the effectiveness gradually increases along streamwise direction except M=0.25. At M=0.25, the small amount of coolant quickly mixes with the mainstream. The effectiveness on the sidewall increases with increasing of blowing ratios, however, the increment is insignificant from M=0.5 to M=1.5. On the lands, the effectiveness level is much lower than on the slots and sidewall (noted the different scale). The effectiveness increases as x/s increases. Toward the trailing edge, the height of the side decreases, therefore, the coolant lateral expansion increases and more coolant crosses over the lands.

Figure 6.10 shows the spanwise averaged effectiveness for the three configurations under the condition of δ/s=2.1. The same configurations (t/s) are denoted by the same color, the different blowing ratios are identified by different symbols. In general, the thin lip gives higher effectiveness (blue>black>pink) at the same blowing ratios. On the slots, the effectiveness level is about the same for the three configurations at same blowing ratios. Moreover, the high effectiveness maintains for a distance about x/s=4. Further downstream, the effectiveness decays faster for the thicker lips. For the

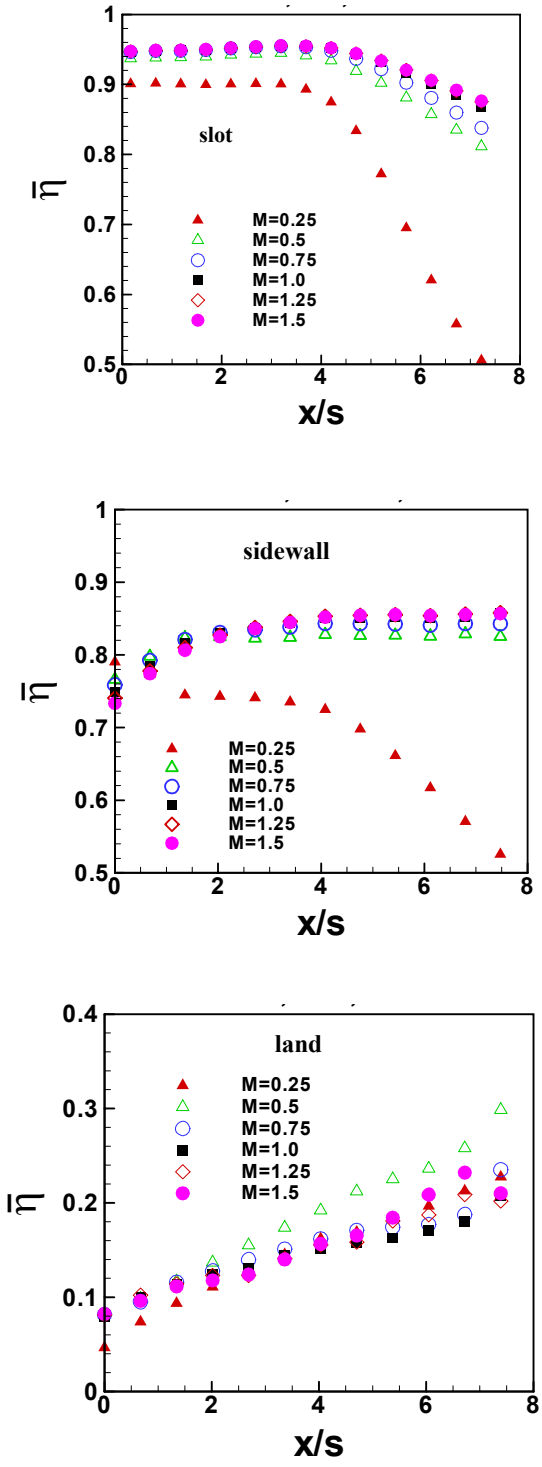

Fig. 6.9 Spanwise averaged effectiveness for baseline configuration (t/s=1.0) without mainstream acceleration (δ/s=2.1)

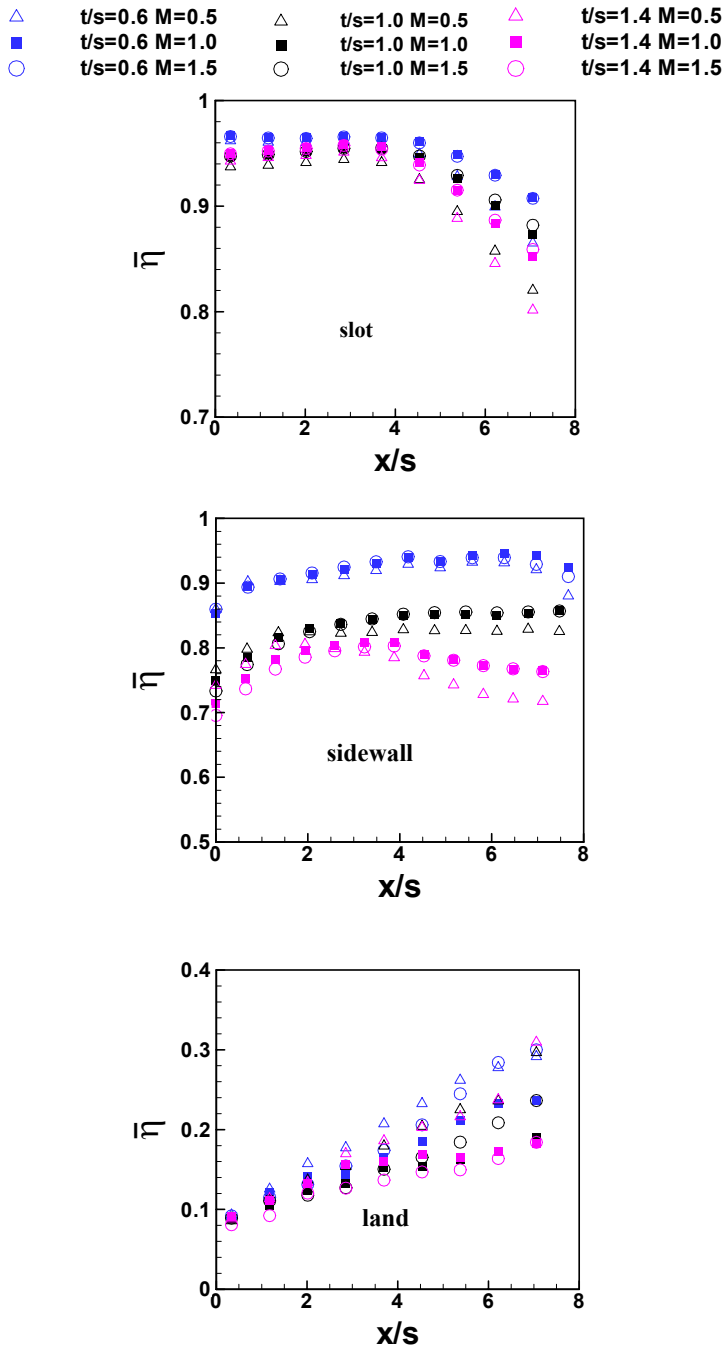

Fig. 6.10 Spanwise averaged effectiveness without mainstream acceleration (δ/s=2.1)

same configuration (t/s), the effectiveness on the slots only slightly increases with blowing ratios. Particularly, at M=1.0 and M=1.5, the increment is not noticeable. On the sidewall, the difference in effectiveness for different lips is more profound. For the thinner lip design, the height of sidewall is correspondingly smaller. Therefore, the coolant jets are able to covered larger area of the side wall with elevated effectiveness. On the land, the effectiveness increases as the flow goes to the trailing edge. Again, the thinner lip exhibits higher effectiveness due to coolant jet expansion and smaller wakes.

Figure 6.11 shows the spanwise averaged effectiveness under the condition of thin boundary layer condition ($\delta/s=1.3$). On the slot floor near the slot exit ($x/s<4$), the thin lip doesn't appear advantage over the thicker lips at the thin boundary layer. The shear mixing is stronger for the thin boundary layer condition. The small step (lip thickness) of the thin lip leads to quick interaction between the mainstream and coolant, and reduces the effectiveness. Further downstream, the vortex shedding is dominant over the shearing mixing, therefore, the thin lips exhibit advantage in effectiveness than the thick lips. On the lands, the combined effect of enhanced shearing mixing and vortex makes t/s=1 performing better than the other lip thickness.

Figure 6.12 shows the effect of boundary layer thickness. In general, the effectiveness slightly increases with increasing boundary layer thickness (open symbols > close symbols) on the slots. While on the lands, the trend is reversed. The thin boundary layer thickness gives better effectiveness. With the thin boundary layer, the mixing between mainstream and coolant enhances and the effectiveness in the slot reduces. However, the enhanced mixing spreads more coolant to the land, therefore, the effectiveness on the lands are higher at thin boundary layer condition.

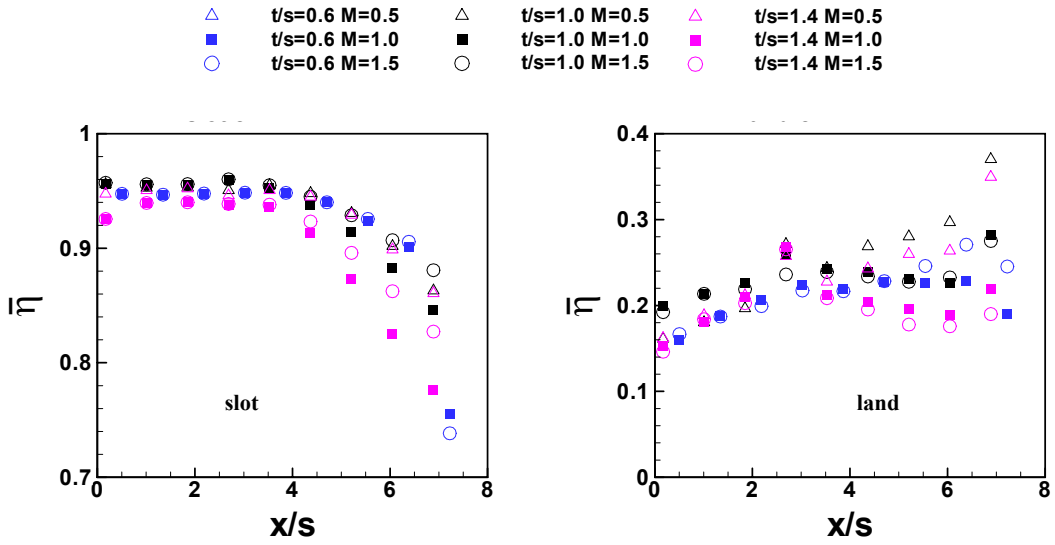

Fig. 6.11 Spanwise averaged effectiveness with mainstream acceleration (δ/s=1.3)

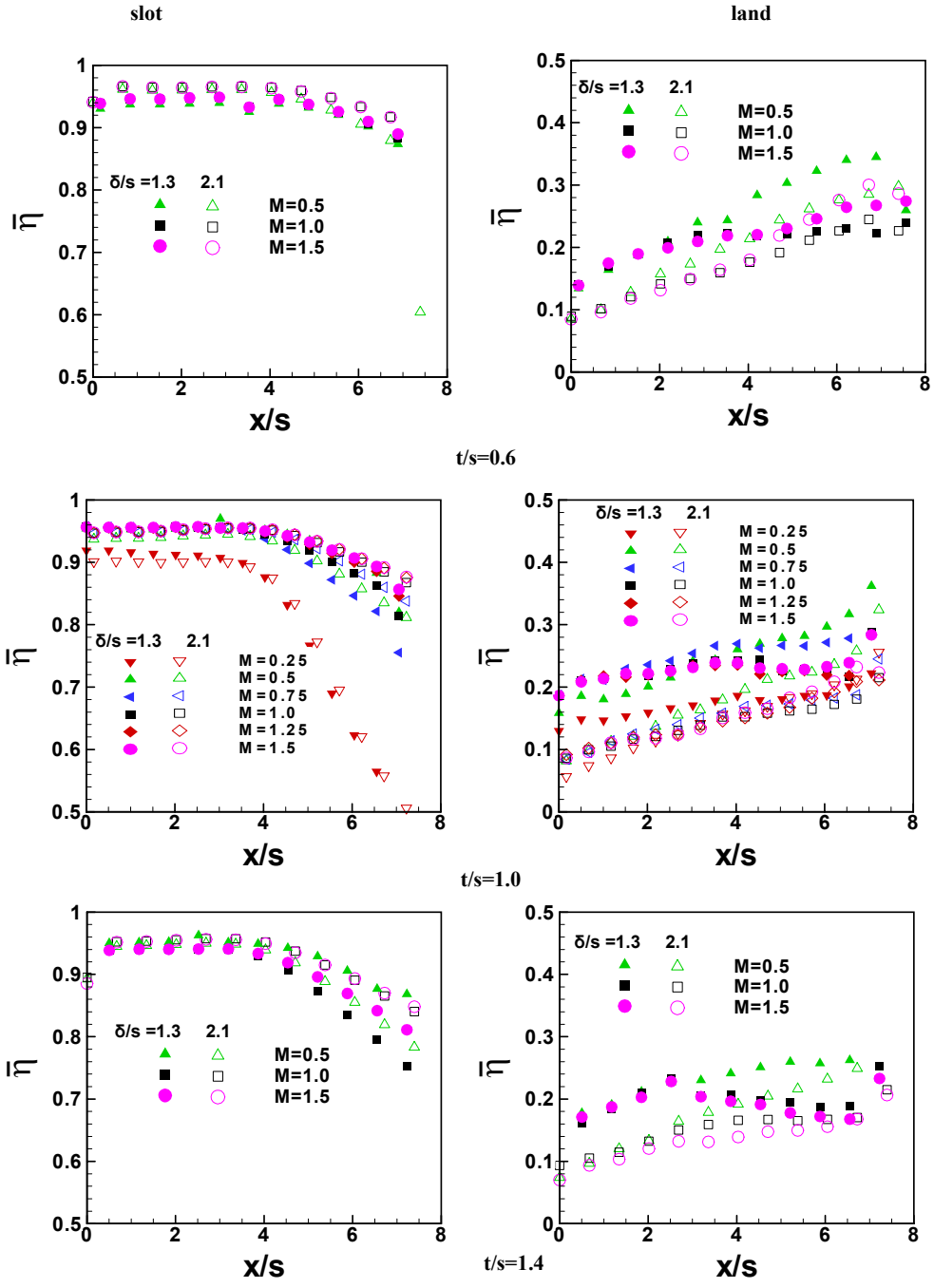

Fig. 6.12 Effect mainstream boundary layer thickness on spanwise averaged effectiveness

Fig. 6.13 shows slot film cooling effectiveness and compares the current data with Taslim's correlation [83]. Near the slot, the current data is lower than the correlation. Further downstream, the data from the current study is higher than the correlation. The difference may be caused by the different trailing edge design and mainstream flow conditions.

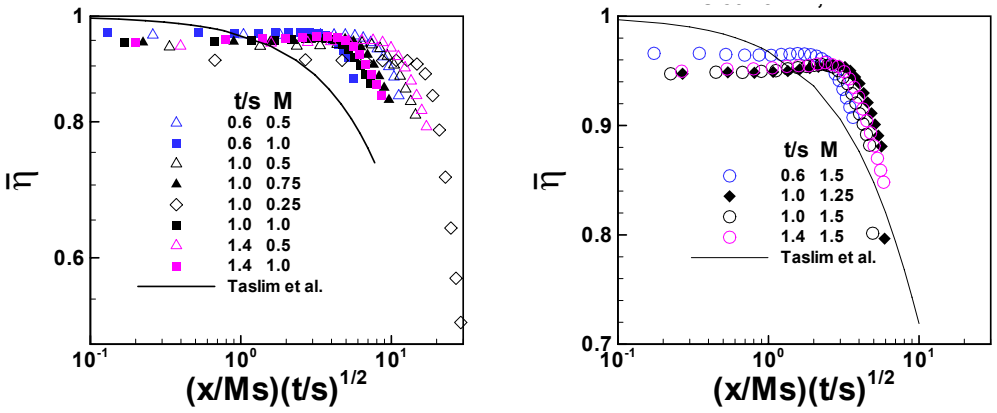

Fig. 6.13 Slot film cooling effectiveness and comparison with correlation [83] for δ/s=2.1

6.3 Conclusions

The effect of the lip thickness on the trailing edge slot film cooling effectiveness was investigated under two mainstream flow conditions and varying blowing ratios. Three trailing edge models with pressure side cutback were presented. Effectiveness data on the slots, lands and sidewalls were measured using pressure sensitive paint technique. Based on the heat/mass analogy, the conduction error in effectiveness data is eliminated in PSP measurement. This is particularly useful for the effectiveness measurement on the narrow land and slot sidewalls. Main findings for the current study are as follows:

1. The film effectiveness on the slot floor (0.8~0.95) is slightly higher than the sidewall (0.7~0.95). The lands receive the lowest film protection, particularly in the region near the slot exit (0.1~0.3).
2. The film effectiveness on the slots, lands and sidewalls increases with increasing blowing ratios. However, the increment is mild from M=0.5 to M=1.5.
3. The thinner lip offers higher effectiveness due to the small wakes. The effect of lip thickness is more evident in the downstream region of the slot floor where x/s>4. In this region, the vortex shedding enhances the interaction (mixing) between the mainstream and coolant. The advantage of thinner lip also presented on the sidewalls and lands with increased overall effectiveness.
4. The interaction of mainstream and coolant enhances with the thinner boundary. More coolant is dispersed from the slots to the lands. Therefore, the thinner boundary layer thickness reduces effectiveness on slots but increase effectiveness on lands.

5. As the sidewall height decrease in the streamwise direction, the lateral expansion of coolant increases. Therefore, the effectiveness increases on the land in the streamwise direction.

7. SUMMARY

Film cooling is commonly used in modern high temperature and high pressure blades as an active cooling scheme. In this study, the film cooling effectiveness in different regions of gas turbine blades was investigated with various film hole/slot configurations and mainstream flow conditions. The study consisted of four parts: 1) effect of upstream wake on blade surface film cooling, 2) effect of upstream vortex on platform purge flow cooling, 3) influence of hole shape and angle on leading edge film cooling and 4) slot film cooling on trailing edge. Pressure sensitive paint (PSP) technique was used to get the conduction-free film cooling effectiveness distribution.

The effect of film cooling hole configurations and upstream wake was studied for a fully film cooled blade. Two hole configurations were considered: axial shaped hole and compound angle shaped hole. The upstream wake was simulated by the stationary rods periodically placed upstream of the blade passage at different phases. Results revealed that the tip leakage vortices and endwall vortices sweep the coolant film on the suction side to the midspan region. Because of the surface curvature, the effectiveness is lower on the pressure surface than that on the suction side. The presence of upstream wake rods results in lower film cooling effectiveness on the blade surface. The compound angle shaped holes outperform the axial angle shaped holes by the elevated film cooling effectiveness, particularly at higher blowing ratios.

The effect of the upstream vane passage vortex on the downstream blade platform film-cooling effectiveness was examined in a five-blade linear cascade. A typical labyrinth-like seal was placed upstream of the cascade blades to simulate purge flow from a stator-rotor gap. Delta wings were periodically placed upstream of the

blades to model the effect of the passage vortex generated in the vane passage on the downstream blade platform film cooling effectiveness. The strength of vane passage vortex was varied by changing the size of the delta wings and mainstream attack angle to the delta wings. The vortex generated by the delta wings has a profound impact on the platform film cooling effectiveness. The upstream vortex creates more turbulent mixing within the blade passage and results in reduced film cooling effectiveness on the blade platform. When the vane induced secondary flow is included, the need for additional platform cooling becomes very obvious.

The effect of hole geometry and angle on turbine blade leading edge film cooling was studied in a low speed windtunnel. The leading edge was modeled by a blunt body with a semicylinder and an afterbody. Two film cooling designs were considered: a heavily film cooled leading edge feathered with seven rows of film cooling holes, and a moderately film cooled leading edge with three rows. Results showed that the shaped holes provide higher film cooling effectiveness than the cylindrical holes, particularly at higher average blowing ratios. The radial angle holes have better effectiveness than the compound angle holes at M=1.0~2.0. The seven-row film cooling design results in much higher effectiveness on the leading edge region than the three-row design at the same average blowing ratio or same coolant mass flow rate.

Film cooling effectiveness was measured for trailing edge models with pressure side cutback. The trailing edge models were cooled by ejecting coolant from spanwise discrete slots located on the pressure side. Two mainstream flow conditions were considered. In one condition, the mainstream flow was not accelerated; a relatively thicker boundary layer was developed upstream of slot exit. In the other condition, the

mainstream flow was accelerated and a thinner boundary layer was developed. The effect of slot lip thickness and blowing ratios on film effectiveness under the two mainstream conditions were investigated. Results showed that the film cooling effectiveness increases with increasing of blowing ratios. Thinner lips offer higher effectiveness. The effect of lip thickness is more evident in the downstream region of the trailing edge with faster decay in effectiveness for thicker slot lips. The film effectiveness on the slots decreases when the incoming mainstream boundary layer thickness decreases.

REFERENCES

[1] Han, J.C., Dutta, S., and Ekkad, S.V., 2000, *Gas Turbine Heat Transfer and Cooling Technology*, Taylor and Francis, New York.

[2] Goldstein, R. J., Eckert, E. R. G., and Burggraf, F., 1974, ‘‘Effects of Hole Geometry and Density on Three- Dimensional Film Cooling,’’ Int. J. Heat Mass Transfer, **17**, pp. 595–607.

[3] Thole, K., Gritsch, M., Schulz, A., and Wittig, S., 1996, ‘‘Flowfield Measurements for Film Cooling Holes With Expanded Exits,’’ ASME Paper No. 96-GT-174.

[4] Gritsch, M., Schulz, A., and Wittig, S., 1997, ‘‘Adiabatic Wall Effectiveness Measurements of Film-Cooling Holes With Expanded Exits,’’ ASME Paper No. 97-GT-164.

[5] Yu, Y., Yen, C.-H., Shih, T. I.-P., Chyu, M. K., and Gogineni, S., 1999, ‘‘Film Cooling Effectiveness and Heat Transfer Coefficient Distributions around Diffusion Shaped Holes,’’ ASME Paper No. 99-GT-34.

[6] Schmidt, D. L., Sen, B., and Bogard, D. G., 1994, ‘‘Film Cooling With Compound Angle Holes: Adiabatic Effectiveness,’’ ASME Paper No. 94-GT-312.

[7] Dittmar, J., Schulz, A., and Wittig, S., 2002, ‘‘Assessment of Various Film Cooling Configurations Including Shaped and Compound Angle Holes Based on Large Scale Experiments,’’ ASME Paper No. GT-2002-30176.

[8] Chen, P. H., Hung, M. S., and Ding, P. P., 2001, ‘‘Film Cooling Performance on Curved Walls with Compound Angle Hole Configuration,’’ *Annals of the New York Academy of Sciences*, **934**, pp. 353–360.

[9] Teng, S., and Han, J.C., 2001, “Effect of Film-Hole Shape on Turbine-Blade Film-Cooling Performance,” Journal of Thermophysics and Heat Transfer, **15**(3), pp. 257-265.

[10] Mhetras, S., Narzary, D., Gao, Z., Han, J.C., “Effect of a Cutback Squealer and Cavity Depth on Film-Cooling Effectiveness on a Gas Turbine Blade Tip” AIAA Paper No. AIAA 2006-3404.

[11] Teng, S., Sohn, D.K., and Han, J.C., 2000, “Unsteady Wake Effect on Film Temperature and Effectiveness Distributions for a Gas Turbine Blade,” ASME J. of Turbomachinery, **122**, pp. 340-347.

[12] Ou, S., Han, J. C., Mehendale, A. G., and Lee, C. P., 1994, ‘‘Unsteady Wake Over a Linear Turbine Blade Cascade with Air and CO_2 Film Injection: Part I—

Effect on Heat Transfer Coefficients,'' ASME J. Turbomachinery, **116**, pp. 721–729.

[13] Mehendale, A. B., Han, J. C., Ou, S., and Lee, C. P., 1994, ''Unsteady Wake over a Linear Turbine Blade Cascade With Air and CO_2 Film Injection: Part II-Effect on Film Effectiveness and Heat Transfer Distributions,'' ASME J. Turbomachinery., **116**, pp. 730–737.

[14] Du, H., Ekkad, S. V., and Han, J. C., 1999, ''Effect of Unsteady Wake with Trailing Edge Ejection on Film Cooling Performance for a Gas Turbine Blade,'' ASME J. Turbomachinery, **121**, pp. 448–455.

[15] Rigby, M. J., Johnson, A. B., and Oldfield, M. L. G., 1990, ''Gas Turbine Rotor Blade Film Cooling With and Without Simulated NGV Shock Waves and Wakes,'' ASME Paper No. 90-GT-78.

[16] Heidmann, J.D, Lucci, B.L., and Reshotko, E., 2001, "An Experimental Study of the Effect of Wake Passing on Turbine Blade Film Cooling," ASME J. of Turbomachinery, **123**, pp. 214-221.

[17] Mhetras, S., Han, J.C., "Effect of Unsteady Wake on Full Coverage Film-Cooling Effectiveness for a Gas Turbine Blade," AIAA Paper No. AIAA 2006-3404.

[18] Narzary, D.P., Gao, Z., Mhetras, S., Han, J.C., 2007, "Effect of Unsteady Wake on Film-Cooling Effectiveness Distribution on a Gas Turbine Blade with Compound Shaped Holes," ASME Paper No. GT2007-27070

[19] Mhetras, S., Han, J.C., "Effect of Superposition on Spanwise Film-Cooling Effectiveness Distribution on a Gas Turbine Blade," ASME Paper No. IMECE 2006-1808

[20] Langston, L.S., 2001, "Secondary Flows in Axial Turbines – A Review," *Annals of the New York Academy of Sciences*, **934**, pp. 11-26.

[21] Chyu, M.K., 2001, "Heat Transfer near Turbine Nozzle Endwall," *Annals of the New York Academy of Sciences*, **934**, pp. 27-36.

[22] Simon, T.W. and Piggush, J.D., 2006, "Turbine Endwall Aerodynamics and Heat Transfer," AIAA J. of Propulsion and Power, **22**, pp. 310-312.

[23] Langston, L.S., Nice, L.M., and Hooper, R.M., 1976, "Three-Dimensional Flow within a Turbine Cascade Passage," ASME Paper No. 76-GT-50.

[24] Langston, L.S., 1980, "Crossflows in a Turbine Cascade Passage," ASME J. Engineering for Power, **102**, pp. 866-874.

[25] Goldstein, R.J. and Spores, R.A., 1988, "Turbulent Transport on the Endwall in the Region between Adjacent Turbine Blades." ASME J. Heat Transfer, **110**, pp. 862-869.

[26] Wang, H.P., Olson, S.J., and Goldstein, R.J., 1997, "Flow Visualization in a Linear Turbine Cascade of High Performance Turbine Blades," ASME J. Turbomachinery, **119**, pp. 1-8.

[27] Takeishi, K., Matsuura, M., Aoki, S., and Sato, T., 1990, "An Experimental Study of Heat Transfer and Film Cooling on Low Aspect Ratio Turbine Nozzles," ASME J. Turbomachinery, **112**, pp. 488-496.

[28] Harasgama, S.P. and Burton, C.S., 1992, "Film Cooling Research on the Endwall of a Turbine Nozzle Guide Vane in a Short Duration Annular Cascade: Part 1 – Experimental Technique and Results," ASME J. Turbomachinery, **114**, pp. 734-740.

[29] Jabbari, M.Y., Marston, K.C., Eckert, E.R.G., and Goldstein, R.J., 1996, "Film Cooling of the Gas Turbine Endwall by Discrete-Hole Injection," ASME J. Turbomachinery, **118**, pp. 278-284.

[30] Friedrichs, S., Hodson, H.P., and Dawes, W.N., 1996, "Distribution of Film-Cooling Effectiveness on a Turbine Endwall Measured Using the Ammonia and Diazo Technique," ASME J. Turbomachinery, **118**, pp. 613-621.

[31] Friedrichs, S., Hodson, H.P., and Dawes, W.N., 1997, "Aerodynamic Aspects of Endwall Film Cooling," ASME J. Turbomachinery, **119**, pp. 786-793.

[32] Friedrichs, S., Hodson, H.P., and Dawes, W.N., 1998, "The Design of an Improved Endwall Film Cooling Configuration," ASME Paper No. 98-GT-483.

[33] Barigozzi, G., Benzoni, G., Franchini, G., and Derdichizzi, A., 2005, "Fan-Shaped Hole Effects on the Aero-Thermal Performance of a Film Cooled Endwall," ASME Paper No. GT2005-68544.

[34] Blair, M.F., 1974, "An Experimental Study of Heat Transfer and Film Cooling on Large-Scale Turbine Endwall," ASME J. Heat Transfer, **96**, pp. 524-529.

[35] Granser, D. and Schulenberg, T., 1990, "Prediction and Measurement of Film Cooling Effectiveness for a First-Stage Turbine Vane Shroud," ASME Paper No. 90-GT-95.

[36] Roy, R.P., Squires, K.D., Gerendas, M., Song, S., Howe, W.J., and Ansari, A., 2000, "Flow and Heat Transfer at the Hub Endwall of Inlet Vane Passages – Experiments and Simulations," ASME Paper No. 2000-GT-198.

[37] Burd, S.W., Satterness, C.J., and Simon, T.J., 2000, "Effects of Slot Bleed Injection Over a Contoured End Wall on Nozzle Guide Vane Cooling Performance: Part II – Thermal Measurements," ASME Paper No. 2000-GT-200.

[38] Oke, R., Simon, T., Shih, T., Zhu, B., Lin, Y.L., and Chyu, M., 2001, "Measurements over a Film-Cooled Contoured Endwall with Various Coolant Injection Rates," ASME Paper No. 2001- GT-0140.

[39] Oke, R.A. and Simon, T.W., 2002, "Film Cooling Experiments with Flow Introduced Upstream of a First Stage Nozzle Guide Vane through Slots of Various Geometries," ASME Paper No. GT-2002-30169.

[40] Nicklas, M., 2001, "Film-Cooled Turbine Endwall in a Transonic Flow Filed: Part II – Heat Transfer and Film Cooling Effectiveness," ASME J. Turbomachinery, **123**, pp. 720-729.

[41] Liu, G., Liu, S., Zhu, H., Lapworth, B.C., and Forest, A.E., 2004, "Endwall Heat Transfer and Film Cooling Measurements in a Turbine Cascade with Injection Upstream of Leading Edge," *Heat Transfer – Asian Research*, **33**, pp. 141-152.

[42] Zhang, L.J. and Jaiswal, R.S., 2001, "Turbine Nozzle Endwall Film Cooling Study Using Pressure-Sensitive Paint," ASME J. Turbomachinery, **123**, pp. 730-735.

[43] Zhang, L.J. and Moon, H.K., 2003, "Turbine Nozzle Endwall Inlet Film Cooling – The Effect of a Backward Facing Step," ASME Paper No. GT2003-38319.

[44] Knost, D.G. and Thole, K.A., 2004, "Adiabatic Effectiveness Measurements of Endwall Film Cooling for a First Stage Vane," ASME Paper No. GT2004-53326.

[45] Cardwell, N.D., Sundaram, N., and Thole, K.A., 2005, "Effects of Mid-Passage Gap, Endwall Misalignment and Roughness on Endwall Film-Cooling," ASME Paper No. GT2005-68900.

[46] Wright, L.M., Gao, Z., Yang, H., and Han, J.C., 2006, "Film Cooling Effectiveness Distribution on a Gas Turbine Blade Platform with Inclined Slot Leakage and Discrete Film Hole Flows," ASME Paper No. GT2006-90375.

[47] Wright, L.M., Blake, S., and Han, J.C., 2006, "Effectiveness Distributions on Turbine Blade Cascade Platforms through Simulated Stator-Rotor Seals," AIAA Paper No. AIAA-2006-3402.

[48] Wright, L.M., Blake, S., and Han, J.C., 2006, "Film Cooling Effectiveness Distributions on a Turbine Blade Cascade Platform with Stator-Rotor Purge and Discrete Film Holes Flows," ASME Paper No. IMECE2006-15092.

[49] Suryanarayanan, A., Ozturk, B., Schobeiri, M. T., and Han, J. C., 2007, "Film Cooling Effectiveness on a Rotating Turbine Platform Using Pressure Sensitive Paint Technique," ASME Paper No. GT2007-27122.

[50] Suryanarayanan, A., Mhetras, S.P., Schobeiri, M.T., and Han, J.C., 2006, "Film Cooling Effectiveness on a Rotating Blade Platform," ASME Paper No. GT2006-90034.

[51] Wright, L.M., Blake, S., Rhee, D. H., and Han, J.C., 2007, "Effect of Upstream Wake with Vortex on Turbine Blade Platform Film Cooling with Simulated Stator-Rotor Purge Flow," ASME Paper No. GT2007-27092.

[52] Luckey, D.W., Winstanley, D.K., Hames, G.J., and L'Ecuyer, M.R., 1977, "Stagnation Region Gas Film Cooling for Turbine Blade Leading Edge Applications," AIAA Journal of Aircraft, **14**, pp. 494-501.

[53] Karni, J. and Goldstein, R.J., 1990, "Surface Injection Effect on Mass Transfer from a Cylinder in Crossflow: A Simulation of Film Cooling in the Leading Edge Region of a Turbine Blade," ASME Journal of Turbomachinery, **112**, pp. 418-427.

[54] Mick, W.J. and Mayle, R.E., 1988, "Stagnation Film Cooling and Heat Transfer Including Its Effect Within the Hole Pattern," ASME Journal of Turbomachinery, **116**, pp. 730-737.

[55] Mehendale, A.B. and Han, J.C., 1992, "Influence of High Mainstream Turbulence on Leading Edge Film Cooling Heat Transfer," ASME Journal of Turbomachinery, **114**, pp. 707-715.

[56] Mehendale, A. B. and Han, J. C., 1993, "Reynolds Number Effect on Leading Edge Film Effectiveness and Heat Transfer Coefficient," Int. J. of Heat and Mass Transfer, **36**, pp. 3723-3730.

[57] Ou, S., Mehendale, A. B., and Han, J. C., 1992, "Influence of High Mainstream Turbulence on Leading Edge Film Cooling Heat Transfer: Effect of Film Hole Row Location," ASME J. of Turbomachinery, **114**, pp. 716-723.

[58] Ekkad, S.V., Han, J.C., and Du, H., 1998, "Detailed Film Cooling Measurements on a Cylindrical Leading Edge Model: Effect of Free-Stream Turbulence and Coolant Density," ASME Journal of Turbomachinery, **119**, pp. 594-600.

[59] Gao, Z., Wright, L.M. and Han, J.C., 2005, "Assessment of Steady State PSP and Transient IR Measurement Techniques for Leading Edge Film Cooling", ASME Paper No. IMECE2005-80146.

[60] Funazaki, K., Yokota, M., and Yamawaki, K., 1997, "The Effect of Periodic Wake Passing on Film Effectiveness of Discrete Holes Around the Leading Edge of a Blunt Body," ASME J. of Turbomachinery, **119**, pp. 292-301.

[61] Ou, S. and Rivir, R. B., 2001, "Leading Edge Film Cooling Heat Transfer with High Free Stream Turbulence Using a Transient Liquid Crystal Image Method," Int. J. of Heat and Fluid Flow, **22**, pp. 614-623.

[62] Nirmalan, N.V. and Hylton, L.D., 1990, "An Experimental Study of Turbine Vane Heat Transfer with Leading Edge and Downstream Film Cooling," ASME J. of Turbomachinery, **112**, pp. 477-487.

[63] Abuaf, N., Bunker, R., and Lee, C. P., 1997, "Heat Transfer and Film Cooling Effectiveness in a Linear Airfoil Cascade," ASME J. of Turbomachinery, **119**, pp. 302-309.

[64] Cruse, M. W., Yuki, U. M., and Bogard, D. G., 1997, "Investigation of Various Parametric Influences on Leading Edge Film Cooling," ASME Paper No. 97-GT-296.

[65] Ekkad S. V., Mehendale, A. B., Han, J. C., and Lee, C. P., 1997, "Combined Effect of Grid Turbulence and Unsteady Wake on Film Effectiveness and Heat Transfer Coefficient of a Gas Turbine Blade with Air and CO2 Film Injection," ASME J. of Turbomachinery, **119**, pp. 594-600.

[66] Cutbirth, J. M. and Bogard, D. G., 2003, "Effects of Coolant Density Ratio on Film Cooling Performance on a Vane," ASME Paper No. 2003-GT-38582.

[67] Mhetras, S.P. and Han, J.C., 2006 "Effect of unsteady wake on showerhead film cooling protection for a gas turbine blade", International Heat Transfer Conference 2006 Sydney, Australia.

[68] Dring, R. P., Blair, M. F., and Hoslyn, H. D., 1980, "An Experimental Investigation of Film Cooling on a Turbine Rotor Blade," ASME J. of Engineering for Power, **102**, pp. 81-87.

[69] Takeishi, K., Matsuura, M., Aoki, S., and Sato, T., 1990, "An Experimental Study of Heat Transfer and Film Cooling on Low Aspect Ratio Turbine Nozzles," ASME J. of Turbomachinery, **112**, pp. 488-496.

[70] Abhari, R. S. and Epstein, A. H., 1994, "An Experimental Study of Film Cooling in a Rotating Transonic Turbine," ASME J. of Turbomachinery, **116**, pp. 63-70.

[71] Ahn, J., Schobeiri, M.T., Han, J.C, Moon, H., 2006, "Film Cooling Effectiveness on the Leading Edge Region of a Rotating Turbine Blade with Two Rows of Film Cooling Holes Using Pressure Sensitive Paint", Transactions of the ASME. Journal of Heat Transfer, **128**(9), pp. 879-88.

[72] Ahn, J., Schobeir, M.T., Han, J.C. and Moon, H.K., 2007, "Effect of Rotation on Leading Edge Region Film Cooling of a Gas Turbine Blade with Three Rows of Film Cooling Holes", **50**, pp. 15-25.

[73] Mouzon, B.D., Terrell, E. J., Ablert, J.E. and Bogard, D.G, 2005, "Net Heat Flux Reduction and Overall Effectiveness for a Turbine Blade Leading Edge", ASME Paper No. GT2005-69002.

[74] Falcoz, C., Weigand, B. and Ott, P., 2006, "Experimental Investigation on Showerhead Cooling on A Blunt Body", International Journal of Heat and Mass Transfer, **49**, pp. 1287-1298.

[75] Kim, Y. J. and Kim, S. M., 2004, "Influence of Shaped Injection Holes on Turbine Blade Leading Edge Film Cooling," Int. J. of Heat and Mass Transfer, **47**, pp. 245-256.

[76] Reiss, H. and Bölcs, A., 2000, "Experimental Study of Showerhead Cooling on a Cylinder Comparing Several Configurations Using Cylindrical and Shaped Holes," J. of Turbomachinery, **122**, pp. 161-169.

[77] Lu, Y., Allison, D. and Ekkad, S.V., 2006, "Influence of Hole Angle and Shaping on Leading Edge Showerhead Film Cooling", ASME Paper No. GT2006-90370.

[78] Uzol, O., Camci, C., Glezer, B., 2001, "Aerodynamic Loss Characteristics of a Turbine Blade with Trailing Edge Coolant Ejection: Part 1- Effect of Cut-Back Length, Spanwise Rib Spacing, Free-Stream Reynolds Number, and Chordwise Rib Length on Discharge Coefficients", ASME J. of Turbomachinery, **123**, pp. 238-248.

[79] Uzol, O., Camci, C., 2001, "Aerodynamic Loss Characteristics of a Turbine Blade with Trailing Edge Coolant Ejection: Part 2- External Aerodynamics, Total Pressure Losses, and Predictions", ASME J. of Turbomachinery, **123**, pp. 249-257.

[80] Holloway, D. S., Leylek, J. H., Buck F.A., 2002, "Pressure Side Bleed Film Cooling: Part 1 - Steady Framework for Experimental and Computational Results", ASME GT-2002-30471.

[81] Holloway, D. S., Leylek, J. H., Buck F.A., 2002, "Pressure Side Bleed Film Cooling: Part 2 - Unsteady Framework for Experimental and Computational Results", ASME GT-2002-30472.

[82] Goldstein, R.J., 1971, "Film Cooling," *Advances in Heat Transfer*, Academic Press, New York and London, **7**, pp.321-379.

[83] Taslim, M.E., Spring, S.D., and Mehlman B.P., 1992, "Experimental Investigation of Film Cooling Effectiveness for Slots of Various Exit Geometries", **6**(2), pp302-307.

[84] Martini, P., Schulz, A., Bauer, H.-J., 2006, "Film Cooling Effectiveness and Heat Transfer on the Trailing Edge Cut-back of Gas Turbine Airfoils with Various Internal Cooling Designs", ASME Journal of Turbomachinery, **128**, pp.196-205.

[85] Martini, P., and Schulz, A., 2004, "Experimental and Numerical Investigation of Trailing Edge Film Cooling by Circular Wall Jets Ejected from a Slot with Internal Rib Arrays, ASME J. of Turbomachinery, **126**, pp. 229-236.

[86] Cunha, F.J., Dahmer, F.T., and Chyu, M.K., 2005, "Analysis of Airfoil Trailing Edge Heat Transfer and its Significance in Thermal-Mechanical Design and Durability," ASME Paper No. GT2005-68108.

[87] Chen, S.P., Li, P.W., and Chyu, M.K., 2006, " Heat Transfer in a Airfoil Trailing Edge Configuration with Shaped Pedestals Mounted Internal Cooling Channel and Pressure Side Cutback", ASME Paper No. GT2006-90019.

[88] Cakan, M. and Taslim, M.E., 2007, "Experimental and Numerical Study of Mass/Heat Transfer on an airfoil Trailing-Edge Slots and Lands", ASME Journal of Turbomachinery, **129**, pp 281-293.

[89] Wright, L.M., Gao, Z., Varvel, T.A., and Han, J.C., 2005, "Assessment of Steady State PSP, TSP and IR Measurement Techniques for Flat Plate Film Cooling," ASME Paper No. HT-2005-72363.

[90] Coleman, H.W., and Steele, W.G., 1989, *Experimentation and Uncertainty Analysis for Engineers*, John Wiley & Sons, New York.

[91] Lau, S.C., Cervantes, J., Han, J.C., and Rudolph, R.J., 2006, "Internal Cooling near Trailing Edge of a Gas Turbine Airfoil with Cooling Airflow through Blockages with Holes," ASME Paper No. GT2006-91230.

VITA

Zhihong Gao received Bachelor of Engineering and Master of Engineering degrees in thermal engineering from the School of Energy Science and Engineering, Harbin Institute of Technology, China. She also earned a Master of Science degree in mechanical engineering, National University of Singapore. She joined the Ph.D. program at Texas A&M University in 2003. She worked as a Graduate Research Assistant at the Turbine Heat Transfer Laboratory in the Department of Mechanical Engineering under the supervision of Dr. Je-Chin Han. She obtained a Ph.D. degree in August 2007.

Permanent Mailing Address

Zhihong Gao

c/o Dr. Je-Chin Han

Department of Mechanical Engineering

Texas A&M University

College Station, TX 77843-3123